TAMPEREEN TEKNILLINEN YLIOPISTO
TAMPERE UNIVERSITY OF TECHNOLOGY

ANU HARJU

PROPERTIES OF HIGH VELOCITY ARC SPRAYED COATINGS

Master of Science Thesis

Examiners: Prof. Petri Vuoristo, M.Sc. Tommi Varis, M.Sc. Davide Fantozzi

Examiners and topic approved by the Faculty Council of the Faculty of Engineering Sciences on 31st May 2017

ABSTRACT

ANU HARJU: Properties of high velocity arc sprayed coatings
Tampere University of Technology
Master of Science Thesis, 118 pages, 21 Appendix pages
May 2017
Degree Programme in Materials Engineering, MSc (Tech)
Major: Metallic and Ceramic Materials
Examiners: Prof. Petri Vuoristo, M.Sc. Tommi Varis, M.Sc. Davide Fantozzi

Keywords: high velocity air fuel electric arc spray, electric arc spray, coating

High Velocity Air Fuel Electric arc spraying (HVAF Arc) is a thermal spraying technology that is quite similar to electric arc spraying. The difference between these two types of spraying equipment is that whereas the electric arc spraying technology uses compressed air as the atomizing gas, HVAF Arc uses the combustion products of propane and air. As HVAF Arc has not been widely researched, information about how the apparatus actually functions and what kind of effect changing its spraying parameters has, was desired.

This thesis consists of theoretical and experimental parts. In the literature review, thermal spraying technologies and the microstructure of thermally sprayed coatings is discussed briefly. Electric arc spraying, High velocity arc spraying (HVAS) and HVAF Arc especially are presented in more detail. In the experimental part, results from tests made to HVAF Arc specimens that have been strayed with different spraying parameters are presented. These tests include composition and thickness analyses, surface roughness tests, Vickers hardness tests, an erosion and a corrosion test.

According to the results, HVAF Arc coatings have fine microstructure, with low porosity, but are quite heavily oxidized. They are typically more oxidized than coatings made without using propane as a process gas, though the HVAF Arc coatings have lower surface roughness, less pores and slightly higher hardness, due to the amount of oxides in the coating. Typically, by changing spraying parameters the coating qualities of HVAF Arc do not change much.

TIIVISTELMÄ

ANU HARJU: Suurnopeuskaariruiskutettujen pinnoitteiden ominaisuudet
Tampereen teknillinen yliopisto
Diplomityö, 118 sivua, 21 liitesivua
Toukokuu 2017
Materiaalitekniikan DI-tutkinto-ohjelma
Pääaine: Metallic and Ceramic Materials
Tarkastajat: Professori Petri Vuoristo, DI Tommi Varis ja DI Davide Fantozzi

Avainsanat: suurnopeusvalokaariruisku, valokaariruisku, pinnoite

Suurnopeuskaariruisku (HVAF Arc) on terminen pinnoituslaite, joka muistuttaa pitkälti tavallista valokaariruiskua. Erona näiden kahden laitteen välillä on se, että HVAF Arc -menetelmässä pinnoitemateriaalin prosessikaasuna toimivat propaanin ja paineilman palamistuotteet, kun taas tavallisessa valokaariruiskussa prosessikaasuna käytetään vain paineilmaa. Koska HVAF Arc -menetelmästä on saatavilla vain varsin vähän tietoa, haluttiin laitteen toimintaa ja sitä, miten erilaisten ruiskutusparametrien muunteleminen vaikuttaa syntyvän pinnoitteen ominaisuuksiin, tutkia.

Tämä työ koostuu teoreettisesta ja kokeellisesta osasta. Teoreettisessa osassa sivutaan lyhyesti termisiä pinnoitusmenetelmiä yleensä ja niillä aikaansaatavaa mikrorakennetta. Tavalliseen valokaariruiskuun, ruiskuun nimeltä High Velocity Arc Spray (HVAS) ja erityisesti HVAF Arc -ruiskuun paneudutaan syvällisemmin. Kokeellisessa osassa selostetaan erilaisten testien tuloksia, jotka on tehty pinnoitteille, jotka on valmistettu erilaisin ruiskutusparametrein. Testeihin lukeutuvat kuva-analyysit pinnoitteiden koostumuksesta ja paksuudesta, pinnankarheustestit ja kovuusmittaukset, yksi eroosiotesti ja yksi korroosiotesti.

Tulosten mukaan HVAF Arc -ruiskulla saadaan aikaiseksi hienorakenteista pinnoitetta, jossa on vain vähän huokosia. Pinnoitteet ovat kuitenkin varsin hapettuneita. Tyypillisesti tulokseksi saatiin, että HVAF Arc -pinnoitteissa hapettuminen on runsaampaa kuin sellaisilla pinnoitteilla, jotka on tehty hyödyntäen kaariruiskua, jossa ei käytetä propaania prosessikaasuna. HVAF Arc -pinnoitteissa on kylläkin tällaisia pinnoitteita vähemmän huokosia, alhaisempi pinnankarheus ja yleensä hieman suurempi kovuus, oksidien määrästä johtuen. Tyypillisesti ruiskutusparametrien muunteleminen ei aiheuta juurikaan muutoksia syntyvän pinnoitteen laadussa.

PREFACE

This master study was done at the Laboratory of Materials Science at Tampere University of Technology in 2016-2017.

I want to thank my examiners professor Petri Vuoristo, M.Sc. Tommi Varis and M.Sc. Davide Fantozzi for surpervising, evaluating and examining my thesis, as well as for their good advice and instructions. Special thanks go to Mr. Mikko Kylmälahti for operating the HVAF Arc spray process at the TSCF laboratory at TUT, and Davide Fantozzi for his time with the SEM studies. I also want to thank Keijo Penttilä and Juuso Pohjola for their help in learning to prepare the samples and make measurements. Thanks also to the employees of the Laboratory of Materials Science for their advice and for pleasant working environment. I also want to thank AK Roll Oy for lending the HVAF Arc equipment, without which making this thesis wouldn't have been possible.

I want to thank my family, especially my father, for the support they have shown to me.

Tampere 24.5.2017

Anu Harju

CONTENTS

LIST OF SYMBOLS AND ABBREVIATIONS

AAS	Activated Arc Spray
AJB	abrasion jet blasting
AS	arc spray
DE	deposition efficiency
EDS	Energy Dispersive Spectroscopy
HVAF Arc	High Velocity Air Fuel Electric Arc
HVOF	High Velocity Oxy-Fuel
PS	plasma spraying
SEM	Scanning Electron Microscope
SL	turbulent shell lining

1. INTRODUCTION

1.1 Background of the study

The basic principles of a thermal spraying technology called High Velocity Air Fuel Electric arc spraying (HVAF Arc) process were developed in mid 1980's at Institute of Reliability and Longevity of Machines, Belarus Academy of Sciences. [32] It seems that the predecessor of HVAF Arc was called activated Arc Spray (AAS) [7], but after a company called Uniquecoat Technologies Inc. made some minor changes to the machine, the company seems to have renamed it as HVAF Arc [32]. Basically, HVAF Arc can be considered as a type of AAS gun.

As an apparatus, HVAF Arc is very alike to electric arc spraying apparatus. The difference between these two types of spraying devices is that whereas the electric arc spraying technology uses compressed air as the atomizing gas, HVAF Arc uses the combustion products of propane and air. The addition of propane is supposed to increase the velocity of the spraying jet [32] and reduce the oxidation potential of the gas phase in the spray jet [2], thus protecting the particles from oxidation.

Coatings sprayed with HVAF Arc are said to have intriguing qualities such as fine microstructure and high density. Therefore, more information about the qualities of HVAF Arc coatings, and functionality of HVAF Arc apparatus, was desired. HVAF Arc has been studied before by Verstak and Baranovski [32], and the predecessor of HVAF Arc, AAS, has been widely studied by Boronenkov and Korobov [2].

1.2 Aims and structure of the study

The aim of this thesis is to investigate the properties of coatings made with HVAF Arc, as well as to study the behaviour of the equipment itself. This study aspires to find out how the HVAF Arc device truly functions, what kind of effect changing the different spraying parameters has on coating qualities, and which of the parameters have most effect on the quality of the created coating. It is also investigated whether coatings sprayed with HVAF Arc differ from coatings made with conventional arc spray gun, and if they do, how exactly.

The thesis begins with literature review, in which thermal spraying in general as well as microstructure of thermally sprayed coatings, electric arc spray technology and HVAF Arc are discussed. The focus is on HVAF Arc and electric arc spraying, while thermal

spraying in general and the microstructure of thermally sprayed coatings is discussed only briefly.

In the experimental part, the effect of several different spray parameters is studied using two coating materials, Metcoloy 4 and Inconel 625. The coating specimens are studied with regards to their composition, microhardness (Vickers hardness) and surface roughness. For analysing the composition of the coatings optical microscope as well as scanning electron microscope (SEM) are used. The corrosion resistance and erosion wear is also investigated in the case of some of the specimens.

2. THERMAL SPRAYING

In thermal spraying, the materials are spray deposited as fine particles to form a coating. The different thermal spraying technologies are quite numerous, as are the applications that use them. In this chapter, the basics about thermal spraying technology are explained, including what the microstructure of thermal sprayed coatings is like.

2.1 Thermal spraying in general

Thermal spraying is a method for creating coatings that protect or modify the behaviour of a substrate material or a component. [10] Actually, there are several different coating processes of which thermal spraying techniques comprise. [33] Thermal spray techniques are used to increase the lifetime of materials or to provide them with a specific property, which can be for example optical or electrical. [4]

What all the thermal spray techniques have in common is that the coating material is spray deposited as fine particles. The particles can be in molten, semimolten or even in fully solid state as they form the coating. In all thermal spraying processes, a heat source is used to melt the feedstock material and accelerate the particles toward the substrate. [33] Whether the particles are softened or outright melted depends on the heating intensity of the heat source. [2] The heat source can be a combustion flame, electric arc, or ionized gas, and the feedstock may be in the form of powder, wire, stick or suspension. The sprayed coatings are formed by the flattened and solidified particles. [33] The substrate remains unmolten during the deposition. [2]

Thermal spray processes are typically classified according to the type of energy source used to heat the material. Depending on the energy source, the processes can also be classified further according to for example gun design or type of feedstock material, among others. The different thermal spray techniques have their own niches and do not overlap greatly in for example performance or coating properties. [33] Below is Figure 1 where the various thermal spraying technologies are classified according to their type of energy source.

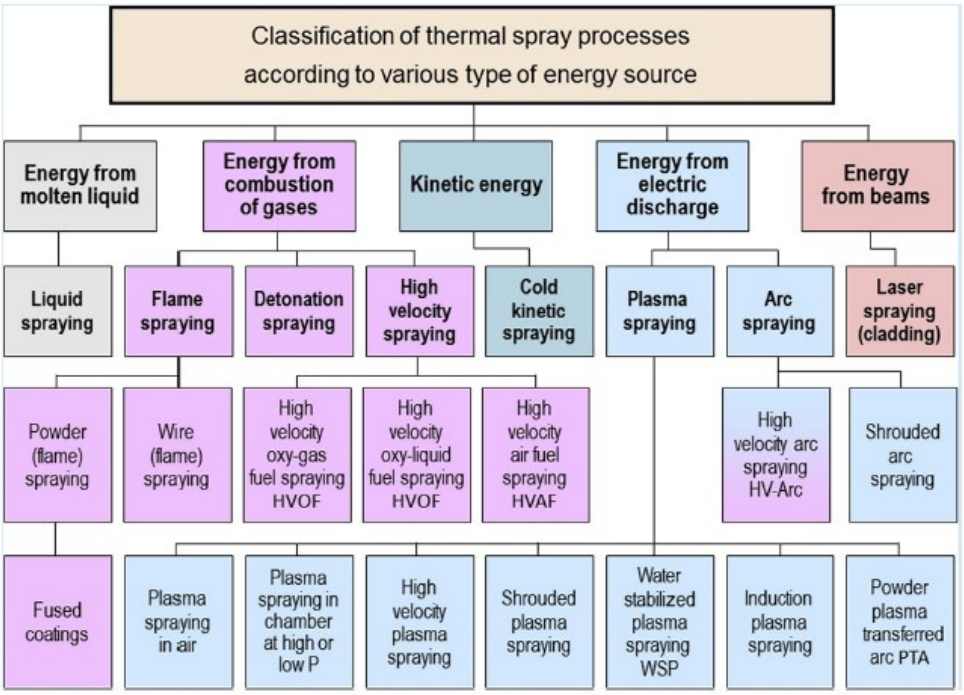

Figure 1. *Classification of thermal spray processes according to their type of energy source. [33]*

In thermal spraying there are quite a lot of different possible coating materials: pure metals, metal alloys, hard metals, oxide ceramics, plastics, cermets, composites, and blended materials. Apart from compounds that decompose irreversibly during melting and the ones that do not have stable meltstate and vaporize excessively in the spray process, almost all materials are suitable for thermal spraying. [33]

The deposition rate in thermal spraying is quite high compared to other deposition technologies. The thickness of the coating layer varies depending on the application; it can be anything from micrometers to several millimetres. [33] Thermal spray processes are also easy to use, and cost little to operate. By using thermal spray coatings, there are cost reductions due to better performance, longer component life and decreased need for maintenance. [10]. Thermal spraying is also a very versatile technology; it can be used on almost any component. [4]

Quite a many industry use thermal spray for many important applications. The applicatio n functions are for example restoration and repair, protection from corrosion or wear, heat insulation or conduction, decorative purposes, and many more. [10] Some of the main application sectors for thermal spray are aerospace, automotive, biomedical, marine, and metal processing industries. [4] In Figure 2 below there are three pictures which show a worn shaft before, during, and after repair.

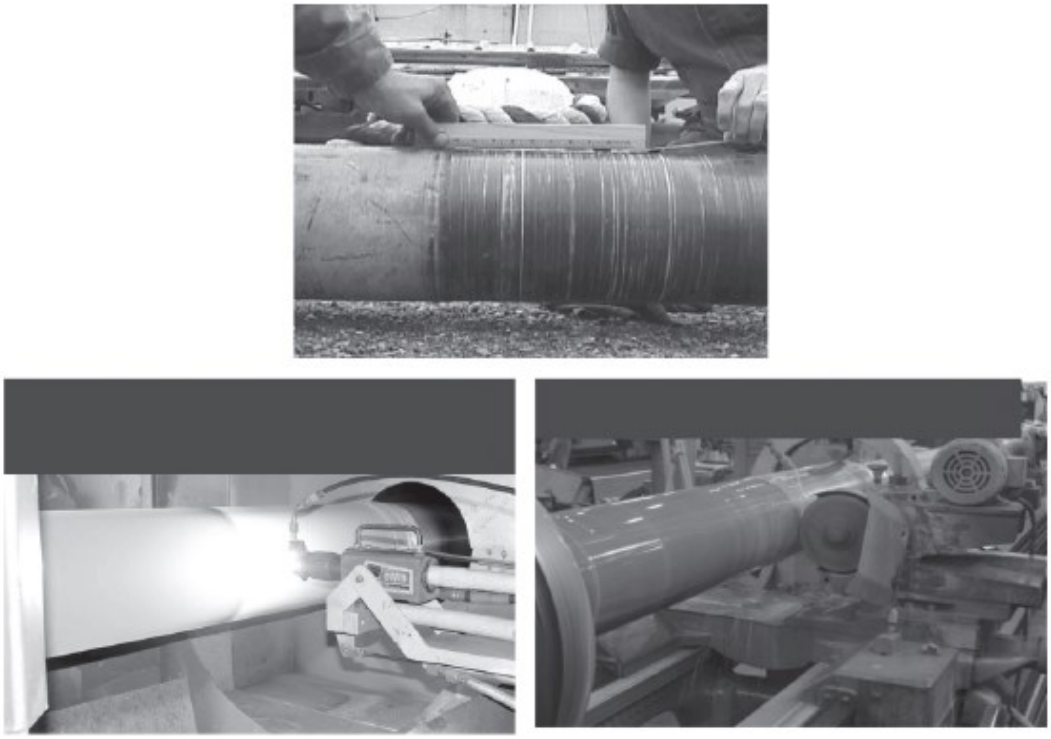

Figure 2. *A worn shaft before, during, and after repair. [9]*

2.2 Microstructure in thermal spray coatings

In the thermal spraying process the particles are first heated by the energy originating from the spray torch. They subsequently melt and are then accelerated by the high temperature, high velocity gas jet. As they impact on the surface, they spread and solidify rapidly and then cool in the next several minutes. [33] The particles take the form of a thin disk as they solidify. [2] Usually, the bonding mechanism between the sprayed particles and the substrate/ previously deposited layer in thermal spray coatings is mechanical, but in some cases it can be also metallurgical. The resulting coating structure is a lamellar, "pancake-like" splat structure. [10] Below is a schematic illustration of thermal spraying process (Fig.3).

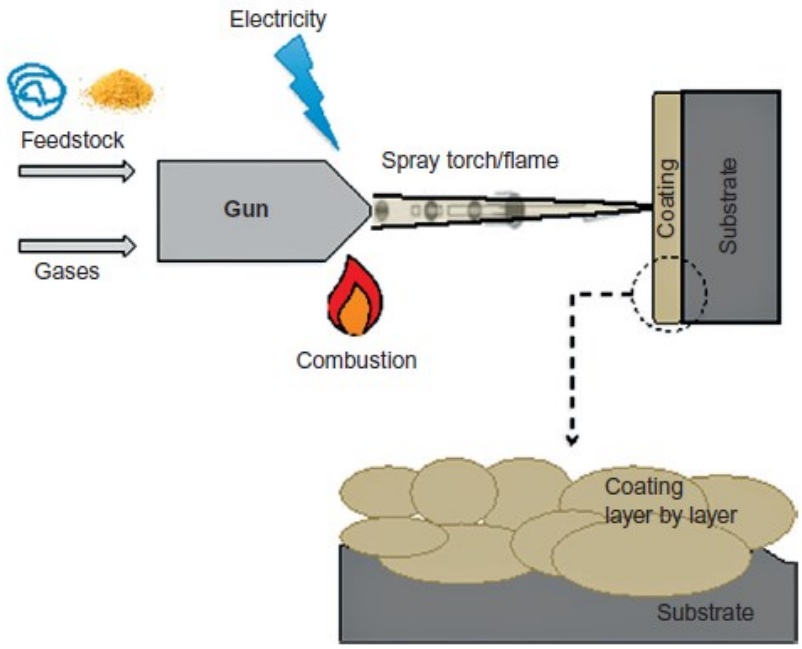

Figure 3. *Schematic illustration of thermal spraying process. [4]*

Though the lamellar structure typically consists of fine grains, it also includes non-homogenous features such as splat boundaries, pores, oxide inclusions, and unmolten particles. [9] There is below Figure 4 where a structure of a thermally sprayed coating is depicted. There can also be reaction products from the interaction between the particulate material and atmospheric gases. These reaction products can be for example stable oxides and nitrides. The interactions can also lead to changes in the phase composition or to selective evaporation of alloying elements. [2] There may also be cracks in the coating caused by residual stresses that form during cooling. In the worst case scenario, the residual stresses can cause the detachment of the entire coating from its substrate. [33]

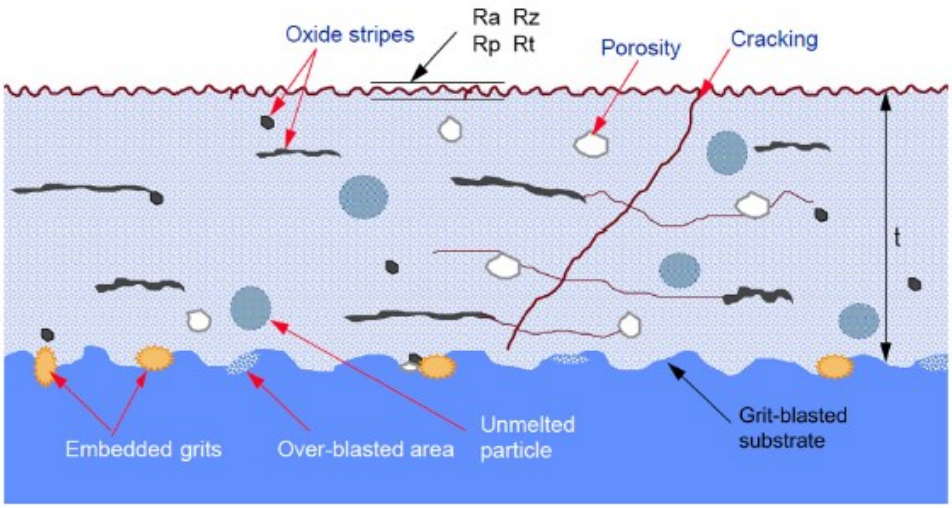

Figure 4. *Structure of a thermally sprayed coating. [33]*

The microstructure of thermal spray coatings is dependent upon the particle conditions at impact, such as the temperature and velocity of the particles, and material properties of the particle and substrate, such as surface roughness. [3] The temperature in the particle bodies strongly influences the microstructure of the coatings because the evolution of the temperature with time determines material solidification and cooling rates, which then influence the formation of crystal phases and crystal size. [33] The particle conditions are determined by the process parameters of the thermal spray. These process parameters, among others, are spray pressure and composition of the atomizing gas, particle velocity and size. [3] This is the reason why it is important to carefully optimize the spray parameters.

3. ELECTRIC ARC SPRAYING

Electric arc spraying is an efficient thermal spraying technology which uses arc produced by two conducting wires as the heat source to melt the wires. In this chapter, the arc spraying process is discussed, as well as the effect the spray parameters have on the arc spraying process. The advantages and disadvantages of the technology are also explained briefly.

3.1 Arc spraying process

Electric arc spraying, sometimes also called twin-wire-arc spraying [23], is a thermal spraying technology in which two wires with opposite polarities are used as the consumable electrodes. The stable arc produced by the end-meet of the wires is utilized as the heat source to melt the continuously fed wires. Compressed airflow is used to atomize the melted metal drops. [36] Usually the wires are made of electrically conductive materials, such as aluminium and copper, but it is also possible to spray non-conductive materials by using cored wires which have the non-conductive materials inside a conductive wire. The wire tips are separated by a distance of about a few tenths of a millimetre from one other. The electric voltage applied on them is about 40 V and causes the arc between the wire tips. [23] Typical arc spraying applications are wear and corrosion resistance, thermal barriers, high dielectric strength, hard dense coatings and decorative coatings, among others. [5]

Different wire-arc spraying systems differ in the geometry of the torch, the wire diameter, the feed mechanism for the wires and the location of the wire tips with respect to the torch geometry. [23] Typical feed mechanisms are driven by either electric or pneumatic motor. They are available in push, pull or push/pull arrangements. The push/pull feed mechanism is the most reliable and farthest reaching. [14] Controllable parameters in arc spray are: material of the wires, type of the atomizing gas, gas pressure, voltage, and wire-feed-rate or arc current. In systems that allow control over wire feed rate, the arc current cannot be controlled, and vice versa. [23]

In the arc spray process, the high temperature of the arc melts the ends of the feedstock wires and a spray of molten metal droplets is formed by the simultaneous flow of an atomizing gas through the arc region. Initially the molten metal is in the form of relatively large droplets which disintegrate further as the high velocity atomizing gas moves them downstream the arc. On impact with the substrate, the droplets spread and solidify as splats, as is typical in a thermal spraying technique. The formed coating has the characteristic thermal sprayed lamellar microstructure which includes also some porosity and

oxides. [15] Below is Figure 5 in which a schematic of electric arc spray is presented, alongside a picture of the typical coating.

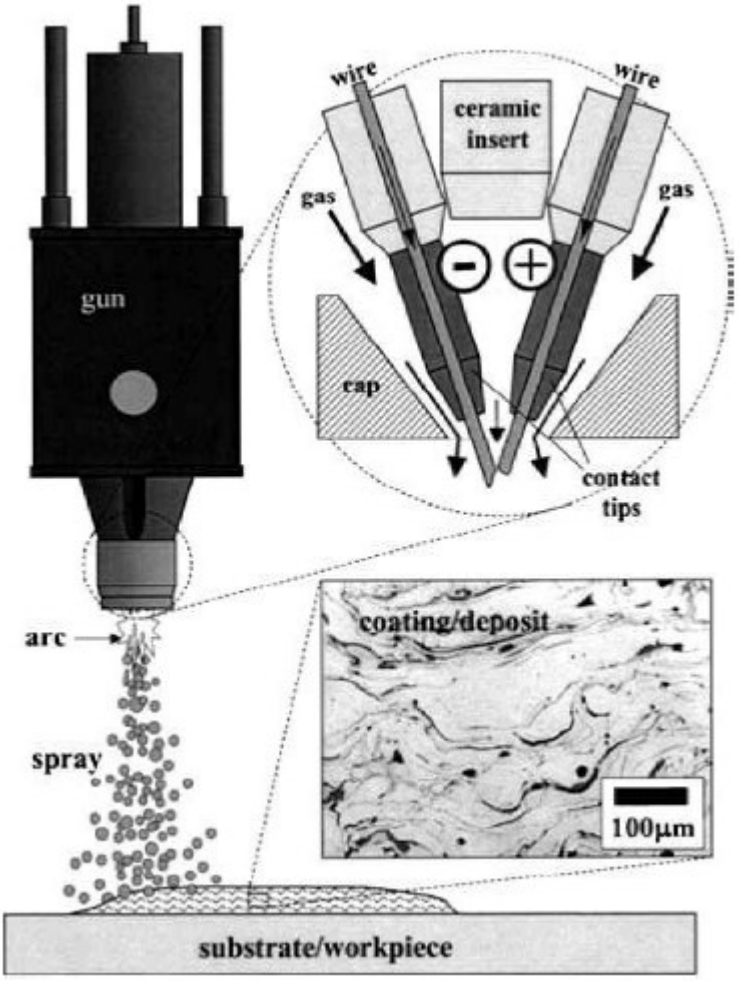

Figure 5. *Schematic of electric arc spray with a picture of a typical coating. [15]*

In arc spraying, the diameter of the droplets affects critically the microstructure, porosity and oxide content of the coating. The droplet diameter is determined by the melting behaviour of the feedstock wires in a direct current arc as well as primary and secondary atomisation processes under the action of the atomizing gas. [15] There are significant differences between the melting phenomena at the cathode and the anode. At the cathode, the arc attachment of the wire is localized, resulting in small molten droplets. The arc attachment at the anode, on the other hand, is more diffuse, the wire heating is more homogenous and the formed droplets are larger in size. [37] The result of these differences is that often the droplet size distribution of arc spraying is bimodal – the size distribution is composed of the larger and smaller droplets [28], [37], so that there are two distinctive particle size ranges. [31] It should be noted, though, that the difference in the average particle sizes lessens after the second atomization and becomes quite small. [11]

Not only are the droplets formed on anode and cathode of a different size, according to Zhu et al, they are also not distributed symmetrically about the centreline of the plume [40]. The maximum particle densities of the anode and cathode materials do not coincide with each other and they are not located at the centreline of the plume. [40] The spray also exhibits asymmetric radial variation of velocity and temperature about the pray cone axis. [17] All in all, these asymmetries result in a coating structure that is quite inhomogeneous. This is detrimental to coating qualities. [40]

The production of the droplets occurs typically in burst or pauses with respect to time. This is because the molten metal forms on the wire tips until the liquid metal volume becomes unstable under the influence of the atomization gas flow, and the liquid material is swept away by the gas flow. During these atomization pulses, the arc changes in length. Usually the arc is first struck directly across the shortest separation between the wire tips. The atomizing gas, however, deflects the arc column downstream and the arc extends. At quasiperiodic intervals, the arc becomes unstable and restrikes upstream at the original position at minimum separation. The periodical changes in arc length cause changes in the voltage across the arc. In Figure 6 below there is a graph of arc voltage as a function of time. At the shortest arc length, the voltage is at minimum and the current at maximum; at the largest arc length, the voltage is at maximum, the current at minimum. It has been suggested that voltage minima coincide with the release of a burst of large droplets from the wire tips. [15] In other words, the molten droplet size varies periodically. [11]

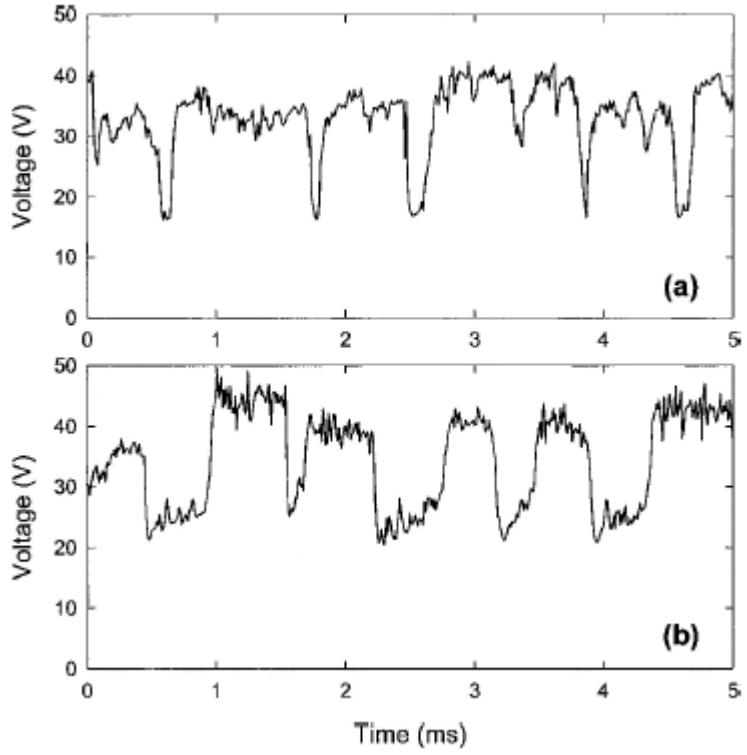

Figure 6. *Arc voltage as a function of time for standard conditions of atomizing gas pressure of 280 kPa and nominal applied arc voltage of 34 V, except with wire feed rate of a) 1*0 gs^{-1} and b) 5*0 gs^{-1}. [15]*

3.2 Effects of the processing parameters in arc spraying

Of different AS spray parameters, the atomizing gas flow rate is the most important influence on particle characteristics. [22] The higher the flow rate, the smaller and quicker the particles. The diameter of the droplets controls the dynamic and thermal behaviour in the spray as well as the splashing and spreading behaviour of the droplets at deposition. The diameter determines the scale of the coating microstructure; it determines the size of the lamellae as well as the size of the pores. If the droplets are substantially solid, they may bounce off the substrate or if they are substantially super-heated, liquid droplets, they may splash on the substrate. [15]

The flattening degree and splashing of the particles increases as flow rate increases. This occurs because the inertia force decreases in favour of viscous force and surface tension force when the flow rate is increased. If the spray distance is increased, the velocity and temperature of the particles decreases but their size remains constant. Other spray parameters have less influence. [22]

Increased flow rate leads also to increased hardness of the deposit, increased oxide content and decreased porosity. The oxide content of the coating increases because the specific surface of the particles in contact with oxygen increases, while the decreasing of porosity is caused by a greater flattening of the particles and a better accommodation of the particles between themselves. [22] On the other hand, a higher droplet velocity also causes a decrease in the time of flight, which in turn induces a decrease in the particle oxidation. In other words, a high droplet velocity has two effects that act contrariwise. [1] The gas flow rate and velocity, in turn, are controlled mainly by atomizing gas pressure. [1] Increasing the gas pressure increases the velocity of the spray, causing more efficient atomization. [17]

When it comes to other parameters, arc voltage has affects both arc temperature and spray velocity; an increase in arc voltage leads to an increase in the arc temperature, which leads to an increase in spray temperature. The spray velocity, however, decreases as arc voltage increases. [17] Increase in voltage causes also increase in the arc length, which increases the enthalpy of the metal droplets. This leads to greater progress of chemical interaction between the drop and substrate. At the same time, because the proportion of the vaporized metal increases, the deposition efficiency rate is reduced. The likelihood of cracking increases at higher arc voltages because the arc length is then greater. [2]

As was already mentioned before, there are periodical changes in the voltage across the arc, caused by changes in arc length. At the shortest arc length, the voltage is at minimum; at the largest arc length, the voltage is at maximum. (The current reacts in opposite way.) Voltage minima seem to coincide with the release of a burst of large droplets from the wire tips. [15]

The higher the current is the higher the processing rate and the heat input to the droplets. This, too, improves the interaction between the drops and the substrate at the moment of impact, which leads to higher adhesive strength. After the current rises above a certain level, the adhesion strength becomes constant and even begins to decrease. In other words, there is a limit after which there is no sense in increasing the current in order to improve adhesion strength of the coating. [2]

Wire feed rate, on the other hand, affects the diameter and production rate of primary droplets at the wire tips. Increase in wire feed rate increases both of them, and there is also an overall decrease in the spray average axial velocity. It should be noted that for any increase or decrease in wire feed rate, the arc spray system produces a calibrated increase or decrease in the current supplied to the arc in an attempt to provide stable melting of more or less material per unit time. [17]

The distance from which the coating is sprayed affects the porosity of the arc sprayed coating. The porosity of the coatings increases sharply when the spraying distance increases over 200 mm (Fig. 7).

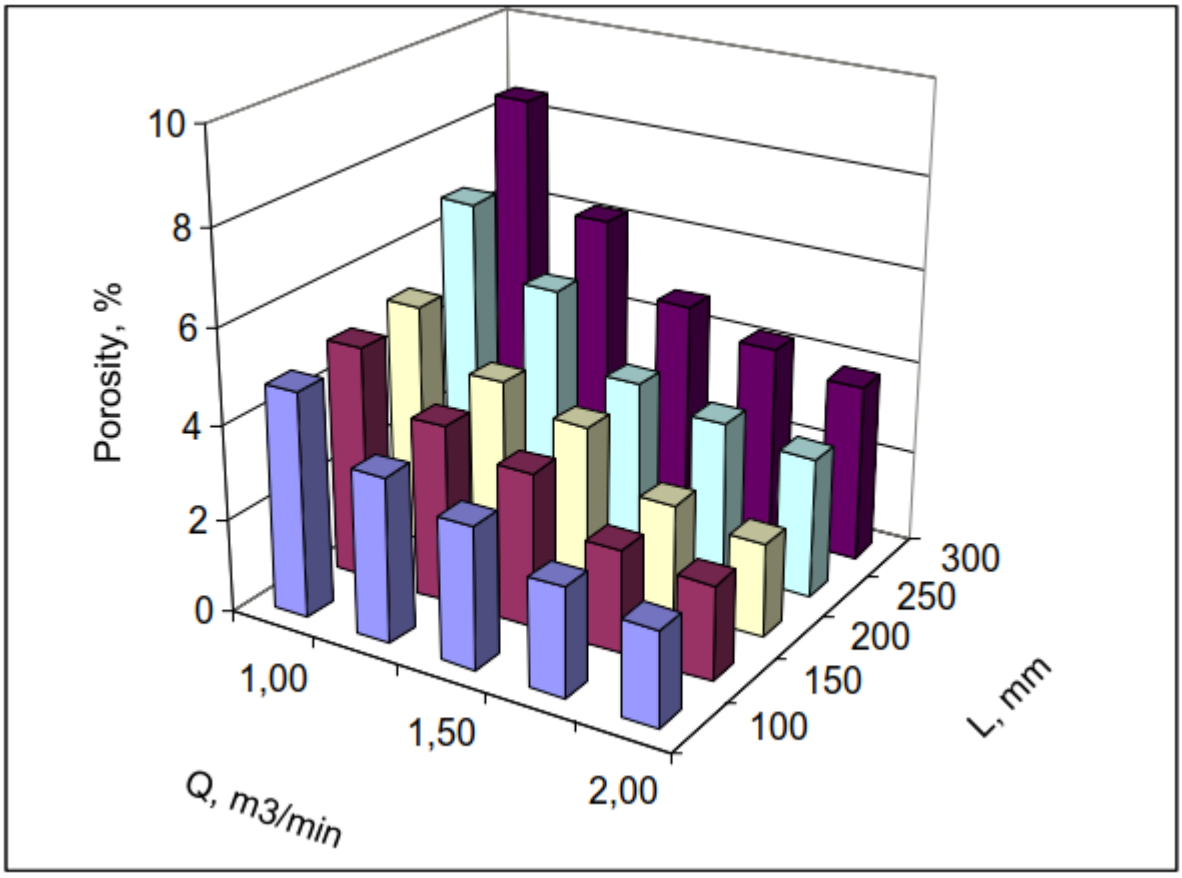

Figure 7. *The dependence between the porosity of the coating and the air flow rate (Q) and spraying distance (L). The wire used in the study was steel 304. [2]*

This sharp increase is especially noticeable when lowest allowable consumption of compressed air of 1-1.5 m^3/min is used. If the consumption of compressed air is increased to the maximum, the porosity decreases monotonically. If the spraying distance is increased more than 200 mm, the velocity and enthalpy of the droplet starts to fall, which creates worse conditions for spreading of the molten metal droplets on the substrate upon impact. This is what leads to increased porosity of the coating. It is recommended to use L=150-200 mm, and Q=1.75- 2 m^2/min to obtain coatings with minimum amount of pores. [2]

3.3 Advantages and disadvantages of arc spraying

The advantages arc spray has over other thermal spraying technologies are for example low operation cost, high efficiency of productivity, low heat input to the substrate and variant materials available for spraying. [36] Low heat input to the substrate prevents damage, distortion and metallurgical changes to the substrate surface. [23] Arc spraying also uses its power source more efficiently than for example plasma spraying. Benefits of using arc spraying also include the possibility to obtain thick coatings and ease of implementation. [2]

Yet another benefit of using arc spraying is that the materials introduced into the system are completely melted and consumed in the process. This eliminates the problems caused by partially melted particles. Almost all other thermal spray processes that use solid particles or powder as feedstock suffer from incomplete melting of particles. [23] Arc spray coatings are also usually denser and stronger than their equivalent combustion spray coatings. Compared to flame sprayed coatings, arc sprayed coatings have better bond strengths and lower porosity levels. [5]

Of course, arc spraying has also some disadvantages. The main one of them is that the coating quality is relatively poor; they usually have high porosity and low adhesion strength. [23] In arc spraying, there is also intense burnout of alloying elements from the metal and saturation of the sprayed layer with atmospheric gases. These phenomena lead to changes in the chemical composition of the sprayed material, lowering the alloying elements concentration. It also leads to excess of oxides in the coating. This decreases the quality of the coatings. [2] While arc sprayed coatings may contain more pores and oxides compared to other thermal spraying techniques, such as plasma or high velocity oxyfuel spraying, the higher deposition rate and low capital cost outweigh these disadvantages in many applications. [15]

Other disadvantages that arc spraying has are that only conductive wires can be sprayed. The high feed rate also causes a large amount of emitted aerosols, high level of noise and ultraviolet and infrared radiation. Therefore high safety requirements are required. [2] On the other hand, the gases used in arc spray are non-flammable, which makes the process safer than the ones that use flammable gases. [23]

The size of the particles in the spray cannot be controlled, unlike in those thermal spray processes that use powders as feedstock and where the size of the particles in the powder determines the size of the molten droplets. Thus the ability to adjust coating characteristics in arc spray is lacking; this narrows the range of arc spray applications. [23] In applications where the coating protects the substrate from corrosion, the corrosive medium in the environment can penetrate into the arc sprayed coatings and even to the substrate due to the porosity and slits between the layers of coating. The result of this is, of course, corrosion of the substrate and corrosion between the layers. [35]

4. HVAF ARC SPRAYING

High Velocity Air Fuel Electric Arc spraying (HVAF Arc) is a thermal spraying process that is very alike the electric arc spraying process. The main difference between the two methods is that with HVAF Arc, the atomizing gas has higher velocity. In this chapter the origins and basics of HVAF Arc process and its predecessor are discussed, as well as the studies concerning the technology. Another arc spraying technology that also uses high velocity spray jet is explained briefly and compared with HVAF Arc and electric arc spraying methods.

4.1 Origins of HVAF arc

The basic principles of HVAF Arc process were developed in mid 1980-s at Institute of Reliability and Longevity of Machines, Belarus Academy of Sciences. [32] It seems that originally the technology as well as the spraying apparatus was called Activated Arc Spray (AAS). [7] After some changes were implemented in the equipment by UniqueCoat Technologies (Ashland, Virginia, USA), the company renamed the device as HVAF Arc. The exact nature of these changes is not known, though it is said that these changes allowed the technology to become commercially available worldwide. [32] Boronenkov and Korobov, who have studied AAS extensively, refer to HVAF arc as a type of AAS gun, so it is evident that the principles of HVAF arc and AAS are the same. [2]

HVAF Arc has been studied somewhat by Verstak and Baranovski. AAS, on the other hand, has been quite extensively studied by Boronenkov and Korobov. Since the principle of the devices is the same, the research about AAS should pertain also HVAF Arc [2]. There is also one small study by Nuzzo regarding HVAF Arc [18].

4.2 Basics of HVAF Arc equipment

HVAF Arc is a coating deposition process similar to electric arc spraying. Its idea is to combine the efficiency of conventional electric arc spraying and the coating quality usually found in high Velocity Oxy-Fuel (HVOF) processes. It is supposed to provide fine particle atomization combined with protection of the sprayed material from in-flight oxidation by excess of propane in the gas jet. [32] Below is a picture of the HVAF Arc equipment (Fig. 8).

Figure 8. *An image of HVAF arc gun head. [29].*

In HVAF arc, two consumable wires are fused by electric arc and atomized by a supersonic jet of air-fuel combustion products. The combustion products are generated in toroidal combustion chamber which rear wall contains a high temperature catalyst. After flame ignition with a spark the rear wall heats up and activates continuously the air-fuel combustion during the spray process. Wire tips are located inside the chamber, and the flow of exhaust gases is directed along them. Wire material is atomized in a short expanding nozzle where the exhaust gas velocity exceeds the sound velocity. [32] Below in Figure 9 is a sketch of the HVAF gun.

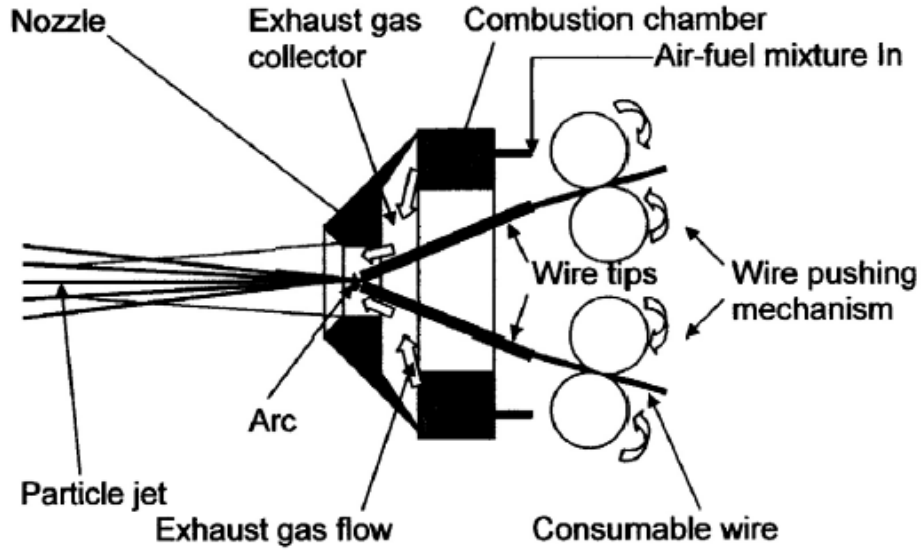

Figure 9. *A schematic of the HVAF Arc gun. [32]*

The average particle size of the atomized particles varies within 2-20 µm range. The size depends on the gas pressure in the combustion chamber and the atomizing nozzle diameter. Average particle velocity is within 150-280 m/s range. Maximal particle velocity is limited by the splats shattering upon impact. [32]

The reduction of the oxidation potential of the gas phase in the arc zone is a critical factor of the HVAF arc process, because the fine spray particles created in the process are prone to rapid in-flight oxidation. [2] To reduce oxidation potential of the gas inside the gun [2], an excess of the fuel gas is provided compared to its stoichiometric composition in air-fuel combustion mixture [32]. A number of fuel gases can be used. The decision of which fuel gas is to be used depends on availability and cost of the gas; the choice of fuel gas doesn't affect coating quality. Propane, propane-butane or natural gas are all widely used. [32]

4.3 HVAF Arc coating microstructure

The microstructure of an HVAF Arc coating seems to be typically fine, with lower porosity than coatings made with conventional arc spraying. For example, in the study by Verstak and Baranovski, the coatings made of alloy 671 and 625 had a very fine structure, with apparent metallographic porosity less than 2%. They were also denser than conventionally arc sprayed coatings or HVOF coatings. [32]

In a study by Boronenkov and Korobov, the coatings made with two types of AAS guns, one with and one without the combustion chamber, had the most preferable structure. [2] The study in question will be discussed more in Chapter 4.5.

4.4 Theories about the effect of propane in HVAF Arc

In conventional arc spraying, the atomizing gas can be either compressed air or compressed air combined with other fuel. The compressed air option is the one that is usually used, since it is the cheapest. When other fuels are used beside the compressed air, as is done in HVAF Arc, the oxidation potential of the gas phase is reduced and the heat generated during the combustion process can be used. [2] The hydrocarbon fuel (denoted as C_xH_y) reacts with the oxygen (the oxidizer; compressed air is about 21% oxygen and 79% nitrogen) in the compressed air, as is shown in the equation (1) below that explains this phenomenon:

$$C_xH_y + oxidizer = CO_2 + H_2O + heat \quad (1)[2]$$

When compressed air only is used as the atomizing gas, the oxide content of the sprayed coating is relatively high, since the molten wire material oxidizes in the wire arc spray process. While the higher oxide content can increase the coating hardness, it may also be detrimental to the coating properties because oxidation may reduce the adhesion strength

between the coating and the substrate. Coatings sprayed with air atomization are also often relatively high in porosity which, too, is detrimental to the coating quality. [37]

The fuels that can be used with compressed air are hydrocarbons like acetylene and propane. Of the hydrocarbon fuels, propane is the most suitable for arc spraying. Propane does not require significant starting costs, since it is already used with many gas-welding and cutting technologies. Propane is also safer than acetylene, though the latter is also widely used in gas welding processes. The relative safety of propane is based on its much lower inflammation velocity which makes it less likely to backfire. [2]

In conventional arc spraying, it is also possible to use an inert gas such as carbon dioxide or nitrogen instead of compressed air. By using them, oxidation of the formed coating may be less than when compressed air is used. Reduced oxidation also increases the adhesion of the coating to the substrate. When alloys such as stainless steels are sprayed, a significant amount of addition elements like chromium may be lost because the oxygen in the compressed air burns them; with inert gases, this phenomenon may be prevented. [1] Still, even when an inert gas is used, there is still some oxidation, because of air entrained from the surrounding atmosphere. Air entrainment can also cause a great drop in temperature and velocity of the gas stream. [1] In HVAF Arc it would not be viable to use an inert gas instead of compressed air to reduce oxidation, since HVAF Arc uses combustion products of propane and air mixture as the atomizing gas.

The spray produced by arc spraying gun can also be shrouded in order to reduce the amount of oxygen the spray encounters. [16] A shroud gas decreases the rate of air in the jet. The method can also decrease the jet divergence somewhat. In the shroud technique, the atomizing gas is protected by an injection of a secondary, inert gas. There are different methods for this injection; it can be located upstream the gun exit, or downwind the gun exit. [1] It might be possible to use a shroud gas in HVAF Arc process to further reduce the oxidation of the spraying material. It could also be said, though, that the function of propane as a process gas is almost the same as a shroud's.

4.5 Studies about the effect of propane on AAS coatings

Boronenkov and Korobov have studied the effect of the process gas atmosphere by using different kinds of arc spraying guns. Their first sample was done with a normal arc spraying gun, EM-14, the second with ADM-10, which uses both propane and air, making it a kind of AAS gun. The third sample was done with ADM-12, which nozzle system is a closed system with a central nozzle, and the fourth was done with the ADM-12 gun using a secondary propane injection as a shroud. In essence, in the case of sample 4, the gun can be considered an AAS gun without a combustion chamber. [2] Below is Table 1 where the parameters and different compositions of the gas can be seen.

Table 1. *Parameters of the stainless steel X40Cr13 coating with a different composition of the process gas. [2]*

Specimen number	Differences			Constant parameters
	gun	$P_в$, MPa	$P_п$, MPa	
1	EM-14 [19]	0.6	0	Initial material – wire X40Cr13, ∅ 1.8 mm; I = 180 A; U = 28 V; $T_{пп}$ = 120°C; L = 100 mm; $V_п$ = 1.8 m/s; δ = 2 mm
2	ADM-10 [20]	0.35	0.3	
3	ADM-12 [21, 22]	0.6	0	
4	ADM-12, [21, 22]	0.6	0.2	

Symbols: $P_в$,$P_п$ - pressure of air and propane; I - current; U - voltage; L - spraying distance; $T_{пп}$ - temperature of samples preheating; $V_п$ - linear velocity of the gun relatively to the sample; δ - coating thickness

The microstructure of the specimens can be seen in Figure 10 below. The numbers correspond to the Table 2 above. We can see that specimen 1, which was sprayed with conventional arc spraying gun, has the coarsest inhomogeneous structure. Specimen 2, for which a type of AAS gun was used, has thinner structure and fewer and smaller voids, and there are fewer extended pores. The samples 3 and 4 were made with the same gun, but in sample 4, an injection of propane was also used. The coating of sample 4 has more homogenous and finer structure than sample 3. [2] It can be concluded that when the gun uses propane, the microstructures of the coatings are preferable to when the gun uses only compressed air.

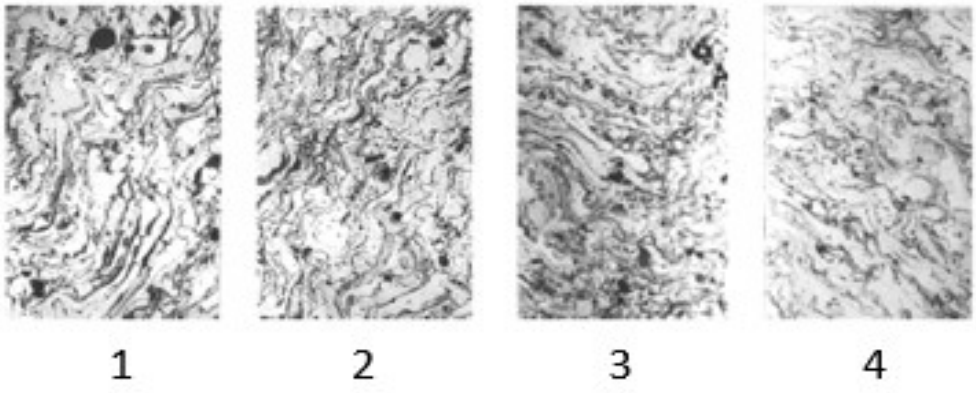

Figure 10. *The microstructure of the stainless steel X40Cr13 specimens. The specimens have not been etched. Magnification is 250. Numbers correspond to the Table 2. [2]*

Below is Figure 11 where the differences in the microstructure of specimens 3 and 4 can be seen more clearly. In sample 4, there are only small, point like pores (the black points in the picture) where as in sample 3, the pores are more extended.

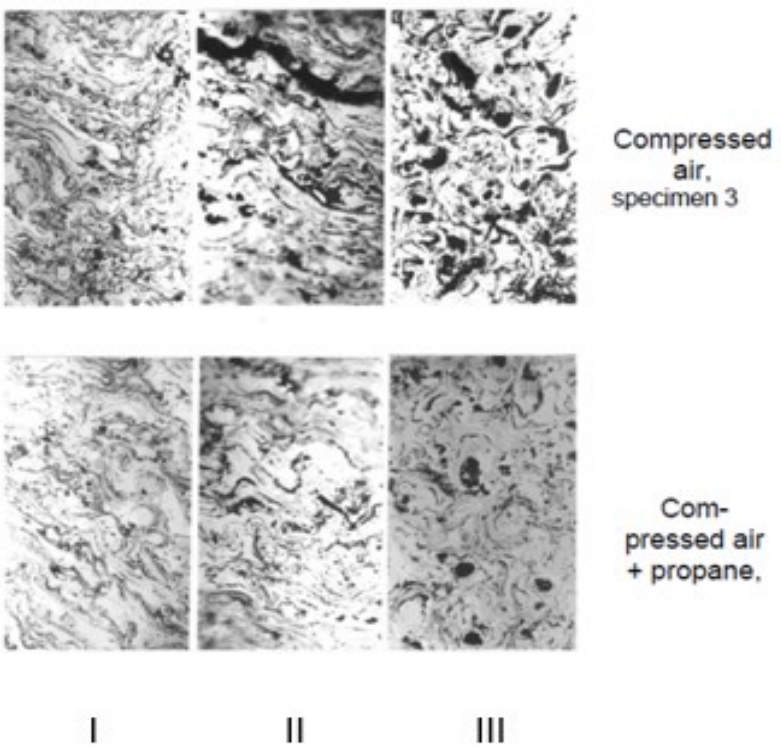

Figure 11. *The microstructure of the stainless steel X40Cr13 coatings with different compositions of the process gas. Magnification is 250x. I - near the substrate; II - a surface layer, thin section perpendicular to the surface; III - surface layer with thin section parallel to the surface. [2]*

When the microhardness of the specimens was compared, it was noted that by using propane, the microhardness was increased. [2] In Figure 12 below, both samples 2 and four have higher microhardness values than specimen one, though specimen 3, where no propane was used, has at least as good, if not better, values as sample 2. Sample 4 seems to have, on average, the highest values.

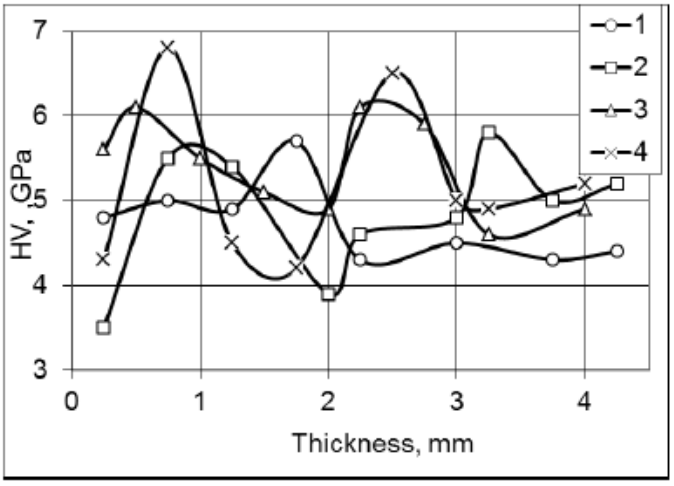

Figure 12. *Comparison of stainless steel X40Cr13 coating microhardness sprayed with propane injection (AAS) and compressed air (AS). 1 – AS, pure metal and portions of the mixed structure; 2 - AS oxides; 3 – AAS, pure metal and portions of the mixed structure; 4 - AAS, oxides [2]*

In another study by the same authors as in the previous case, a gun that used supersonic jet of combustion products as the carrier gas, making it a type of AAS gun, was compared to typical arc spray gun and a plasma gun. The coatings were made of stainless steel. [2]In Table 3 below the results can be seen. The coatings made with supersonic gun have reduced porosity, better hardness and better adhesion strength than the coatings made with other guns.

Table 2. *Comparative properties of the stainless steel coatings. AS = arc spray, Ps = plasma spray.[2]*

№	Coating method	Poros-ity, %	Hard-ness, HRc	Phase micro-hardness, MPa		Adhesion strength, MPa	Friction coefficient *
				light	dark		
1	Super-sonic AS	2…3	35…37	1200	16000	65	0,15
2	PS	6…8	28…30	1000	13000	50	0,7
3	Typical AS	10…12	22…25	900	11000	35	0,3

* - the average value at a load of 5 ... 10 MPa

An analysis of the stainless steel coatings sprayed in the study (apart from those that were sprayed with the plasma gun) was made using a diffractometer. It was noted that the phase compositions of coatings made with the supersonic gun and conventional arc spray were the same, yet it was also found out that adding propane increases the amount of carbon in the coating, which leads to an increase in the amount of residual austenite. [2] Below is Figure 13 where the diffractogram of number four is the one from a specimen made with the gun that used propane.

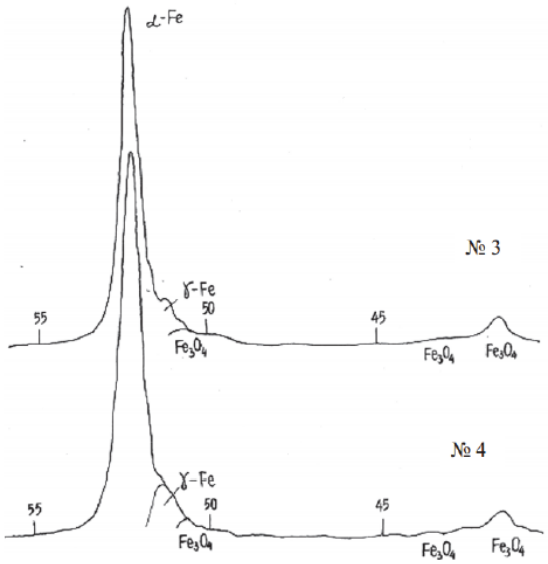

Figure 13. *Diffractograms of specimens 3 and 4. [2]*

Boronenkov and Korobov have also studied how different ratios of propane and air, or in other words, different degrees of particle oxidation, affect the wear resistance of coatings made from steel 20X13. Specimen made with conventional arc spraying gun (EM-14) was used as a standard in the study. It was compared to specimens sprayed with the AAS gun ADM-10, which had different coefficient of oxidant excess in the process gas when different specimens were sprayed. [2] The results can be seen below in Figure 14. When the coefficient of oxidant excess is smallest, the coating's wear resistance is highest, since then the oxidation degree of droplets and thus coating oxidation degree is smallest [2].

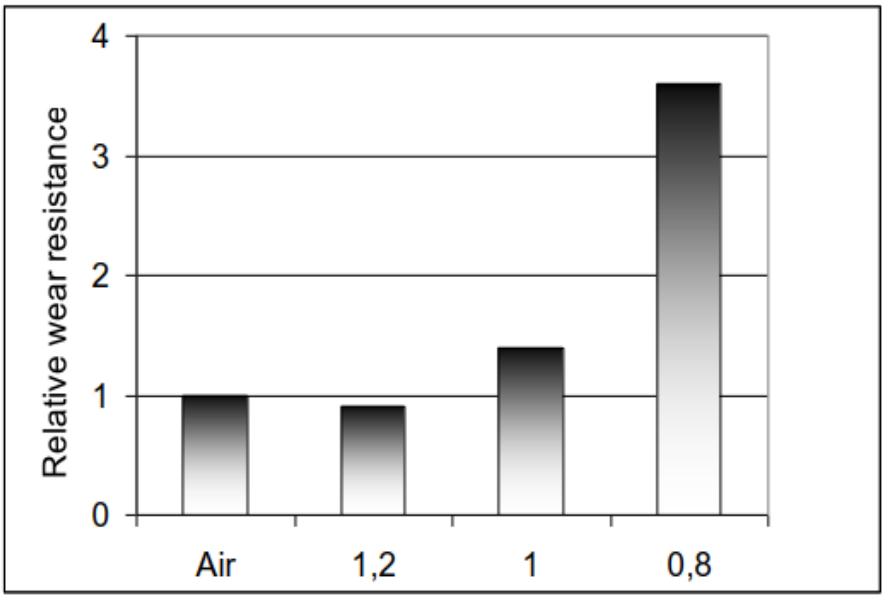

Figure 14. *Wear resistance of AAS coatings with different coefficients of oxidant excess. [2]*

Boronenkov and Korobov conclude that based on the studies made about the effect of the carrier gas there is a critical number of oxides in the coating, which corresponds to the maximum of the wear curve for the specific material. They also show in the Chapter 2 of their book how to calculate the oxygen delivery to a spraying drop, which can be used to estimate interval of process parameters which need to be implemented to get the required amount of oxides. [2]

4.6 Theories about the effect of high velocity

In arc spraying in general, a higher atomizing velocity leads to higher particle acceleration [37]. This leads to a higher impact velocity, which means that the particles deform more intensely on the substrate [2]. The higher velocity also leads to a higher particle temperature at impact, because the particles have a shorter flight time and therefore less time to be cooled by entrained air. The higher temperature results in lower viscosity and better wettability of the particle material, which leads to better conformal coatings. [37] If the particles are overheated, however, the overheating contributes to excessive heat in-put

into the coating, which causes an increase in the level of residual stresses in the coating. Increasing the velocity of the particles also leads to decreasing porosity. [2] So by using a gun with high atomizing velocity, coatings of better quality can be achieved.

The velocity of the particles can be increased in two ways. First way means increasing the mass flow rate of carrier gas, in other words, increasing its velocity, pressure or density, or increasing the cross-section of the nozzle. The other way is to reduce the particle size to reduce its aerodynamic resistance. This can be done at arc spraying by increasing pressure and velocity of the gas and lowering the arc voltage. The latter is limited by a threshold of stability disturbance at droplet separation. [2] In HVAF Arc, it seems, the high velocity is achieved by having high gas pressure in the combustion chamber.

4.7 Studies about particle velocity and its effect in AAS coatings

In a study by Boronenkov and Korobov, the velocity of the particles was measured from AAS and an arc spraying gun without combustion chamber by using velocity rate meter intended for luminous objects. The device's operation is based on the principle of a rotating mirror. The current used in this test was 210 A, voltage 30V, combustion chamber pressure equaled 0.32 MPa, and the pressure in the spraying head was between 0.22-0.23 MPa. The wire material used was steel X20Cr13, with a diameter of 1.6 mm. Measurement results are in Table 3 below. The scatter of the values is related to the difference in velocities of the particles of different diameters. [2]

Table 3. *Results of the steel X20Cr13 particles' velocity measurements at arc spraying, m/s. [2]*

Results of the particle's velocity measurements at arc spraying, m/s

The distance from the nozzle face, mm		50	100	150
Spraying head with a combustion chamber	Velocity at the upper border of the interval, m/s	134	125	120
	Velocity at the lower border of the interval, m/s	110	100	100
Spraying head without a combustion chamber	Velocity at upper border of the interval, m/s	62	75	70
	Velocity at the lower border of the interval, m/s	42	52	46

Particle size distribution of arc sprayed steel solid wires was conducted by spraying into water. The resulting powder was collected and dried at elevated temperature. The fractional composition of the particles was determined by sieve analysis method by weight share. The experiments were conducted using a type of AAS gun, with a current of 200 A and voltage of 30 V. The spraying distance was 100 mm, and the wire used was steel wire X20Cr13, just like in the particle velocity study. [2] The results of the test are in Table 4 below.

Table 4. *Fractioned composition ofsteel X20Cr13 particles according to experiments. [2]*

Particle sizes intervals, microns											
0-20	20-35	35-40	40-50	50-63	63-71	71-80	80-100	100-125	125-160	160-200	200-315
Fraction weight content, %											
7.0	6.6	6.6	8.2	7.6	10.0	11.8	12.0	10.0	7.8	6.0	6.4
Area share of fraction, %											
38.9	10.4	3.9	6.6	7.7	4.8	4.9	8.1	6.5	4.1	2.3	1.9

In another study made by Boronenkov and Korobov, the magnitude of open porosity decreases sharply with increasing the velocity and decreasing the particle size. In this study, average particle velocity of conventional arc spraying gun was 55 m/s and the particle size was 1-600 µm. It seems that steel wire X20Cr13 was used as the coating material. When using a type of AAS gun, the average particle velocity was 120 m/s. The share of droplets with a diameter of 20-125 µm was about 75% and the size of particles all in all was up to 315 µm. Their analysis showed that at the coating thickness of 0.05 mm, open porosity of AAS and conventional arc spray differ by almost one order at different spraying distances (Figure 15 below). The porosity of the coating surface decreases in the study also due to the reduction of roughness. The roughness is directly related to the size of the particles impinging on the surface. [2]

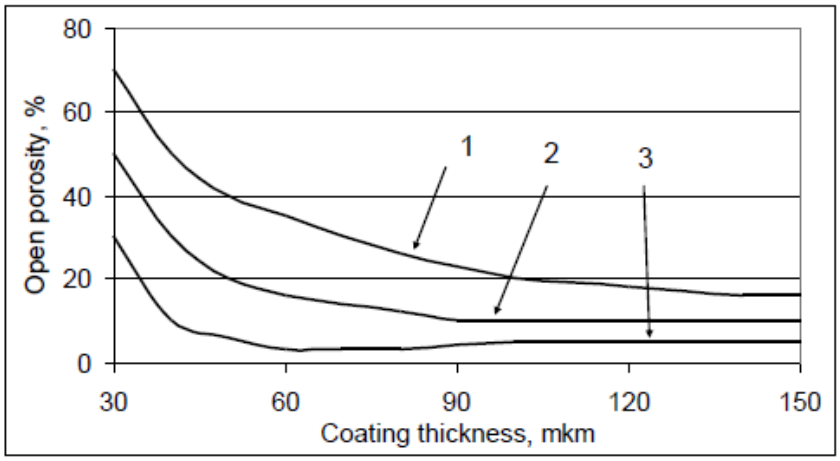

Figure 15. *Influence of the coating thickness on the open porosity. 1- AS, 2,3 – AAS, 1,3 – L = 100 mm, 2 – L = 50 mm. [2]*

The difference in the open porosity leads to an even greater difference in the gas permeability. For AAS coating, this quantity is two orders of magnitude smaller than in the case of typical arc spray, with a coating thickness greater than 0.1 mm. With a layer thickness of 0.05 - 0.1 mm the difference is 4 - 5 orders of magnitude. This can be seen from the Figure 16 below.

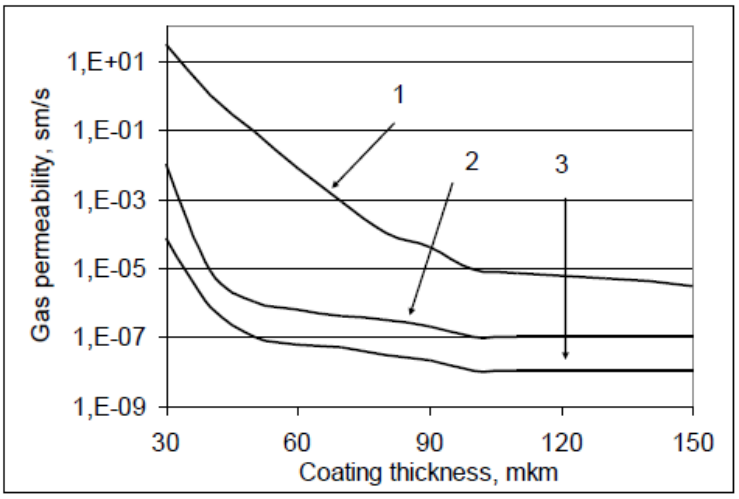

Figure 16. *Effect of coating thickness on gas permeability. 1 – sprayed with conventional arc spray gun; 2,3 – sprayed with AAS; 1,3 - L = 100 mm; 2 - L = 50 mm. [2]*

4.8 Hardness of HVAF Arc coatings

The hardness of HVAF Arc coatings seems to be better than that of coatings made with conventional arc spray. In the study made by Verstak and Baranovski, Fe-Cr-B-C cored wire coatings made by HVAF Arc had similar microhardness to those sprayed with conventional arc spray, yet their macrohardness was better. The hardness test was made with impact tester. In Table 5 below are results of the both hardness tests. [30] In another study by Boronenkov and Korobov, the microhardness of AAS coatings was better than that of conventional arc spray coatings. [2]

Table 5. *Hardness and elevated temperature erosion resistance data for HVAF Arc and conventional electric arc sprayed hardface coatings. [32]*

Coating	Micro-hardness HV_{300}	Macro-hardness HRC	Thickness loss due to erosion, μm
Armacor M Arc	740 +/-95	51.5 +/- 1.5	116
Armacor M HVAF Arc	750 +/- 100	58.5 +/- 2.0	70
Duocor Arc	755 +/- 85	52.6 +/- 2.2	161
Duocor HVAF Arc	785 +/-90	55.0 +/- 1.8	53

In study made by Nuzzo, three iron based coatings made with HVAF Arc sprayed at three different spray distances were investigated. The materials used were Metcoloy 2, Tafa 45CT, and Kanthal SW 010. Their Vickers microhardness was measured (Table 6) and their microstructure and oxide content was evaluated using optical micrographs. It was

found that the oxide content in the cross section of the coatings increases with an increase of the spray distance. [18]

Table 6. *Microhardnesses of Metcoloy 2, Tafa 45CT, and Kanthal SW 010 HVAf Arc coating, as well as the distances they were sprayed from. [18]*

Sample name	Mean Hardness (HV)	Minimum value (HV)	Maximum value (HV)
M130	485	436	526
M150	491	440	539
M200	494	436	530
T130	364	326	412
T150	372	353	432
T200	382	360	398
K130	320	239	366
K150	354	300	416
K200	351	298	399

The spray distances appear to have relatively little effect on hardness of the coatings, even though the increase in the oxide content should also raise hardness. Nuzzo attributes this to the fact that the coatings were already so oxidized that the small increase of oxide content caused by the increased spray distance doesn't significantly affect the coating hardness. [18] In the micrographs in Figure 17 can be seen that the samples are quite oxidized. There can also be seen dark, oxidized ridges in the image of Metcoloy 2.

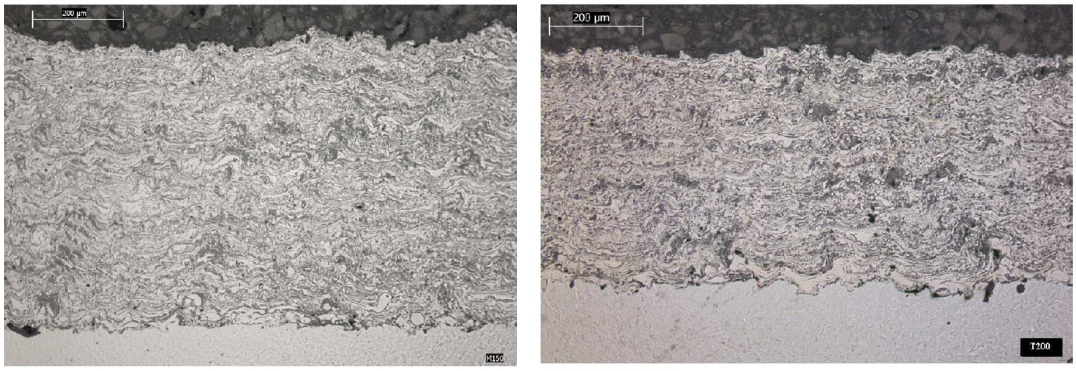

Figure 17. *Optical micrographs of Metcoloy 2 coating cross-section sprayed at 150 mm, on the left, and of Tafa 45CT coating cross-section sprayed at 200 mm, on the right above. [18]*

4.9 Oxidation of HVAF arc coatings

When it comes to oxidation, in the study made by Verstak and Baranovski, in HVAF Arc coatings made of aluminium there were no oxide scales, but there were isolated oxide inclusions. Their amount was controlled by spray parameters. Apparent metallographic porosity of the coatings was less than 1%. The coating also became practically impermeable to gas at thickness of 100-120 micron (which is quite low). On the other hand, when the coatings were made of alloy 671 and 625, respectively, the amount of oxides in the coatings was similar to conventional electric arc spraying. [32]

4.10 Corrosion resistance of HVAF Arc coatings

In a study by Verstak and Baranovski, the alloy 671 HVAF Arc coating outperformed conventional arc spray and HVOF coatings in elevated temperature sulfidation test at 400 ˚C (Table 7). In oxidation test at 700 ˚C, the alloy 671 and 625 HVAF Arc coatings outperformed conventional, but were inferior to HVOF (Table 8) coatings. [32]

Table 7. *Weight gain and X-ray microanalysis data of sulfur and chlorine permeation into alloy 671 coatings after testing in N_2-1%H_2S-1%HCl gases at 400 °C during 1440 hours. [32]*

	Electric arc coating	HVOF coating	HVAF Arc coating
Weight gain due to corrosion, mg/cm^2	5.64	5.28	4.75
Sulfur inside the coating	Yes	Yes	Yes
Sulfur at coating-substrate interface	Yes	No	No
Chlorine inside the coating	Yes	No	No
Chlorine at coating-substrate interface	Yes	Yes	No

Boronenkov and Korobov conducted an express corrosion resistance test in the atmosphere of water vapor. It showed that the resistance of AAS coatings with thickness of 150 microns matches the value of typical arc sprayed coating with thickness of 200 microns. [2] So the test would indicate that the corrosion resistance of AAS coatings might be better than that of conventional arc spray coatings.

Table 8. *Weight gain and scan electron microscopy data for alloy 671 and alloy 625 coatings after testing in air at 700 °C during 1000 hours. [32]*

	Electric arc coating	HVOF coating	HVAF Arc coating
Weight gain due to oxidation, mg/cm^2 Alloy 671 Alloy 625	 3.23 3.49	 1.89 2.29	 1.68 2.91
Substrate oxidation beneath the coating	Yes	Yes	Yes
Depth of inter-granular oxidation of the substrate, μm	150	50	50

Boronenkov and Korobov have also studied cored wires made with AAS gun and the heat resistance of the cored wire coatings. They were interested in finding out what kind of effect the conditions of coating formation have on those characteristics of alloying system Fe-Cr-Al that affect their heat resistance. They used cored wires with diameter of 2.0 mm and with a shell of low carbon steel. The contents of the wires were titanium and silicon. [2] Chemical compositions of the coatings of the wires are shown in Table 9 below.

Table 9. *Calculated chemical compositions of the cored wire coatings. [2]*

Component	Chemical composition, wt. %		
	1	2	3
Aluminum	6.0	6.0	6.0
Chrome	28.0	28.0	28.0
Titanium	1.7	less 0.5	less 0.5
Silicon	less 0.5	1.3	less 0.5
Ferrum	Substrate		

In the study, the initial composition of the wires was chosen so that their content of chromium and aluminum were similar to heat-resistant alloy grade CrAlTi 23-5. Chromium and aluminum contents were chosen to be held constant for all the cored wires so that the effect of silicon and titanium on the heat resistance of the coatings could be determined. The cored wire combinations for their spraying are in Table 10. The coating specimens were held for 24 hours at a temperature of 700°C in air. [2]

Table 10. *Combinations of cored wires (CW) used for spraying. The combination numbers refer to Table 9. [2]*

Cored wire combinations	Symbol for the cored wire coating
3 and 3	a
3 and 2	b
3 and 1	c

Their study revealed that the lamellae in the coatings were separated by thin oxide films. They didn't find any significant differences in the structures of the different types of coatings (Fig. 18). The main coating phase in structure was formed by solid solution of chromium, aluminum and other elements present in iron. The predominant oxide present was iron oxide Fe_2O_3; there were also some of oxides inclusions of Al_2O_3 and Cr_2O_3. From figure 19 below can be seen that specific weight loss of the coating specimens was 2.3-0.4 g/(m^2*h). This is significantly lower than similar values for pearlitic and martensitic-ferritic steels. [2]

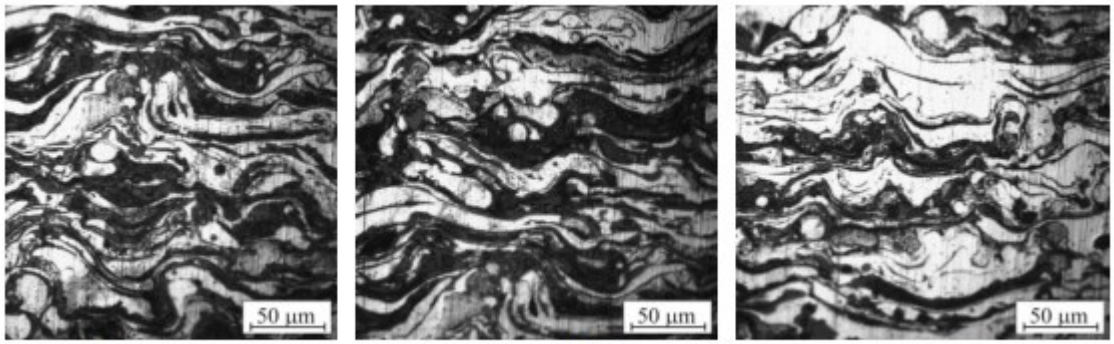

Figure 18. *Microsturctures of the cross-sections of coatings. The a, b, and c correspond to cored wire combinations in Table 10. [2]*

Based on Table below, the best heat resistance belongs to the coating alloyed with the largest amount of titanium.

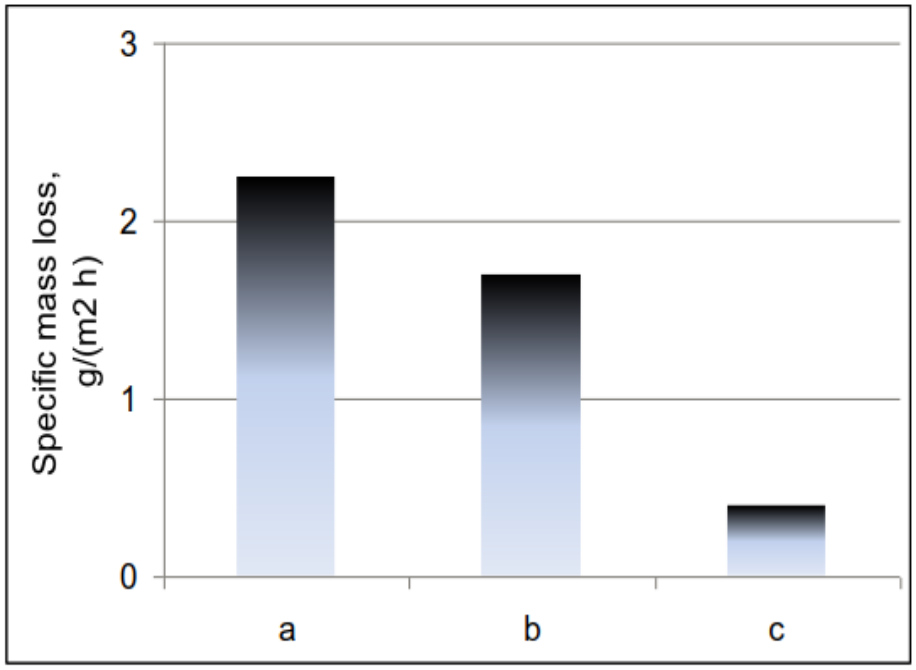

Figure 19. *The specific mass loss of specimens of heat resistant coatings after holding for 24 hours at a temperature of 700 ° Celsius. The a, b, and c refer to cored wire combinations in Table 10. [2]*

Based on the EDS results in upper part of Table 11 below, which show the composition of the coating before the heat resistance test, in the calculating the compositions for Table 9, the error was not more than 15%. From the chemical composition of the coating after the heat resistance test, Boronenkov and Korobov deduced that the individual particles of sizes 1-10 micrometers contain an increased amount of titanium (5-6 wt%), while the total content of Ti in the coating does not exceed 1.6 wt%. They say that the particles are located at the grain boundaries in the coating and the oxide film Al_2O_3, and that spectra corresponding to the localization zones of these particles also exhibit the several times increased content of aluminum and oxygen with several times reduced chromium and iron, compared with the average values for the coating, seen in lower part of Table 11. They presume that the particles are TiC, since they are thermodynamically the likeliest option. [2]

Table 11. *EDS spectrum interpretation for coating Fe-Cr-Al-Ti before the heat resistance test (the upper results) and after the heat resistance test (the lower results).[2]*

Element		Al	Si	Ti	Cr	Fe	Totals
Content	wt.%	6,16	0,26	1,60	29,30	62,68	100
	at. %	11,66	0,48	1,71	28,79	57,36	100

Element		O	Al	Ti	Cr	Fe	Totals
Content	wt.%	49,58	35,65	3,70	5,98	5,09	100
	at. %	65,89	28,09	1,64	2,45	1,94	100

Based on the data, Boronenkov and Korobov conclude that in the coatings, the formation of averse structural components like ferritic carbides $(Fe, Cr)_7C_3$ and aluminum nitride AlN is prevented. The reason for this is the formation of thermodynamically stable and heat-resistant carbides TiC and a layer of oxides that function as a diffusion barrier. Since there are no averse structural components, the film of aluminum oxide Al_2O_3 is mainly formed on the surface during heating, based on first EDS analysis before heat treatment (Table 11, upper part), which ensures a high level of heat resistance. The authors conclude that by adding an increased quantity of titanium and silicon into the charge of the base alloying system Fe-Cr-Al, the formation of averse structural components can be averted. [2]

Boronenkov and Korobov also note that the adhesion coating strength of the base alloying system Fe-Cr-Al, when titanium is introduced into the initial charge of wire (variant c from Table 10) is 44MPa. This is comparable with values for cored wire coatings with similar purpose. [2] In Table 12 below the adhesion strengths of different coating techniques can be seen.

Table 12. *Adhesion strengths of various coating technologies, [2]*

CW grade	developed	PMet 731	EuTronic Arc 509	TAFALOY 26CA
Adhesion strength, MPa	44	43	46	54

In table below, the total porosity of the coating (variant c) can be seen. The total porosity of the coating, including the open and closed porosity, is 2.8%. The maximum pore size is 44.1 micrometers, while the minimum pore size is 0.5 micrometers. [2]

Table 13. *The total share of pores of long-accumulate mode, %. The coating the pores belong in is the variant c from Table 10. N is the numerical share of the pores, A is share area, and V is share by volume. [2]*

D, micron	0-2	2-4	4-6	6-8	8-10	10-12	12-14	14-16	16-18	18-20	20-22
n*	9.7	45.2	67.5	78.7	84.1	90.6	92.8	94.8	95.5	97.0	97.8
A*	0.3	4.6	12.5	20.2	26.2	37.3	42.7	49.3	52.4	60.4	64.9
V*	0	0.7	2.7	5.4	8.0	14.2	17.7	22.8	25.3	33.1	37.8

The authors of the study estimate that the amount of pores that have a size up to 22 micrometers is about 97.8% of the coating, and major part accounts for pore size to 10 microns. According to the authors the coating is formed from particles with a diameter up to 100 mm (weight content of 69.8%), and thus the data demonstrates the stability of the process of cored wire spraying. Based on these solutions, heat resistant AAS coatings were developed to increase service life of power equipment parts that are used in conditions of gas corrosion. [2]

4.11 Tribological properties of HVAF Arc coatings

Verstak and Baranovski conducted a study where the HVAF Arc Fe-Cr-B-C cored wire coating outperformed conventional arc spray coatings in elevated temperature erosion tests. [32] The results can be seen in Table **5**. Boronenkov and Korobov have also studied quite widely the tribological properties of AAS coatings. For example they used the apparatus in Figure 20 below for testing impact abrasion. [2]

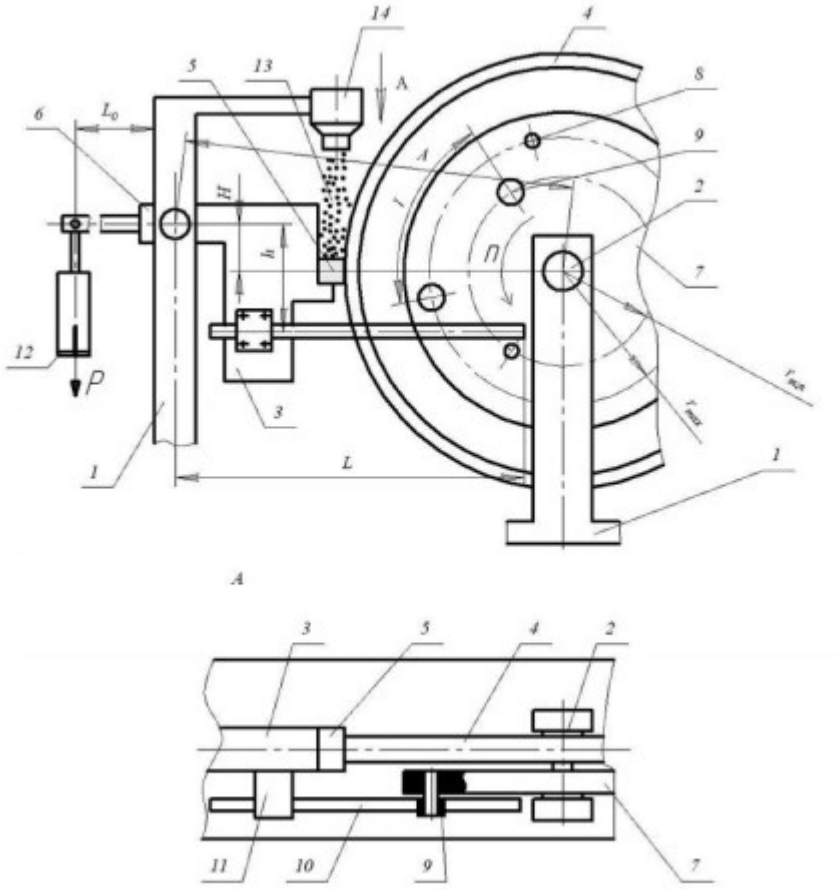

Figure 20. *Impact tester used for testing abrasion resistance. [2]*

They compared the abrasion resistance, or loss in weight, of various materials typically used in spraying. They used current of 160 A, voltage of 28 V, electrode diameter 1.6 mm, spraying distance of 100 mm, compressed air pressure of 0.3-0.4 MPa, and pressure of propane of 0.3-0.4 MPa when coating the specimens with an AAS gun [2]. In Table 14 below the test modes they used in their study are shown.

Table 14. *Wear resistant testing modes. [2]*

Regime number	Contact pressure, MPa	Single impact energy, J	Friction path, m
1	233	0	30
2	129	72.8	30
3	233	133.6	30
4	233	133.6	122

The results of the abrasion study can be seen from Figure 21 below. The relative durability of the coatings tested in the experiment is higher than that of the standard cast steel. If the specific load is reduced, like in mode 2, or if the sliding path is increased, like in mode 4, wear resistance of coating from high-chromium steel X20Cr13 becomes several times higher than that of other materials (depicted as the violet bars in the figure). [2]

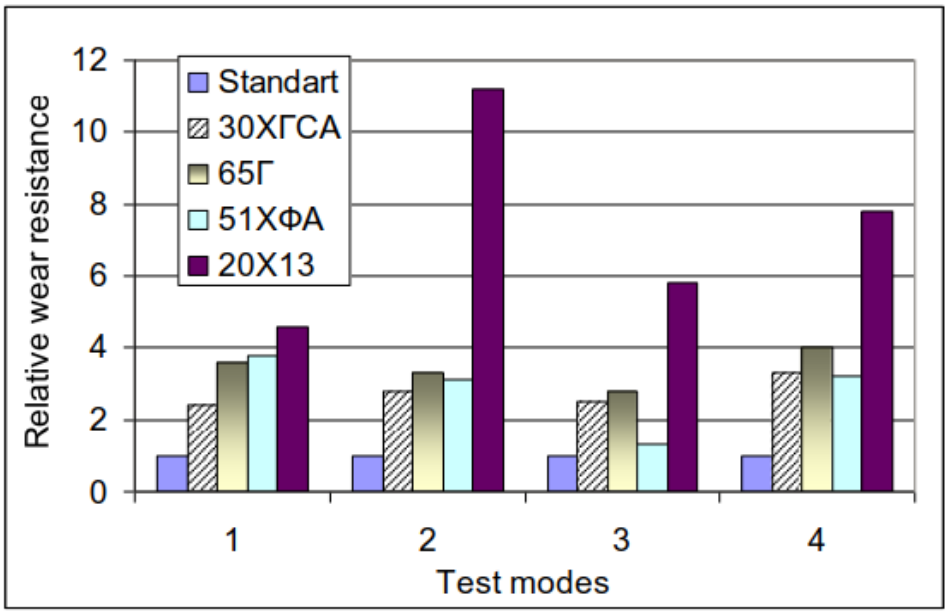

Figure 21. *Wear resistance of AAS coatings. The standard is cast steel iron similar to steel 5120. Test modes refer to Table 14. Tested steels 30ХГСА, 65Г, 51ХФА, 20Х13 correspond to steels like 30CrMnSi, 1566, 6150, 420. [2]*

In another tribological study made by Boronenkov and Korobov, an AAS Babbitt coating with steel solid substrate are compared with Babbitt coatings made with turbulent shell lining (SL), gas surfacing, and plasma spraying (PS). From Figure 22 below can be seen that the AAS Babbitt coatings (marked as AS in the figure) have the smallest friction coefficient no matter the pressure used and clearly smaller wear rate than shell lining and plasma spraying. [2]

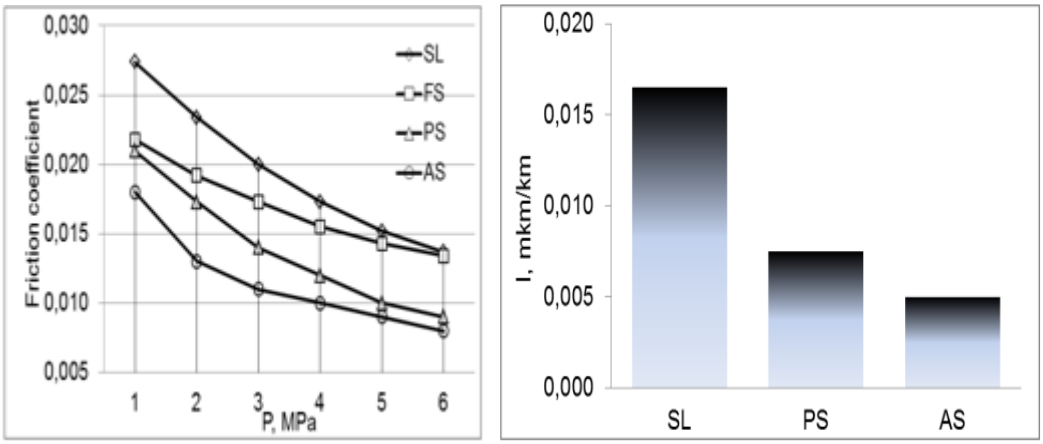

Figure 22. *Tribological characteristics of alternative Babbitt B 83 layers. On the left, friction coefficient at different pressures, on the right, the wear rate. [2]*

Boronenkov and Korobov think that the decrease in the friction coefficient at increasing pressure may be because of the changes in the ratio of hard intermetallic compounds in the coatings and the substrate playing the role of a soft interlayer. The authors also think that the lower friction coefficient and wear rate of AAS and plasma sprayed coatings compared with shell lining and gas surfacing are probably caused by the smaller size and greater uniformity of intermetallic phases in the AAS and plasma sprayed coating. The intermetallic phases are the hardest components of Babbitt coatings. Sprayed coatings also have high oil ability due to porous acting layer which leads to less wear when lubrication is insufficient. The wear is increased in plasma sprayed coatings compared to AAS coatings probably because plasma sprayed coatings have less fatigue strength, since they have higher thermal stresses, because there is excessive heat input to the spray material in plasma spraying in comparison with AAS. [2]

According to Boronenkov and Korobov the friction coefficient of a type of AAS coating (shown, and called supersonic AS, in the Table 15) is lower than that of plasma and typical AS coatings sprayed using similar initial core wires. The authors of the study claim this is probably connected to the differences in conditions of the coating formation, and velocity and oxidation ability of the carrier gas in plasma spraying and standard arc spray. [2]

Table 15. *Anti-friction properties of the coatings. Determined by ball- on -disc method, load 5-10 MPa. [2]*

Coating method	Supersonic AS	Plasma spray-ing	Typical AS
Friction coeffi-cient	0.03	0.05	0.15

4.12 Relationship between bonding strength and permeability in HVAF Arc coatings

Boronenkov and Korobov studied also the relationship between bonding strength and permeability of AAS coatings made from stainless steel wire. The steel wire was similar to steel ASTM 304, with wire diameter of 1.6mm. A substrate of low carbon steel similar to A570-36 was used. The specimens were jet blasted before the coating was sprayed. The dependence of the roughness on the size of the abrasive was obtained at a distance of 50-150 mm (Table 16 below). The angle of the jet to the surface was 90° degrees. For comparison, unblasted surface was used. [2]

Table 16. *Dependence of the surface roughness on the grit size and distance processing. The grit is of chipped steel. AJB means abrasive jet blasting. [2]*

Grit size, mm	0.1…0.3	0.4…0.8	0.5…1.2	0.8…1.4	0.8…1.9
AJB distance, 50 mm					
Rough-ness, µm	12	16	21	28	37
AJM distance, 100 mm					
Roughness, µm	16	20	25	35	45
AJM distance 150 mm					
Roughness, µm	14	18	23	34	44

The results for the effect of surface roughness of the substrate on the permeability of the coatings can be seen in Figure 23 below. The authors of the study came to the conclusion that corrosion resistance of the coating with increased surface roughness is reduced by its increasing permeability. [2]

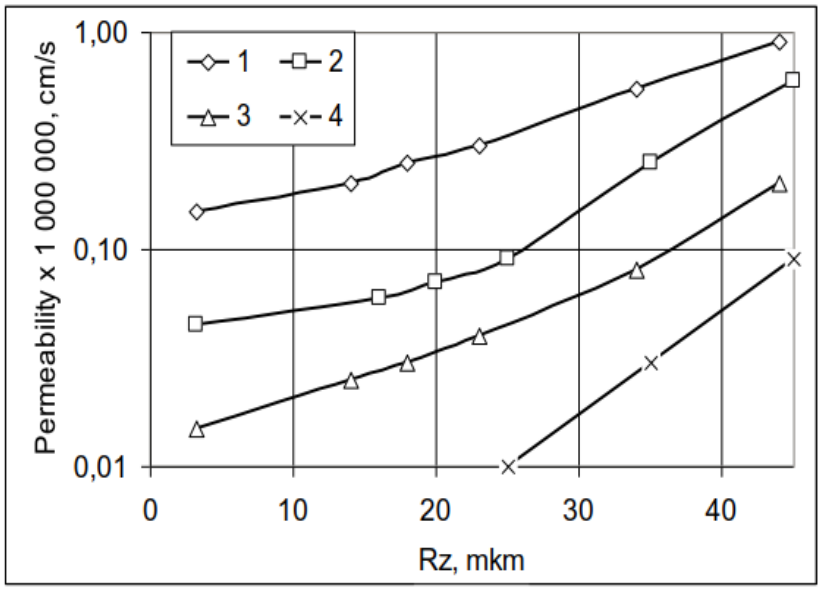

Figure 23. *The effect of surface roughness of the substrate on the permeability of coatings. Wire: steel 340. The thickness of layers 1, 2 is 0.15 mm,and thickness of layers 3, 4, is 0.20 mm. Spraying distance: 1, 3 – 150 mm, 2, 4 - 100 mm. [2]*

From Figure 24 below can be seen that like permeability, adhesion strength of the AAS coating increases as the roughness of the substrate increases. Increasing the height of surface roughness of the substrate up to Rz40 leads to increased adhesion strength. It can also be seen that if the roughness increases further, Rz is not noticeably affected. The authors think the results are similar to plasma spraying, indicating that AAS coatings are similar in quality to plasma sprayed coatings. [2]

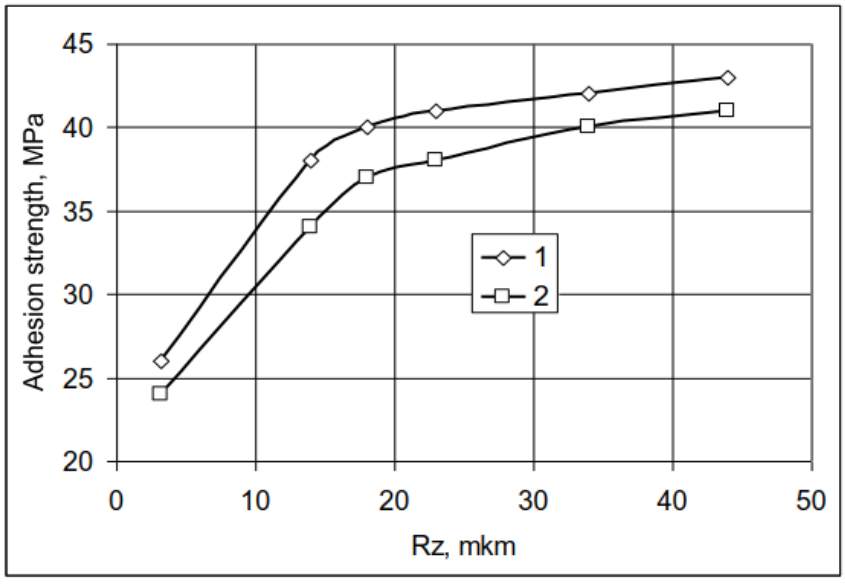

Figure 24. *The effect of base surface roughness on the adhesion strength of coatings. Wire: steel 304. Layer thickness is 0.15 mm, spraying distance: 1 - 150 mm, 2 - 100 mm. [2]*

It is also noted in the study that deposition efficiency (DE) increases with increasing roughness (Fig. 25). At least, deposition increases up to to Rz 40. Further than that it starts to decrease slightly.

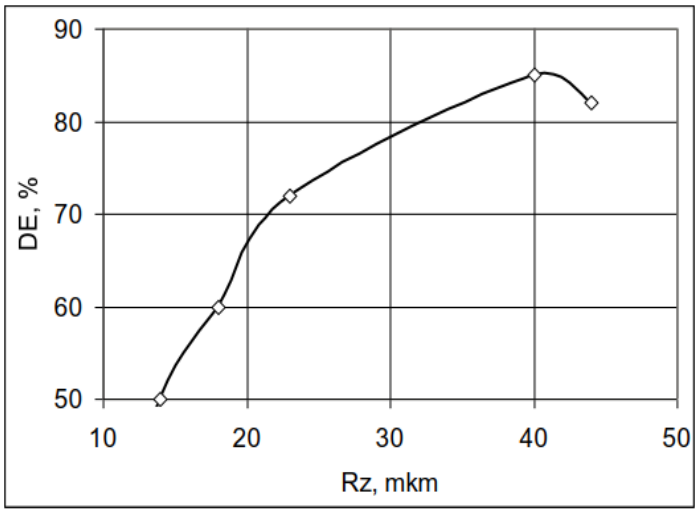

Figure 25. *The effect of surface roughness of the substrate on deposition efficiency. Coating material is steel 304. Layer thickness - 0.15 mm; spraying distance - 150 mm. [2]*

4.13 HVAS

High Velocity Arc Spraying (HVAS) is a coating deposition process which has a principle very similar to conventional electric arc spraying. They differ in their atomization type; ordinary arc spray uses subsonic, HVAS supersonic atomization. In supersonic atomization, the particles are more evenly distributed and gain higher velocity, which can lead to better coating quality. [34] The droplets can be accelerated up to 350 m/s. [39] and arc temperature can be produced up to 4000K. [6] In the Figure 26 below there is a sketch of the principle of the HVAS gun.

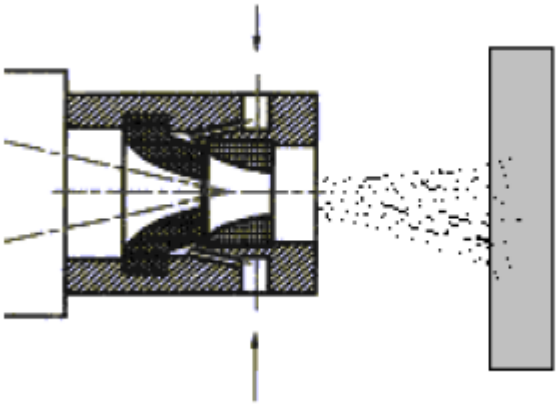

Figure 26. *Sketch of the principle of the HVAS gun. [12]*

In HVAS, two wires, acting as consumable electrodes, are drawn from spools, form a liquid droplet due to arc heating, and are atomized by supersonic gas. The gas is accelerated by convergent-divergent nozzle (LAVAL nozzle). The gun has a special cooling method to avoid the particles adhering to the nozzle. [34] In the Figure 27 below there are schematics of both the convergent divergent nozzle and of the conventional straight bore nozzle.

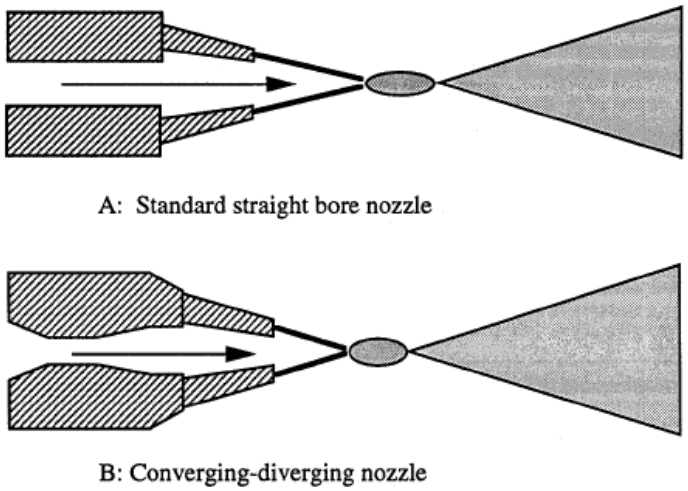

Figure 27. *Schematic of a) standard straight bore nozzle and b) converging-diverging nozzle. [37]*

In arc spraying, the nozzle design affects the efficiency of the spraying process greatly. The arc spraying system is supplied with compressed gas, and because of it, the external jet may underexpand at the nozzle exit. This underexpansion may increase particle jet spreading, which is detrimental to coating quality. A converging-diverging nozzle can be used to solve this problem. A converging-diverging nozzle increases the gas velocity at

the wires intersection point. The nozzle also causes a decrease in the mean droplet size. [1] The conventionally used nozzle is a straight bore nozzle. [37] Thanks to converging-diverging nozzle, the coating structure of HVAS tends to be finer, the porosity lower and oxide content higher. [11] Below in Figure 28 can be seen an image of HVAS coating as well as a coating sprayed with conventional arc spray gun.

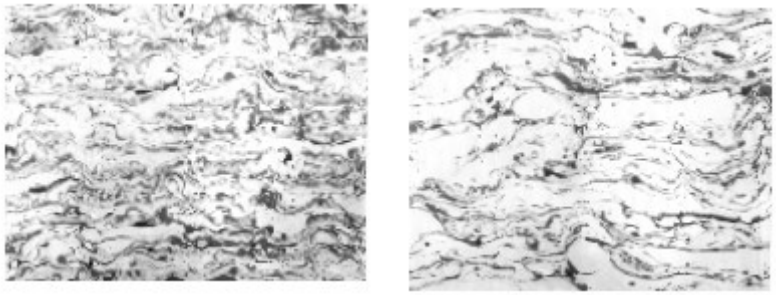

Figure 28. *On the left, an image of HVAS 7Cr13 coating, and on the right, 7Cr13 coating sprayed with conventional arc spray gun [37]*

In the Figure 28 below the formation of shock structures in the straight bore nozzle and converging-diverging nozzle can be seen. The strong shock structure and non-uniformity of the gas stream produced with the straight bore nozzle cause rapid velocity decay (Fig. 29a). There is weaker shock structure and longer high velocity potential core in the gas stream produced by converging-diverging nozzle (Fig.29b). [37]

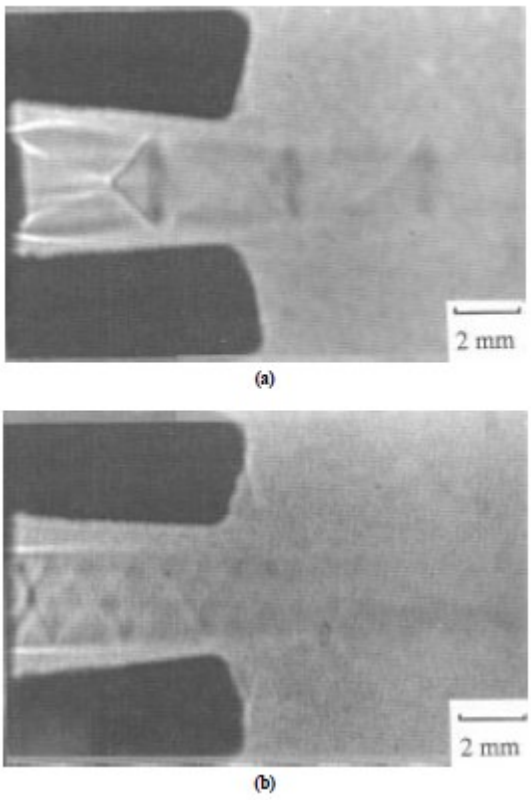

Figure 29. *Shock structure of the gas stream produced by a) straight bore nozzle and b) convergent-divergent nozzle. [37]*

For example, in a study using 3Cr13 as coating material, the HVAS coating has finer crystalline structure and only half the amount of porosity in conventional arc spray coating. In this case, the HVAS coating has a higher oxide content, which the authors of the study attribute to refining of the atomizing particles. The exact amounts of oxide can be seen in Table 17 below.

Table 17. *Chemical composition and oxide content of 3Cr13 coatings [38]*

Arc spray gun	Coating materials	Fe	Cr	O	Oxide
HVAS	3Cr13	80.905	13.745	5.341	16.9
AS	3Cr13	81.750	15.061	3.189	10.1

In another study, 4Cr13 was sprayed with HVAS, conventional arc spray gun and a third gun which had a secondary gas atomization nozzle. From table … below can be seen that the 4Cr13 coating sprayed with HVAS (the 2#nozzle in the Table 18) has more oxides and lower amount of pores than the 4Cr13 coating sprayed with conventional arc spray gun (the 1#Nozzle in the Table 18) [33]

Table 18. *Contents of 4Cr13 coatings. Nozzle 1 is a conventional arc spray nozzle, nozzle 2 is a HVAS nozzle and nozzle 3 is a secondary gas atomization nozzle. [33]*

	Porosity (%)	Oxide (%)	Microhardness (%)	Particles Diameters (μm)
4Cr13				
1#Nozzle	1.98	37.94	452.33	39.95
2#Nozzle	1.04	40.98	480.30	39.98
3#Nozzle	1.16	56.76	497.58	31.49

The bond strength in HVAS coatings seems to better than that of coatings made with conventional arc spray. For example, in a study by Wang et al. the average bond strength in 3Cr13 HVAS coating was 60 MPa. In ordinary arc sprayed coatings it was only 20MPa [34]. In a study using TiB_2/Al_2O_3 cored wires, coatings adhered well with the substrate. With HVAS, higher adhesive bond strength (average value up to 49.8 MPa), tighter microstructure and lower porosity than in conventional arc spraying was achieved. [6] In yet another study, the bonding strength of HVAS Al and 3Cr13 coatings are 35.1 and 42.8MPa, 2.12 and 1.52 times that of AS Al and 3Cr13 coatings. The exact values can be seen from the Table 18 below. [38]

Table 19. *Bonding strength of Al and 3Cr13 HVAS coatings [38]*

Arc spray gun	Coating materials	Microhardness (HV)
HVAS	Al	69.7
HVAS	3Cr13	460
AS	Al	55.8
AS	3Cr13	380

The hardness of HVAS coatings seems to be generally higher than that of conventionally sprayed coatings. For example, in a study using TiB_2/Al_2O_3 as the coating material, the Surface Rockwell hardness was higher in HVAS coating, having average value up to 57HR30N. [6] In another study, the average value of the microhardness of HVAS FeCrAl coating is significantly higher than that of AS FeCrAl coating (Fig. 30), while the average profile roughness coefficient value of HVAS FeCrAl coating is lower than that of the AS one. Both coatings have the same composition. [12]

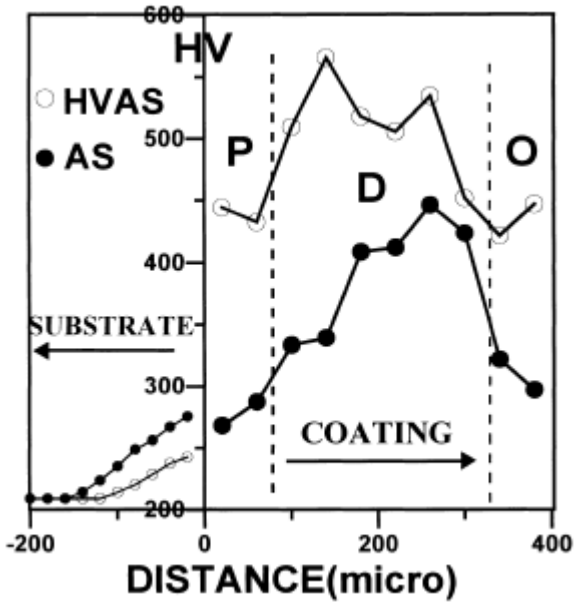

Figure 30. *Vickers microhardnesses (HV) of AS and HVAS FeCrAl coatings and their substrates as a function of distance (mm) from the coating– substrate interfaces. [12]*

In a third study, 3Cr13 HVAS coatings also had higher hardnesses than coatings of the same material sprayed with conventional arc spray gun. The increased hardness also co-incided with the increase of oxides in the coating, shown earlier in Table 17. In Table 20 below, the values of microhardness obtained in the study can be seen. The increase in oxides also resulted in better wear resistance in this study; in the study, the relative wear resistance of HVAS coatings is about twice that of regular arc sprayed coatings. [38]

Table 20. *Microhardness of 3Cr13 HVAS coatings [38]*

Arc spray gun	Coating materials	Microhardness (HV)
HVAS	Al	69.7
HVAS	3Cr13	460
AS	Al	55.8
AS	3Cr13	380

4.14 Comparison of HVAF Arc, HVAS and conventional arc spraying

The main difference between HVAF Arc and conventional electric arc spray gun is the type of gas used – compressed air and propane in HVAF Arc [32] and compressed air only in arc spray gun [36] – and the velocity of the atomizing gas, which is supersonic in HVAF Arc [32] and subsonic in arc spray [34]. In HVAS, too, the atomizing gas has supersonic velocity [34]. The difference between HVAS and HVAF Arc is that the high velocity in HVAS is achieved by using a convergent-divergent nozzle [34] and in HVAF

Arc it seems to be achieved mainly by having higher pressure in the combustion chamber [32].

In the study by Nuzzo, the average Vickers hardness of stainless steel Metcoloy 2 HVAF Arc coatings was 485-494 HV, depending on the spraying distance [18], while in the study by …, the Vickers hardness of stainless steel HVAS 3Cr13 coating was 460 HV [38]. Based on Table 21 below, it can be said that Metcoloy 2 and 3Cr13 have compositions that are quite close to each other, so their Vickers hardness values should be comparable. Their hardness values are relatively close to each other, which indicates that HVAF Arc and HVAS produce quite similar coatings.

Table 21. *Composition of Metcoloy 2 and 3Cr13*

	C	Si	Mn	P	S	Cr	Ni	Fe	
Metcoloy 2	0.35	0.5	0.35	0.02	0.02	13	0.5	Bal.	[26]
3Cr13	0.26-0.35	1	1	0.035	0.03	12.0-14.0	0.6	Bal.	[25]

The microstructure in HVAF Arc coatings is finer and more homogeneous than in arc spray. Their hardness is higher and their porosity lesser. [32] The HVAS coatings, too, have finer microstructure than arc sprayed coatings [11] [34] [38]. However, apart from the hardness results of the two studies mentioned before, the studies about HVAF Arc and HVAS either do not use the same materials, or if they do, the tests themselves are quite different. Therefore, it is difficult to say exactly how similar or dissimilar the coating quality of the two arc guns is. It seems safe to say that HVAF Arc coatings are at least as good as HVAS coatings – after all, both kinds of guns have supersonic atomizing gas velocity, and inclusion of propane in HVAF Arc should not have any negative effects.

The main difference between HVAF Arc and HVAS may be the amount of oxides in the coating: while there was one study [32] where HVAF arc coating had oxide content as high as arc spray coating, there were no studies where it was mentioned that the oxide content was higher. On the other hand, the oxide content in HVAS coatings is thought to be generally higher than in typical arc sprayed coatings [11]. Since the main difference between the guns is that in HVAS, the combustion flame is not used, which purpose in HVAF Arc is to reduce the oxidizing potential of the spraying gas [2], it would make sense that HVAS coatings would be more vulnerable to oxidation.

5. RESEARCH METHODOLOGY AND MATERIALS

In this chapter, the coating materials and coating preparations used in the studies made for this thesis are discussed. The different research methodologies used in the studies are also explained.

5.1 Coating materials

Mild steel Fe37 was selected as the substrate material. The substrates were sandblasted with Al_2O_3 particles which size was 330 microns and grade NKV. The blasting angle was approximately 90 ° degrees and the blasting distance was about 250 mm. Metcoloy 4 and Metco 8625 were selected as the coating materials to be deposited. Metcoloy 4 is an iron-based stainless steel, which is able to resist organic and non-oxidizing organic acids [20]. The latter is similar to Inconel 625, and is henceforth called Inconel 625 in this thesis, since it is presumably the name which is more familiar to the readers. Inconel 625 is a nickel-chromium alloy that has high strength, very good fabricability and outstanding corrosion resistance [24]. The wire diameter used was 1.6 mm. The composition of the wire materials can be seen in Tables 22 and 23, respectively.

Table 22. Nominal chemical composition of Metcoloy 4 wire. [20]

Chemical composition of Metcoloy 4 (wt.%)							
Elements	Cr	Ni	Mo	Mn	Si	C	Fe
Composition	17	12	2.5	2	1	0.08	Bal.

The size of specimens used was for the samples denoted HV1-HV11 and iHV1-iHV6 5×50×330 mm. The samples iHV1-iHV6 were cut in half, so that the size of those specimen that were used in this study was 5×50×170 mm. The rest of the samples were of size 5×50×100 mm, and were sprayed in batches of three so that the three samples were sprayed simultaneously while attached to a holder that kept them at different distances.

Table 23. Nominal chemical composition of Metco 8625 wire. [19]

Chemical composition of Metco 8625 (wt.%)				
Elements	Cr	Mo	Nb+Ta	Ni
Composition	21	9	4	Bal.

5.2 Coating preparations

The spraying parameters that were used in spraying with HVAF Arc can be seen in Tables 24-27. There were also some reference samples deposited by using conventional arc spray unit SmartArc (Oerlikon Metco, Wohlen, Switzerland); the spraying parameters used in making these are listed in Table U, and the samples for which SmartArc was used have either prefix "SA" or "iSA" before the sample number. In all the spraying sessions, step was chosen as 6 mm and gun traverse speed as 500 mm/s. Apart from Metcoloy samples HV1, HV2, and HV3, which we sprayed in six passes, the spraying was conducted in seven passes.

The first three samples that were sprayed used Metcoloy 4 as the coating material. The arc parameters for this session were chosen by adjusting the voltage level until the sound of the arc was stable. The gas parameters were aiming to alter the total gas flow and that way affect the gas flow velocity. Other parameters were kept constant. The parameters used in session one can be seen in Table 24 below.

Table 24. *Spraying parameters used in spraying session 1*

Sample name	**Air**	**Propane**	**total pressure**	**Voltage**	**Wire feed rate**	**Current**	**Spray distance**	**Material**
	(psi)	(psi)	(psi)	(V)	(%)	(I)	(mm)	
HV1	78	72	150	33	54	126	150	Metcoloy 4
HV2	82	76	158	33	54	126	150	Metcoloy 4
HV3	86	80	166	33	54	126	150	Metcoloy 4

During the second spraying session, which was conducted using Inconel 625 as the spraying material, apart from gas pressure, also voltage and wire feed were varied in series of threes. Only one parameter at time was varied, apart from gas parameters, which were both varied simultaneously. One sample (HV7) was also sprayed without propane, using only air as the spraying gas. The gas parameters of sample HV8X did not work; the flame went out after three passes. The parameters used in session two are shown in Table 25 below. It should be noted, though, that wire run out in the middle of spraying sample

HV11. It was sprayed in five passes only, instead of the seven passes which it should have.

Table 25. *Spraying parameters used in spraying session 2*

Sample name	**Air**	**Prop**	**total pressure**	**Voltage**	**Wire feed rate**	**Current**	**Spray distance**	**Material**
	(psi)	(psi)		(V)	(%)	(I)	(mm)	
HV4	80	70	150	33	60	150	150	Inconel 625
HV5	86	76	162	33	60	145	150	Inconel 625
HV6	70	60	130	33	60	150-160	150	Inconel 625
HV7	80	-	80	33	60	170	150	Inconel 625
HV8X	86	80	166	33	60	148-155	150	Inconel 625
HV8	80	70	150	33	54	136-140	150	Inconel 625
HV9	80	70	150	33	70	170-180	150	Inconel 625
HV10	80	70	150	35	54	143-146	150	Inconel 625
HV11	80	70	150	37	54	145-150	150	Inconel 625

In the third spraying session, Inconel 625 was once again used. This time, voltage and distance parameters were varied, one at a time. Two samples, iHV2 and iHV6, were sprayed without the propane, using otherwise same parameters as samples iHV1 and iHV5, respectively. The parameters used in session three are listed in Table 26 below.

Table 26. Spraying parameters used in spraying session 3

Sample name	**Air**	**Prop**	**Total pressure**	**Voltage**	**Wire feed rate**	**Current**	**Spray distance**	**material**
	(psi)	(psi)		(V)	(%)	(I)	(mm)	Inconel 625
iHV1	80	70	150	32	54	150	160	Inconel 625

iHV2	80	-	80	32	54	160-170	160	Inconel 625
iHV3	80	70	150	36	54	130-140	160	Inconel 625
iHV4	80	70	150	36	60	150-170	160	Inconel 625
iHV5	80	70	150	36	60	150-160	120	Inconel 625
iHV6	80	-	80	36	60	160-200	120	Inconel 625

In the final session, both Inconel 625 and Metcoloy 4 were used as wire materials. The parameters of spray session four are in Table 27.

Table 27. *Spraying parameters used spraying session 4*

Sample name	**Air**	**Prop**	**total pressure**	**Voltage**	**Wire feed rate**	**Current**	**Spray distance**	**material**
	(psi)	(psi)		(V)	(%)	(I)	(mm)	
iHV7	80	70	150	36	60	187-195	150	Inconel 625
iHV8	80	70	150	36	60	187-195	175	Inconel 625
iHV9	80	70	150	36	60	187-195	200	Inconel 625
iSA1	40.6	-	40.6	35-36	-	200	150	Inconel 625
iSA2	40.6	-	40.6	35-37	-	200	175	Inconel 625
iSA3	40.6	-	40.6	35-38	-	200	200	Inconel 625
Hv12	80	70	150	33	60	135-143	150	Metcoloy 4
HV13	80	70	150	33	60	135-144	175	Metcoloy 4
HV14	80	70	150	33	60	135-145	200	Metcoloy 4
SA1	40.6	-	40.6	34	-	198-206	150	Metcoloy 4

SA2	40.6	-	40.6	34	-	198-207	175	Metcoloy 4
SA3	40.6	-	40.6	34	-	198-208	200	Metcoloy 4

5.3 In-flight parameters

The velocity and temperature of the particles produced by HVAF Arc were measured in-flight using SprayWatch 4i (Oseir Ltd, Tampere, Finland). SprayWatch uses a fast shutter CCD camera to create digital images of the spray. An algorithm identifies individual particles in the images taken with short exposure time and measures their position, direction and velocity. The camera also takes simultaneously another image using a longer exposure time to measure the average particle temperature in the spray. Particle velocity is measured by time-of-flight method; the image processing algorithm measures the length of the particle traces on the CCD detector and is converted to velocity by dividing by the known camera shutter time. Temperature of the particles is measured by using two-color pyrometry; the spray is imaged on the CCD in two different wavelengths so that it is possible to calculate the lateral distribution of the average particle temperature in the spray using calibration information. [21] Below in Table 28 the parameters used in the monitoring system can be seen.

Table 28. *The SprayWatch4i settings*

Spray Watch 4i				
Focus distance	250 mm		Streak length min	15
Aperture	4		Streak length max	600
Pexp	5			
Texp	800 (1-7)	150 (8)		

In Table 28, it should be noted that 800 was used as the exposure time (T exp) in measuring all except the last measuring session, in which the exposure time 150 was used. Below in Table 29 the parameters used in spraying during the in-flight analysis of particles can be seen.

Table 29. *The spraying parameters used during in-flight analysis of particles*

	Air	Prop	Total pressure	Voltage	Wire feed rate	Current
	(psi)	(psi)	(psi)	(V)	(%)	(I)
1	80	70	150	32	70	170

2	82	69	151	32	70	170
3	80	70	150	32	60	145
4	86	76	162	33	60	145
5	70	60	130	33	60	145
6	70	60	130	37	60	150
7	70	60	130	31	60	140
8	80	-	80	33	60	170

5.4 Optical microscope images and SEM images

From each specimen, one cross-section sample was made. First a small piece was cut from the specimen by using Struers Discotom-10 cutter. Struers 56A25 was selected as the cutting disc. The small pieces were hot mounted into PolyFast resin with Struers Citopress-10 machine. PolyFast is conductive, so samples mounted in it can be examined at SEM. The samples were ground with the parameters listed in Table 30. Between each step mentioned in the Table 30, the samples were washed with water and ethanol. When the polishing cloths were used, the samples were washed with a detergent, as well, before using water and ethanol. Semi-automatic sample preparation machine Struers Tegramin-30 was used in grinding and polishing the samples. A sample holder was used in the grinding and polishing processes. With the polishing cloths, about ten drops of the lubricant was added at the beginning of the polishing process and then at one minute intervals. Lastly, the samples were washed in the ultrasound washer for three minutes.

Table 30. *The parameters used in polishing the cross-sectional samples*

Surface	Suspension	Lubricant	Load (N) per sample	Time (min)
SiC 200		water	30	1
SiC 500		water	30	1
SiC 1200		water	30	1
MD-Dac	Dac 3µm		30	3
MD-Nap	Nap-B 1µm		30	3
MD Nap-R	Nap-R ¼ µm		15	1

Optical microscope Leica DM 2500M and the computer program accompanying it, Leica Application Suite, were used to obtain images of the cross-sections of the samples with magnifications of 10, 20, and 50, respectively. The images with the magnification 10 were used in calculating the thickness of the coatings; using computer program ImageJ, the thickness was measured from each sample at six different locations in the image, chosen so that the cursor was at x=1,0; …;6,0. Using magnification 50, at least two images were

taken of each sample. These images were used to analyze with ImageJ the amount of oxides, pores, and pure metal in the coatings. In some images there were some smudges, but these were discounted from the analysis.

The cross-sections of samples were used in measuring microhardnesses of the samples. A load of 300 g was used in the measurements. For each sample, ten measurements were made. For two samples, a load of 1 kg was used to study the fracture behavior and whether there is any difference whether between samples made with or without propane. The measurements were carried out with Matsuzawa MMT-X7, and the hardness it measures is Vickers hardness.

For certain samples, also SEM images were taken for porosity analysis. The SEM used was Scanning Electron Microscope Philips XL-30. For the porosity analysis, five images with magnification of 500 were taken. Also, at least three energy dispersive spectra (EDS) were taken per sample: one with magnification 200, to represent the whole area, and two others with magnification of 1000, to represent metal and oxide spots, respectively. From some samples, more than one oxide EDS spectrum was taken, because in these samples there could be seen occasional oxide spots which looked different from most of the oxide spots in the sample.

5.5 Surface roughness tests

Surface roughness tests were made on the specimens with Mitutoyo Surftest SJ-301 using standard SFS-EN ISO 4287. The parameters used are displayed in Table 31.

Table 31. *Surface roughness test parameters*

Surface roughness test parameters	
λc	2.5 mm
N	5
standard	ISO '97
speed	0.5mm/s

In the surface roughness tests, arithmetical mean deviation of the assessed profile (Ra) and maximum height of profile (Rz) were measured.

5.6 Corrosion test

Pieces of approximately of dimensions of 40×50×5 were cut off from the specimens. A plastic tube was glued to each piece by using epoxy resin, making it water-tight. The tubes were filled about halfway with salt content of 3.5 wt.% NaCl. The open circuit potential (OCP) of each coated sample surface, exposed to the corrosive media, was measured relative to an Ag/AgCl-reference electrode. The OCP of a coating keeps changing as the

corrosive media is penetrating the coating material. The test was carried on for ten days, during which the OCP of each sample was measured once every hour for first six hours of the experiment, twice a day during the second and third days of the experiment, and once a day for the rest of the duration of the test. A few samples had to be eliminated from the experiment, since they started leaking so much.

5.7 Erosion test

For erosion test, three pairs of specimens were selected so that of each pair, one had been deposited with and the other without the propane flame of HVAF Arc. Samples of size 15× 25× 5 were prepared from the specimens and ground with grit paper which roughness was 200, 500, and 1200, respectively, until the surface of each sample was smooth and there were no visible oxides to be seen on it. Samples were weighted before and after the tests.

The selected test equipment was an erosion tester which uses centrifugal force as accelerator at room temperature [27]. There is an image of the equipment in question in Figure 31. The chosen angle was 30° degrees, the velocity was 3003-3004 RPM, and amount of quarzt used per run was 3 kg. As abrasive, quarzt from a Finnish supplier was selected (NFQ quarzt, Sibelco Nordic Oy Ab, Nilsiä, Finland). The particle size of the quarzt was 0,1 - 0,6 mm.

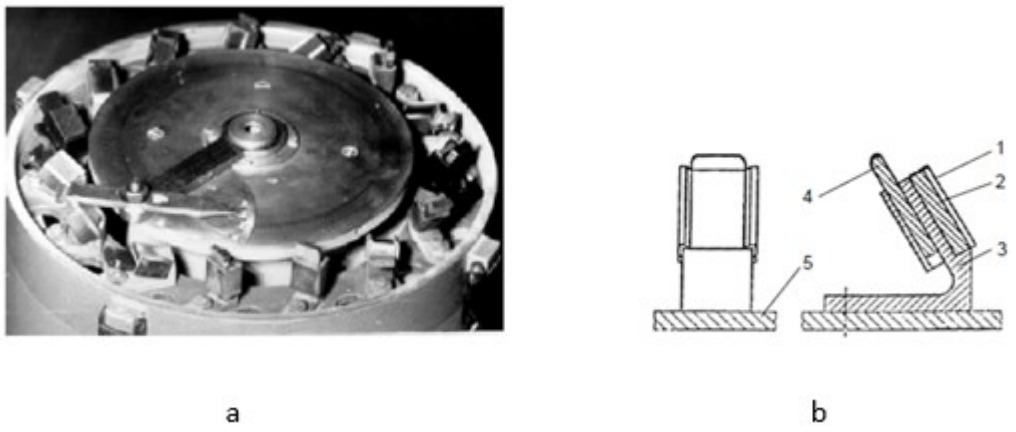

Figure 31.*a) An image of the erosion test equipment, b) overall view of the fixation of the specimen. 1 – clamp, 2 – specimen, 3 – specimen holder, 4 – wedge, 5 – bottom ring. [8]*

6. RESULTS

In this chapter, the results of the studies conducted for this thesis are explained. The functioning of the spraying equipment is also discussed briefly. Especially the results from varying spray parameters are explained in detail.

6.1 Functioning of the spraying equipment

At first it was planned that the ratio of propane to air would be varied during the spray sessions. It became clear, however, that if the ratio of the gases was changed greatly from 7:8, the flame would go out. For that matter, if the gas parameters were changed too much from 70 psi (propane pressure) and 80 psi (air pressure), the same occurred. So about 80 psi of air and 70 psi of propane seems to work best, regardless of the coating material.

It was also not possible to adjust voltage very much, or the spray jet cut out. The best voltage for spraying Inconel seemed to be around 36 V, while for Metcoloy, 33 V was quite enough. It was also noted that if the wire feed rate is high, the voltage needs to be relatively high, and vice versa. Since the wire feed rate affects the current, this makes sense. Wire feed rate of 70 % is too high to be of much use, since it results in a coating so thick it starts to flake off the edges. Feed rate of 52-60 % seems to work best, for both Metcoloy 4 and Inconel 625. All in all, it seems that the range of parameters that can be used in HVAF Arc is quite limited. The spray jet stays stable when the machine keeps making a high "keening" noise; if the noise gets down, the flame is going to go out. If the user of the device wishes to adjust the gas parameters, it can be done just based on what the machine sounds like.

During spraying session three, the wires got frequently stuck, usually one at a time. In the previous spraying session there were not as many problems with that, though the wires got stuck once or twice. The material used in both sessions was Inconel, though since the wire run out during session two, new wires were used for session three. Both the anode and the cathode wire would get stuck; there was not any difference noted between them in this behavior. The reason for the sticking was poor clamping of the wires; the machine has only one Wire Drive Roller per wire [30], which cannot be adjusted much. This causes problems with a softer material like Inconel, since the clamping is not tight enough to keep it from spinning. In the final spraying session, when Inconel was used, it took three tries before the machine would start spraying without the wires getting stuck. When Metcoloy was used, there were no problems with the wires, though since only six Metcoloy coatings were sprayed, and of the six, three were sprayed simultaneously, it cannot be said for sure that they do not have same kind of tendency of getting stuck as the Inconel wires.

6.2 SprayWatch results

The results of the measurements made with SprayWatch 4i are listed below in Table 32. Basically, only by changing total gas pressure could the particle flux be changed in any meaningful way. The velocity and temperature stayed the same regardless of which gas pressure, voltage, or wire feed rate was used, apart from the one time when the combustion flame was not used at all. This caused the temperature of the particles to rise quite a bit, but affected the velocity and flux relatively little.

Table 32. *Results for the in-flight analysis of particle temperatures and velocities*

T (°C)	T std (°C)	v (m/s)	v std (m/s)	Flux	flux std
2110	110	81	2	386	156
2100	128	81	1	427	177
2110	106	81	2	349	154
2120	98	81	1	341	122
2150	135	80	2	367	181
2130	109	80	2	319	137
2120	164	80	2	285	173
3000	175	72	6	306	91

The velocities obtained with SprayWatch are significantly lower than the ones mentioned in the Table 4 from a study in which AAS gun was used. Even though the spraying parameters are not the same in this study as in the study from which Table 3 is [2], it does not seem likely that they alone could cause a discrepancy this great; the velocity of the particles when combustion flame was not used in this study is significantly higher than in the velocities from typical arc spraying machines in Table 3. SprayWatch can measure particles that are bigger than 10 microns. In Table 4, it seems that very few particles are smaller than that in the spray jet of HVAF Arc, so SprayWatch should be able to measure the vast majority of the particles in the jet. Perhaps the differences in the measured velocities are simply caused by having a different measuring equipment. Also, the camera distance was relatively long in the particle velocity measurement made for this thesis, which causes relatively short particle traces. This means that the differences in parameters cannot be captured, due to limited resolution of SprayWatch.

6.3 Micrographs

Below in Figure 32 can be seen an image of a Metcoloy HVAF Arc coating, which is a quite typical result found in this study. An optical image taken with magnification 10 of the every sample can be seen in appendix A. The darker oxide columns or ridges in the image can be seen in all of the Metcoloy coatings made with HVAF arc, though usually

they are not quite as prominent. They are present in some of the Inconel coatings, too. However, they cannot be found either in the SmartArc coatings of either material, or in the coatings made with HVAF Arc without using the combustion flame. Therefore, it seems that the oxide columns are a by-product of the high velocity of the spray jet in HVAF Arc.

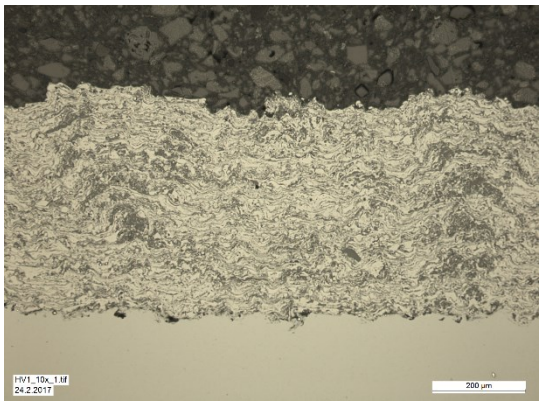

Figure 32. *Image of cross-section of Metcoloy 4 sample HV1*

Below in Figure 33 are images of samples HV2 and HV3. If compared with the image above, which is of HV1, it can be seen that HV3 especially is thinner, denser, and has less clear oxide ridges. HV1 has been sprayed with higher total pressure than HV2 and HV3, otherwise their spraying parameters are identical. It would seem that in Metcoloy samples, increasing pressure causes a kind of densification of the coating.

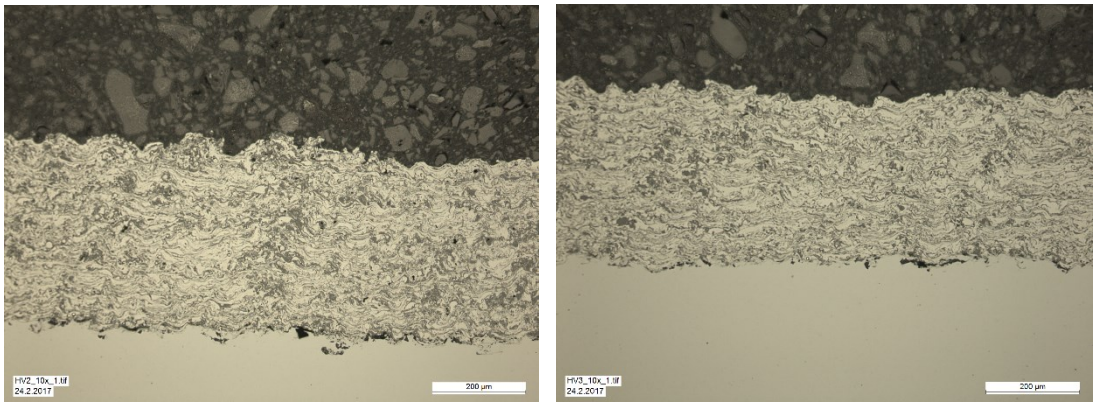

Figure 33. *Images of Metcoloy 4 cross-sections of samples HV2 (on the left) and HV3 (on the right)*

Below images of two Inconel samples can be seen (Fig. 34). If compared to Metcoloy samples above, they look less oxidized, less dark, but have similar dense and tight looking structures. This is typical to the Inconel samples. HV6 has those same kind of more oxidized columns as Metcoloy samples generally have. These samples too, were sprayed with different total pressures, but otherwise same parameters, HV6 with lower total pressure than HV5. The same kind of densification, however, cannot be seen in these Inconel

samples as in the previous Metcoloy samples; these Inconel samples have approximately the same thickness, and their structure looks very similar to each other.

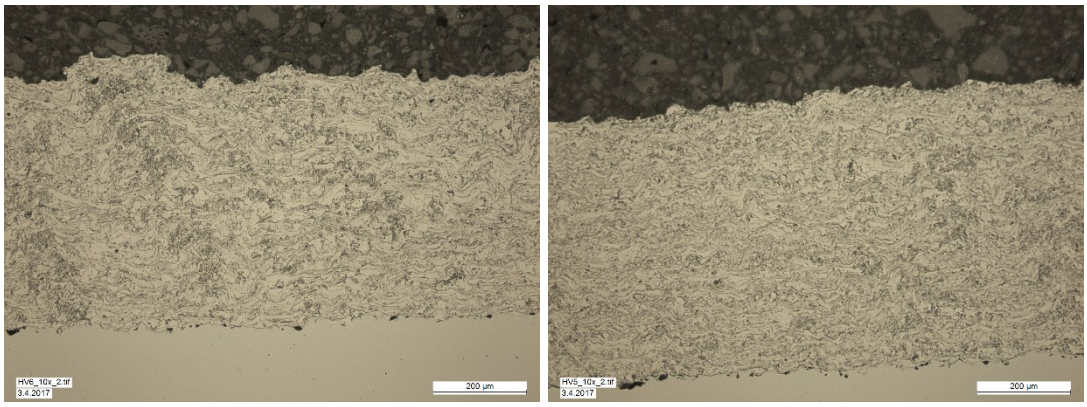

Figure 34. *Cross-sectional images of Inconel 625 samples HV6 (on the left) and HV5 (on the right)*

Below in Figure 35 can be found an example of what Metcoloy and Inconel microstructures look like, respectively. An optical images with magnification 50 of every sample can be seen in Appendix B. The image is from sample HV3 (left) and HV5 (right). In Metcoloy, the oxides form larger areas, while in Inconel, the oxides are more dispersed and smaller altogether.

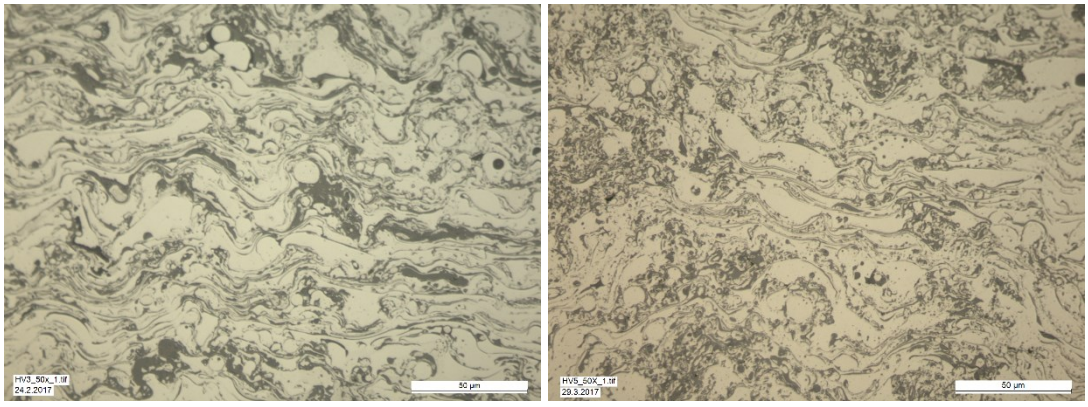

Figure 35. *Image of microstructure of Metcoloy 4 sample HV3 (on the left) and Inconel 625 sample HV5 (on the right)*

If HVAF Arc is used without the combustion flame, like a conventional arc spraying device, the resulting coating looks strikingly different from the coatings that were produced using propane. In Figure 36 below two images of an Inconel sample that was sprayed without the combustion flame can be seen. The structure is clearly less dense and has more pores than either the Inconel or Metcoloy samples discussed previously. Its oxides are also less dispersed than in Inconel samples mentioned previously.

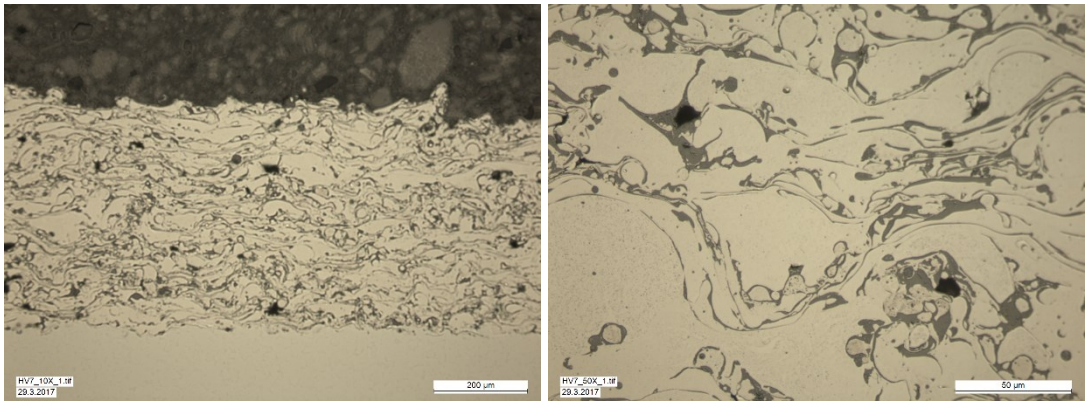

Figure 36. *Inconel sample HV7, sprayed without propane. On the left, magnification is 10, while on the right, magnification is 50.*

Two of the Inconel samples were tested with Vickers hardness load of 1 kg to see whether the two samples break differently. Of the samples, HV4 was sprayed with the combustion flame, the HV7 without. An image of the indentation and breaks it causes are presented in Figure 37. The cracks at the edges of the indentation in HV7 look somewhat worse than the breaks at the edges of HV4.

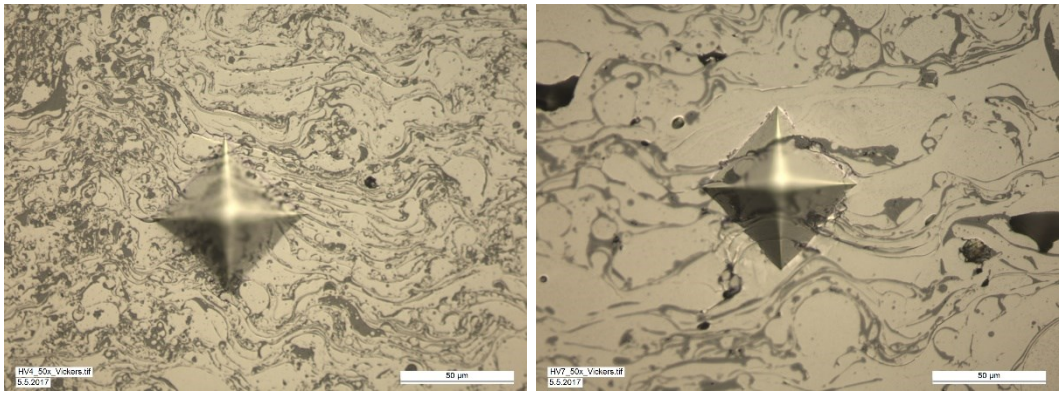

Figure 37. *Image of the cross-section of Inconel 625 sample HV8*

Below in Figure 38 are images of two Metcoloy samples, of which the one on the left was sprayed with HVAF Arc using the combustion flame, the one on the right with SmartArc. SmartArc coatings looks somewhat similar to HVAF Arc coatings that were sprayed without the combustion flame. When the two images below are compared, it can also be noted that while the HVAF Arc image seems to contain only one kind of oxide, and that dark grey, the SmartArc coating seems to have two kinds of oxidized areas: dark areas similar to those in the HVAF Arc coating, and lighter grey areas which probably actually comprise of lots and lots of tiny individual oxide spots.

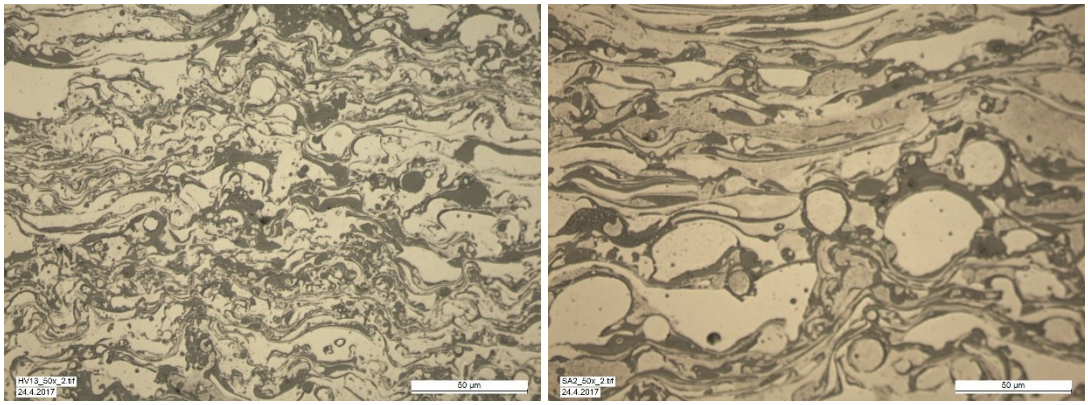

Figure 38. *Microstructures of Metcoloy 4 samples HV13(on the left) and SA2 (on the right).*

In Inconel samples made with SmartArc, there is similar difference to be seen in the tightness of the coating structure (Fig. 39) as in the Metcoloy image above. However, in the Inconel sample made with SmartArc (the image below right), there are not those light grey areas composed of tiny dots that can be seen in the Smartarc Metcoloy coating.

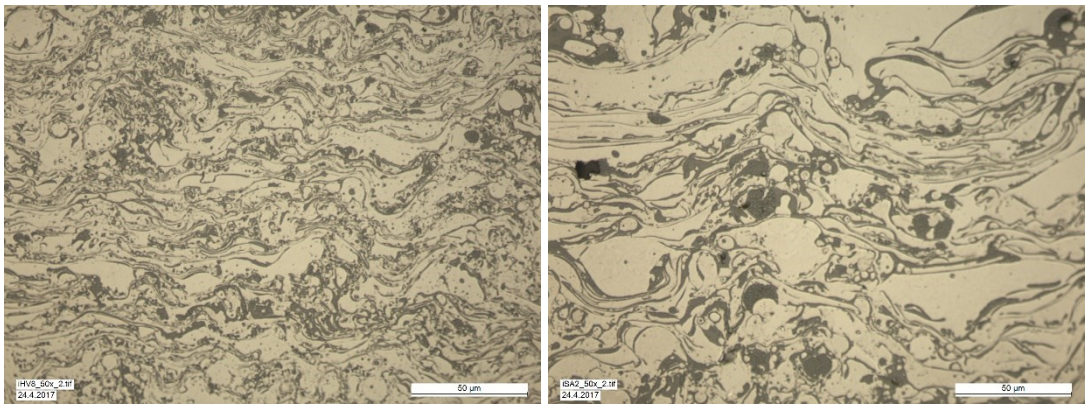

Figure 39. *Microstructures of Inconel 625 samples iHV8(on the left) and iSA2 (on the right)*

From the SEM images it was found out that there were some black areas in the images from the interfaces of the coatings. The dark areas are probably alumina residues from the grit blasting of the substrates. All the images taken from the interfaces more or less like the image in Figure 40 below.

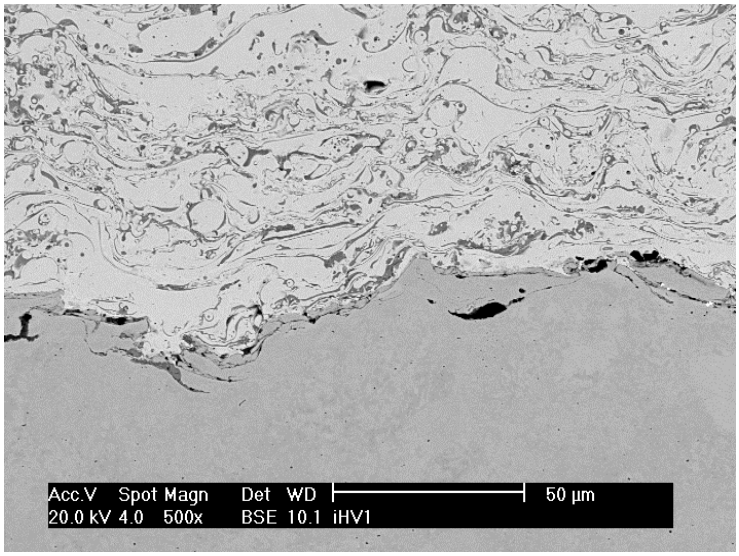

Figure 40. *SEM image of interface of Inconel 625 sample iHV1*

6.4 Compositions of wires and comparison of image analysis results

Below are the EDS quantitative analyses' results from the wires that were used. The Metcoloy wire from the first spraying session could not be obtained. The sessions mentioned in the Table 33 refer to spraying session mentioned in Experimental part of this thesis. Inconel wire that was used in third session has somewhat more iron and lesser amounts of chromium and niobium than the other Inconel wires, but apart from that, the amounts of different elements are quite similar to each other in the Inconel wires. The amounts listed in Table 33 below match relatively well the compositions in Tables 22 and 23 where the data from a supplier of wires is shown. The aluminum in the coatings is not present in the compositions given by the supplier.

Table 33. *Compositions of the wires used in spraying based on EDS analysis*

(wt.(%))		Al	Nb	Si	Mo	Cr	Fe	Ni
session 2	Inconel	0.54	3.63	0	9.75	19.28	0.64	66.16
session 2	Inconel	0.43	3.39	0	8.63	19.31	0.63	67.62
session 3	Inconel	0.6	2.72	0	9.15	15.89	2.27	69.37
session 4	Inconel	0.29	3.53	0	9.31	18.59	0.21	68.07
session 4	Metcoloy	0	0	0.85	3.79	18.67	63.68	13

Below in Figures 41 and 42, the results of image analyses both from optical and SEM images can be seen. While the amounts of oxides, pores, and metal are not identical – typically, the amounts of oxide obtained from optical microscope images are greater -

they show similar trends. This can be seen especially when it comes to pores; if the sample contains lots of pores, it is seen in both results.

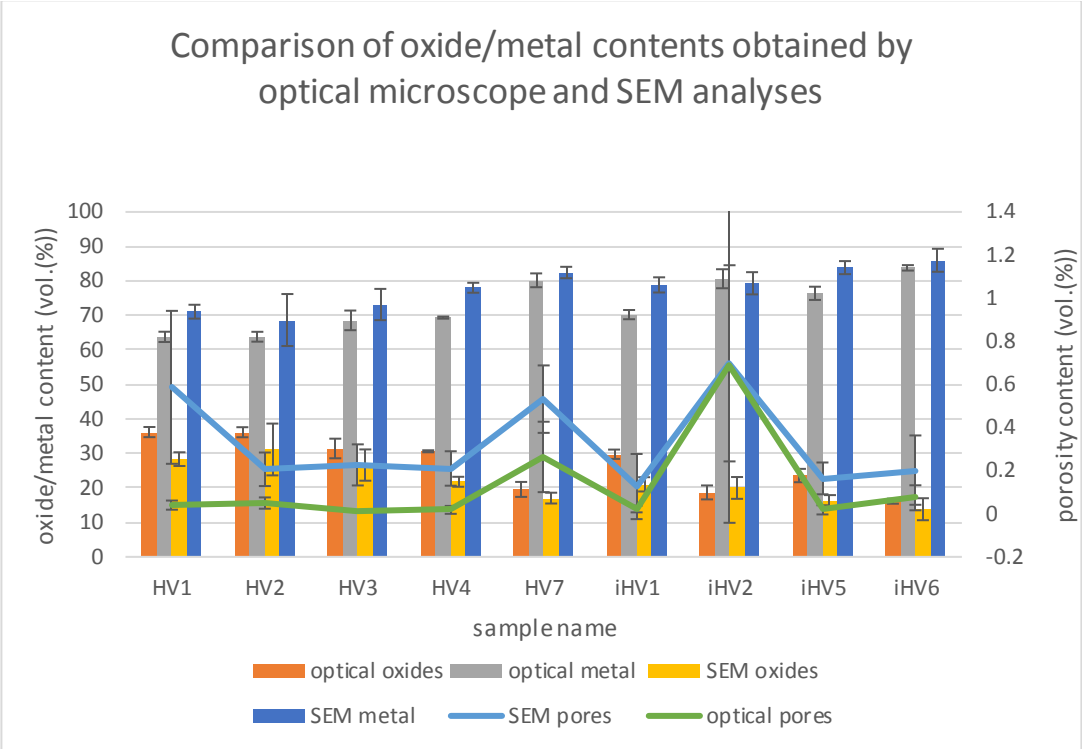

Figure 41. *Comparison of the mean amounts of oxides, pores, and metal from optical microscope image and SEM image analyses*

In Figure 42 below, the results from optical images are compared with maximum amounts of pores and oxides (and least amounts of metal) obtained from the SEM images. These sets of results are not identical, either. They seem to differ from each other about as much as the results in Figure 40 above, with the exception that in Figure 42 below, some of the SEM results are greater than the results from the optical images.

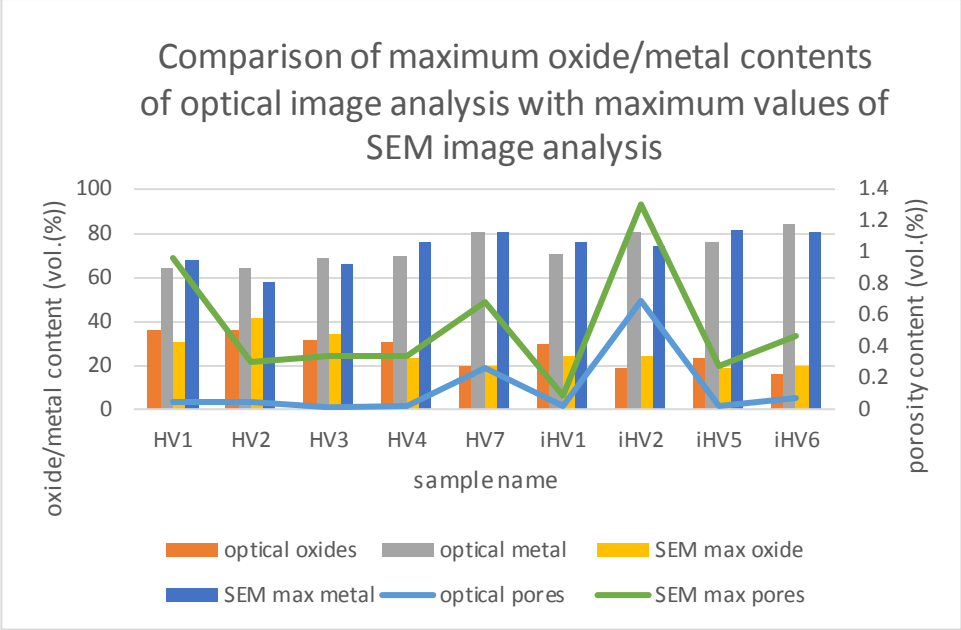

Figure 42. *Comparison of mean amounts of oxides, pores, and metal from optical microscope image analysis and maximum amounts of oxides and pores and minimum amount of metal from SEM image analysis*

From Figures 41 and 42 can be seen that the analysis results from optical and SEM images of Metcoloy samples (samples HV1, HV2, and HV3) differ from each other somewhat. In the case of HV2 and HV3, the mean values for oxide content from the optical images are under the highest value from the SEM images, while for HV1, the results from optical images are much greater than even the maximum values from SEM images. It's hard to say where this discrepancy comes from – it may simply be that coincidentally, more heavily oxidized images where chosen for optical image analysis than for the SEM analysis in the case of sample HV2. The SEM images have better contrast, and have been taken with higher magnification, so the results from the SEM images are the more reliable ones, especially when it comes to pores. On the other hand, while the exact values for the contents obtained from optical images should be regarded as unreliable, they can be used in comparing the samples, since they show similar trends as the values obtained from the SEM images.

When it comes to the results from Inconel images, the results of analyses made from samples sprayed without propane (HV7, iHV2, and iHV6) match quite well, at least when it comes to the amount of oxides and metal. In their optical and SEM images, the oxides form wider and clearer areas, whereas in the images taken from samples sprayed with propane, the oxides are much more dispersed, making image analysis more difficult, especially when it comes to optical images. In the Inconel samples that were sprayed by using propane, the results differ about as much from each other as in the three Metcoloy samples.

In Table 34 below, the results from EDS analysis of the Metcoloy samples are shown. From the full area analyses of the samples can be seen that the amount of oxygen rises in the coatings from sample HV1 to sample HV3. The oxides in the coatings are typically mainly chromium oxide, since the amount of chromium is usually greater in the oxides than in the full area analysis results.

Table 34. *Compositions from EDS analyses of samples HV1-HV3. The oxides A and B of sample HV2 refer to an image that is presented later.*

sample	element	O	Al	Si	Nb	Mo	Cr	Fe	Ni
HV1	full area	-	-	0.62	-	3.11	19.27	63.84	13.16
	oxide	14.38	-	0.19	-	2.32	21.96	56.98	4.18
	metal	-	-	0.4	-	3.46	16.84	65.81	13.48
HV2	full area	5.15	0.54	0.56	-	3.19	17.82	60.47	12.27
	oxide A	21.12	-	3.03	7.37	1.38	44.88	20.98	1.24
	oxide B	15.17	-	0.85	-	3.08	19.44	55.12	7.64
	metal			0.43		2.75	17.73	66.14	12.96
HV3	full area	5.91	-	0.46	-	3.09	17.88	60.06	12.6
	oxide	14.68	-	0.45	-	2.37	18.85	57.73	5.92
	metal	2.13	-	0.52	-	3.19	17.65	63.28	13.05

In the Figure 43 below the oxides A and B mentioned in Table 34 for sample HV2 are shown and explained. EDS analysis indicates that oxide is mainly chromium oxide in both oxides A and B. There is also some niobium oxide in oxide A that is not present in oxide B.

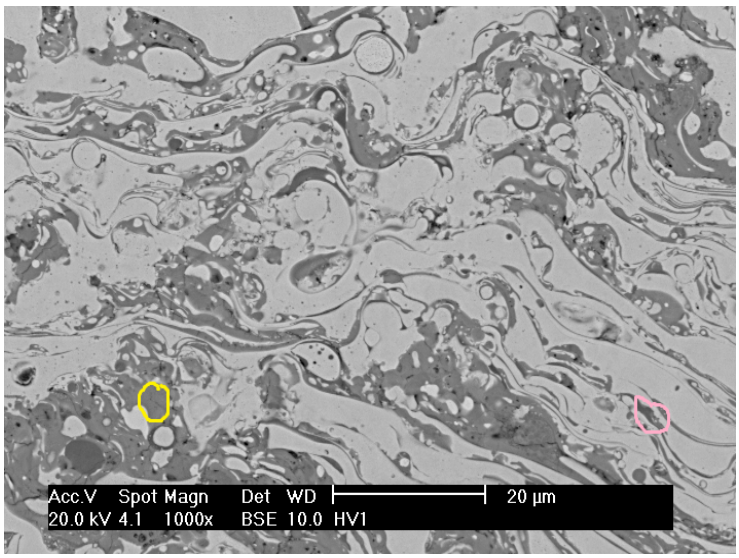

Figure 43. *A SEM image of sample HV2. The oxide circled in pink is oxide A, and the oxide circled in yellow is oxide B in Table 31*

In Table 35 below, the EDS analysis results for the Inconel samples can be seen. In these samples, too, the oxides are typically chromium oxide. The different oxides mentioned in the Table 35 are explained in images below the Table 35. It should be noted that for example oxide A of HV4 and iHV5 are not necessarily of the same material; the oxides are named A, B, etc. based strictly on the order they appear in the Table 35.

Table 35. *Compositions from EDS analyses of samples HV4, HV7, iHV1, iHV2, iHV5, and iHV6. The oxides A and B of the samples refer to images that are presented later.*

sample	ele-ment	O	Al	Si	Nb	Mo	Cr	Fe	Ni	Mg	Ti
HV4	oxide A	7.27	1.44	-	15.96	6.11	40.18	0.44	28.6	-	-
	oxide B	18.82	0.28	-	9.08	17.45	37.68	1.35	15.35	-	-
	metal	-	-	-	3.4	10.69	18.4	0.6	66.9	-	-
HV7	full area	4.72	0.51	-	4.65	10.22	19.62	0.85	59.43	-	-
	oxide A	17.1	3.62	-	28.54	2.11	43.98		4.64	-	-
	oxide B	20.48	0.43	-	10.53	14.28	26.68	2.39	25.21	-	-
	oxide C	18.94	22.71	-	14.08	-	37.09	-	3.61	0.73	2.85
	metal		-	-	3.27	11.09	18.8	0.87	65.97	-	-
iHV1	full area	4.58	-	-	3.8	8.96	19.04	1.87	61.75	-	-
	oxide	16.45	-	-	5.29	11.33	36.88	2.49	27.56	-	-
	metal	-	-	-	2.66	9.56	18.52	1.91	67.36	-	-
iHV2	full area	4.53	-	-	3.98	8.89	19.44	1.72	61.45	-	-
	oxide A	21.43	21.09	-	14.66	1.6	3.89	32.36	4.98	-	-
	oxide B	15.41	1.66	-	16.67	4.16	46.36	0.92	14.83	-	-
	metal	-	-	-	3.19	9.97	18.72	1.86	66.27	-	-
iHV5	full area	4.06	-	-	3.49	9.07	19.34	1.95	62.09	-	-
	oxide A	1.52	-	-	-	1.84	3.42	0.75	92.47	-	-
	oxide B	18.54	-	-	7.81	15.2	37.02	2.35	19.08	-	-

	metal	2.22	-	-	2.5	9.84	17.59	1.63	66.22	-	-
iHV6	full area	4.39	0.63	-	3.96	9.2	19.78	1.8	60.24	-	-
	oxide	16.09	0.6	-	10.23	14.4	42.5	1.93	14.26	-	-
	inclu-sion	2.24	0.32	-	2.56	10.92	15.14	1.75	67.07	-	-
	metal	2.18	0.42	-	3.68	9.55	19.17	1.66	63.34	-	-

In Figure 44 below the oxide circled in pink is referred in the Table 35 as HV4 oxide A, and the oxide circled in yellow is referred in the Table 35 as HV4 oxide B. Based on their compositions, they are both mostly chromium oxide, though both contain also niobium oxide and aluminum, oxide A more than oxide B.

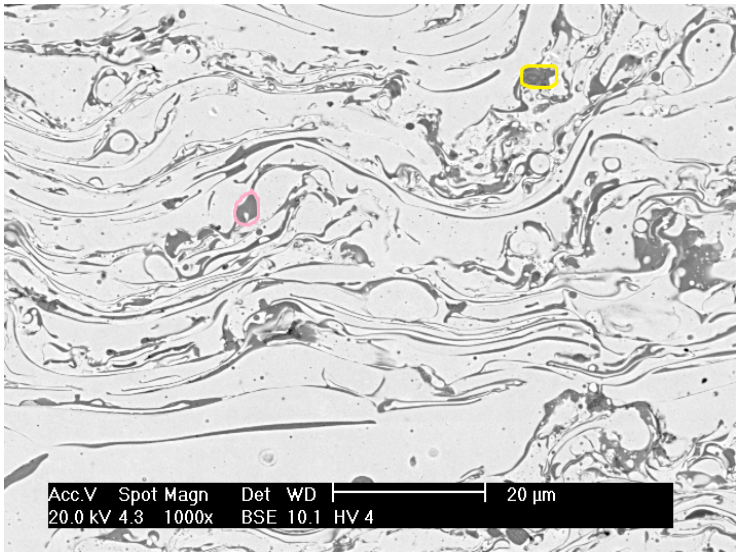

Figure 44. *A SEM image of sample HV4. The oxide circled in pink is referred in the Table 32 as HV4 oxide A, and the oxide circled in yellow is referred in the Table 32 as HV4 oxide B*

In Figure 45 below the oxide circled in pink is referred in the Table 35 as HV7 oxide A, and the oxide circled in yellow is referred in the Table 32 as HV7 oxide B. Oxide A contains more niobium and chromium than oxide B, which contains more nickel than oxide A. It seems oxide B contains less of chromium and niobium oxide and more nickel than oxide A.

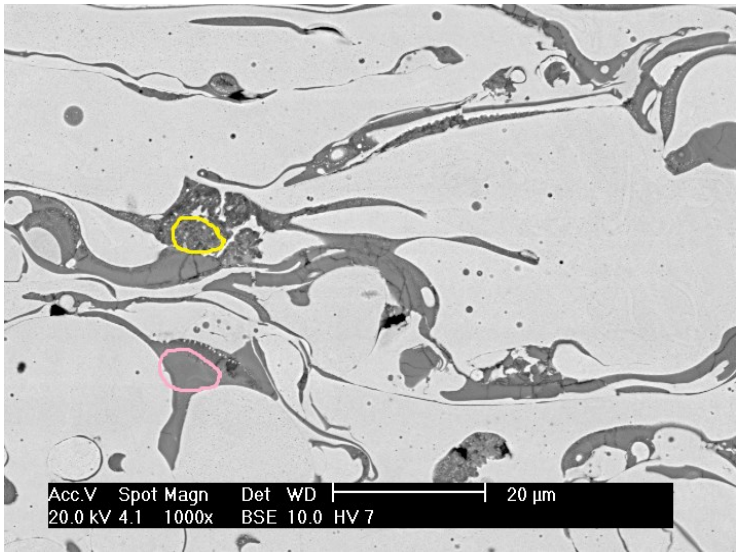

Figure 45. *A SEM image of sample HV7. The oxide circled in pink is referred in the Table 32 as HV7 oxide A, and the oxide circled in yellow is referred in the Table 32 as HV7 oxide B*

In Figure 46 below the oxide circled in pink is referred in the Table 35 as HV7 oxide C. From the Table 35 it can be seen that oxide C contains quite a bit of aluminum, which probably explains the color. It also contains minute amounts of magnesium and titanium, which cannot be found in any of the other samples, or in the other oxides, metal, or full area analysis of sample HV7, either. Neither of those elements should be in Inconel based on the data from the supplier. In the images of the sample, oxide C is much rarer in HV7 than either oxide A or oxide B.

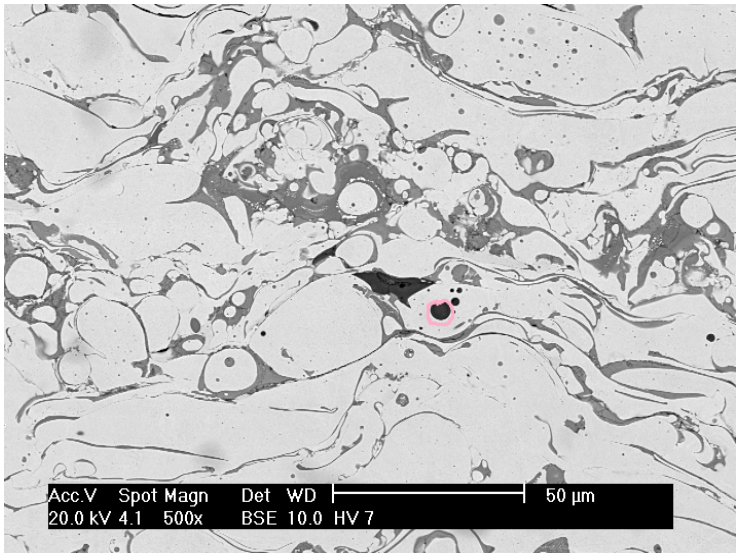

Figure 46. *A SEM image of sample HV7. The oxide circled in pink is referred in the Table 32 as HV7 oxide C.*

In Figure 47 below the oxide circled in pink is referred in the Table 32 as iHV2 oxide A, and the oxide circled in yellow is referred in the Table 32 as iHV2 oxide B. Oxide A is

much rarer than oxide B in iHV2. Oxide A contains more aluminum and iron than oxide B, which contains more chromium. It seems that oxide A is mostly aluminum oxide while oxide B is mostly chromium oxide.

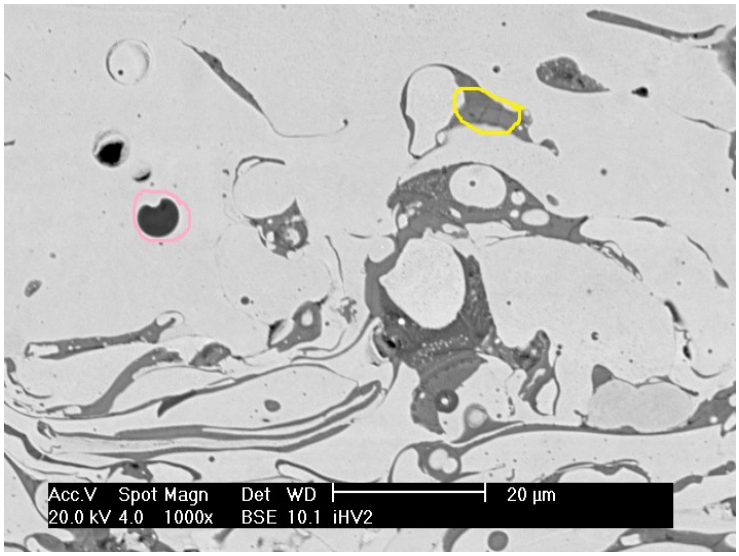

Figure 47. *A SEM image of sample iHV2. The oxide circled in pink is referred in the Table 32 as iHV2 oxide A, and the oxide circled in yellow is referred in the Table 32 as iHV2 oxide B.*

In Figure 48 below the oxide circled in pink is referred in the Table 35 as iHV5 oxide A, and the oxide circled in yellow is referred in the Table 35 as iHV5 oxide B. Oxide A contains more nickel and less oxide and chromium than B. Oxide A likely isn't oxide at all, but pure nickel, and oxide B consists mostly of chromium oxide.

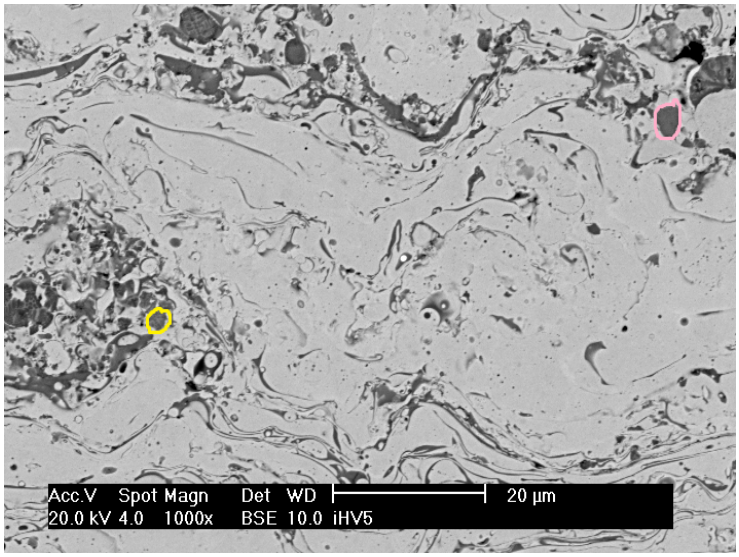

Figure 48. *A SEM images of sample HV5. The oxide circled in pink is referred in the Table 32 as iHV5 oxide A, and the oxide circled in yellow is referred in the Table 32 as iHV5 oxide B.*

In Figure 49 below the oxide circled in pink is referred in the Table 35 as iHV6 oxide, and the small round dark thing circled in yellow is referred in the Table 35 as iHV5 inclusion. The inclusion is mainly nickel.

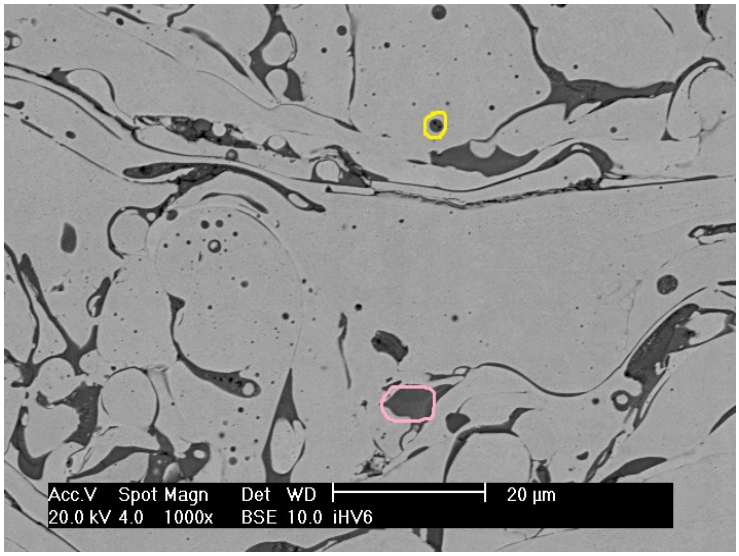

Figure 49. A SEM image of sample iHV6. *The oxide circled in pink is referred in the Table 32 as iHV6 oxide, and the small round dark thing circled in yellow is referred in the Table 32 as iHV6 inclusion*

6.5 Effect of gas pressure

In Figure 50 below, the effect of total gas pressure on the oxide and metal contents on three Metcoloy samples can be seen. Total pressure is the sum of air and propane pressure used during the spraying of the coating. In the three samples the amount of oxides in the coating goes slightly down as the pressure increases. The first two samples have almost the same amount of oxides, though.

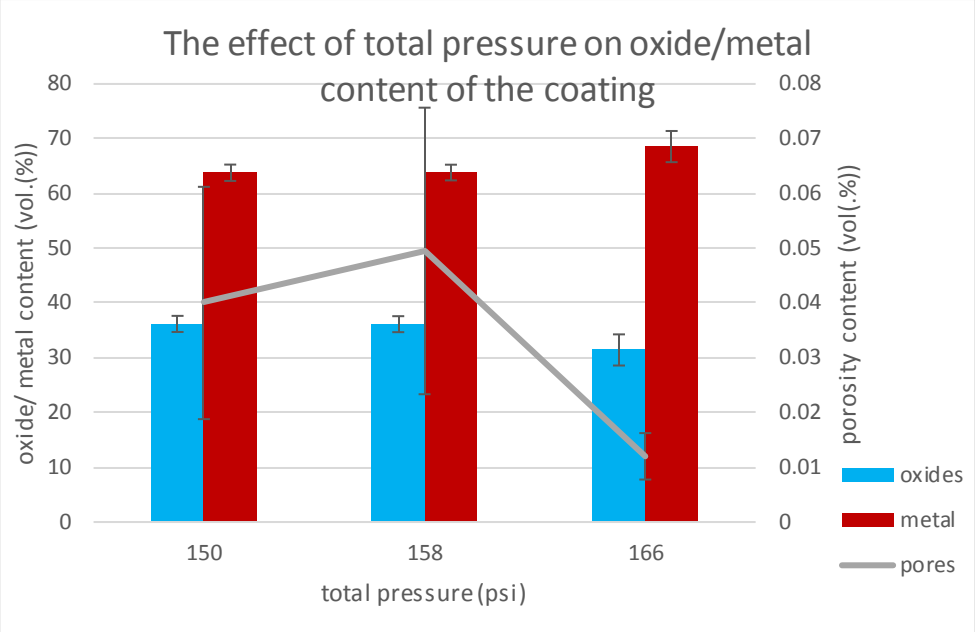

Figure 50. *The effect of pressure on coating composition of Metcoloy 4 samples. The spraying parameters for the samples can be found from Table 21*

With the three Inconel samples, shown in Figure 51 below, the amount of oxides goes slightly up as the total pressure increases. Higher gas pressure causes higher gas velocity, and high gas velocity atomizes the particles into finer particles than lower gas velocity [22]. Finer particles in turn oxidize more than bigger particles [22]. In other words, in the case of the Inconel samples, higher total gas pressure increases oxidation, because it produces finer particles than lower total gas pressure. On the other hand, a higher droplet velocity also causes a decrease in the time of flight, which in turn induces a decrease in the particle oxidation [1]. This may be the reason why in the Metcoloy samples the amount of oxides decreases as the total gas pressure increases. Two of the Metcoloy samples were sprayed with higher total pressures than the Inconel samples. Maybe after certain total gas pressure, 158 psi for example, the effect of total gas pressure changes from increasing the amount of oxides into decreasing the amount of oxides? It is also possible that Metcoloy 4 and Inconel 625 respond differently to the changes in total gas pressure because the materials themselves are somewhat different, or there may other factors affecting the coatings.

In both Metcoloy and Inconel samples, the pressure of propane is always ten psi lower than the pressure of air. In other words, the propane to air ratio stays the same in all the samples. In both Metcoloy and Inconel samples, the amount of pores increases from the first sample to the second, but then the amount of pores in the third sample is lower than in either of the first two. In any case, the amount of pores is extremely low in all of the samples of both materials, and the margin of error is quite great, so the exact amounts of pores cannot be regarded as reliable.

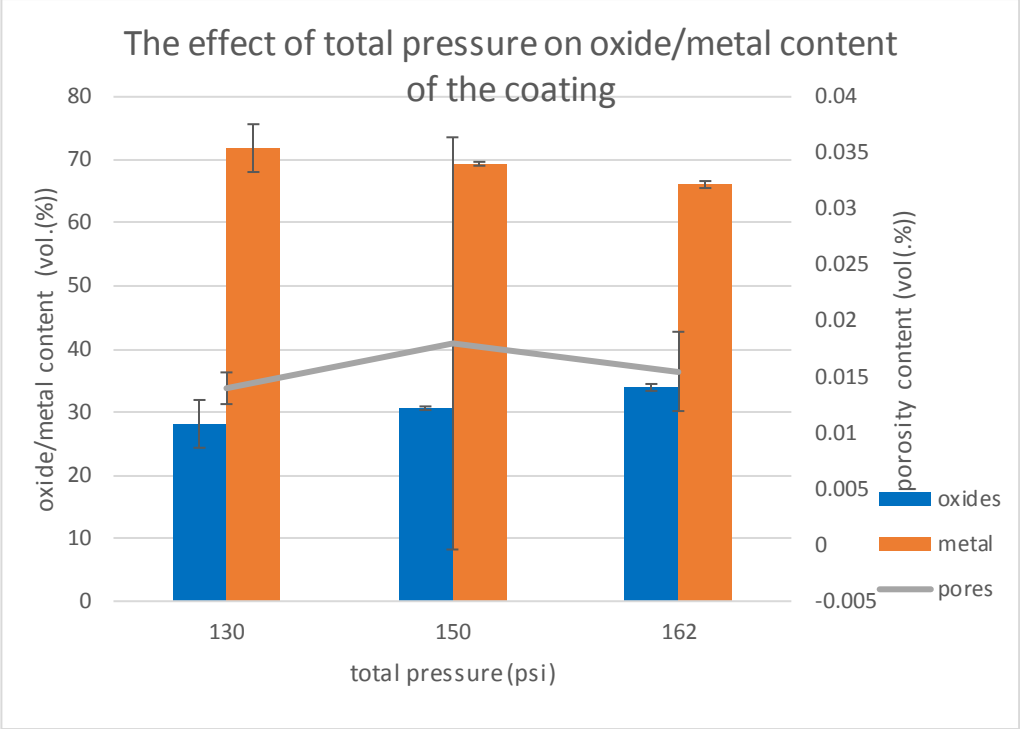

Figure 51. *The effect of pressure on coating composition of Inconel samples. Spraying parameters for the samples can be found in Table 25.*

The effect of increasing pressure on hardness of the three Metcoloy samples can be seen in Figure 52 a below. The hardness values increase from first sample to second, but then the final sample has a hardness that is slightly lower than that of the second sample. The maximum values for the hardness of Metcoloy samples, however, increase as the total pressure increases. In Inconel samples the hardness and maximum value of hardness increases as the pressure increases. This can be seen in Figure 52 b below.

In the Inconel samples, the increase in hardness coincides with the increase in oxide content of the coating. Amount of oxides and coating hardness also correlate in the Metcoloy samples, since the sample sprayed with total pressure of 166 has both the lowest oxide content and hardness, while the other two samples have higher oxide content and higher hardnesses. This correlation between oxide content and coating hardness is quite expected, since it usually occurs in arc sprayed coatings [22].

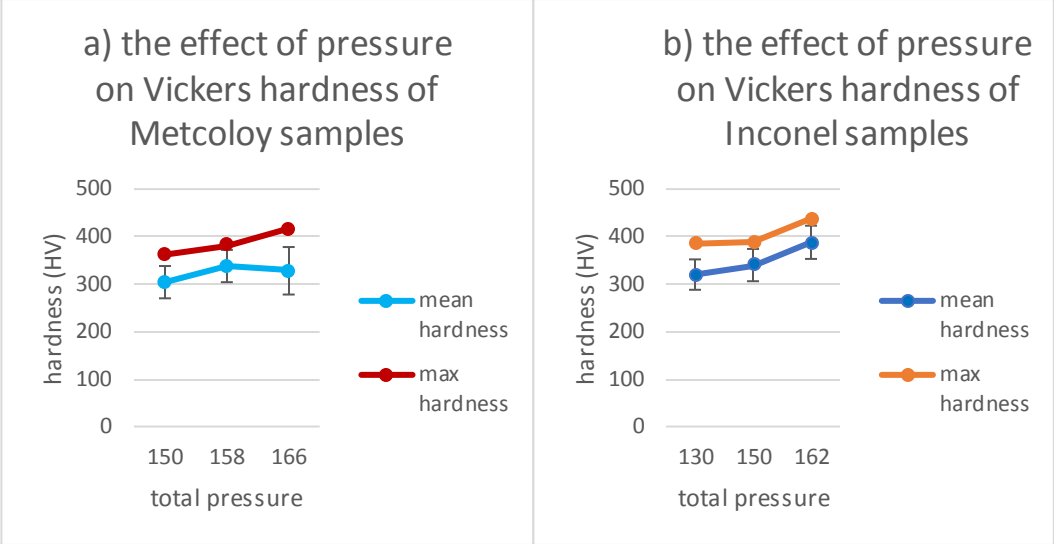

Figure 52 *The effect of total pressure on the mean and maximum Vickers hardness of a) Metcoloy 4 coatings and b) Inconel 625 coatings.*

When it comes to surface roughness, shown in Figure 53 a below, in the three Metcoloy samples, Rz decreases slightly as pressure increases, but the Ra-values stay much the same regardless of the total pressure used. In the three Inconel samples (Fig. 54 b) both the Ra and Rz values increase slightly after the second sample, while the first two samples have almost the same values with each other. It would seem that increasing the total gas pressure decreases slightly the Rz-values in Metcoloy samples and increases slightly the Rz-values in Inconel samples, but doesn't have an effect on the Ra-values of either coating material.

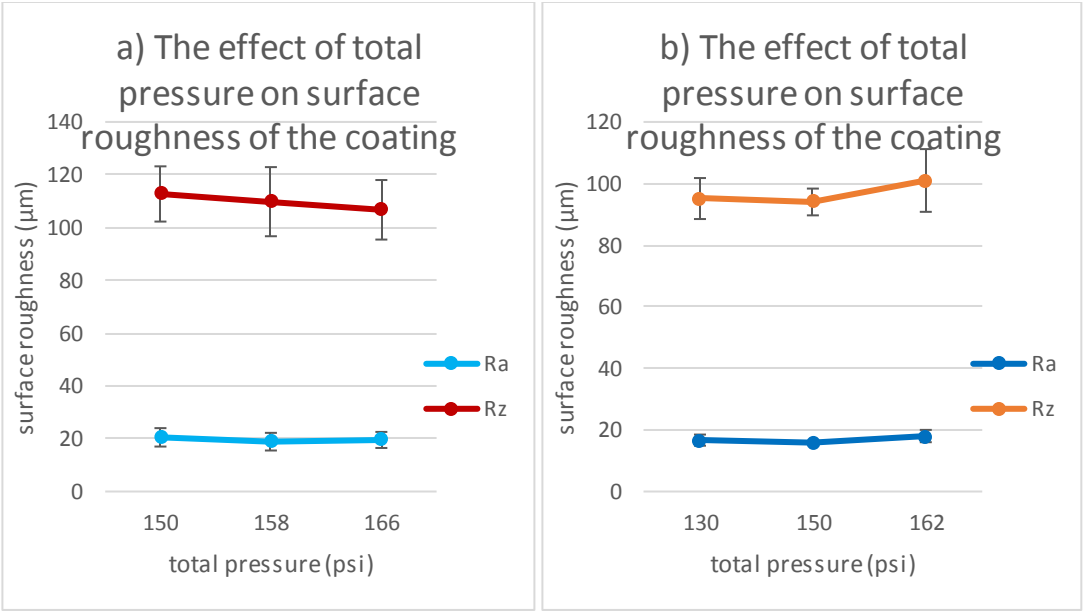

Figure 53 *The effect of total pressure on surface roughness of a) Metcoloy 4 samples and b) Inconel 625 samples.*

From the Figure 54 below can be seen that while the thickness of Inconel samples increases as the total pressure increases, the opposite occurs in the Metcoloy samples. The differences in thickness are greater in Metcoloy samples, even though the differences in total pressure level are greater in the Inconel samples. This coincides with what can be seen in the optical microscope images of the samples; increasing total pressure seems to produce denser Metcoloy 4 coatings, while in the Inconel samples this effect does not seem to exist.

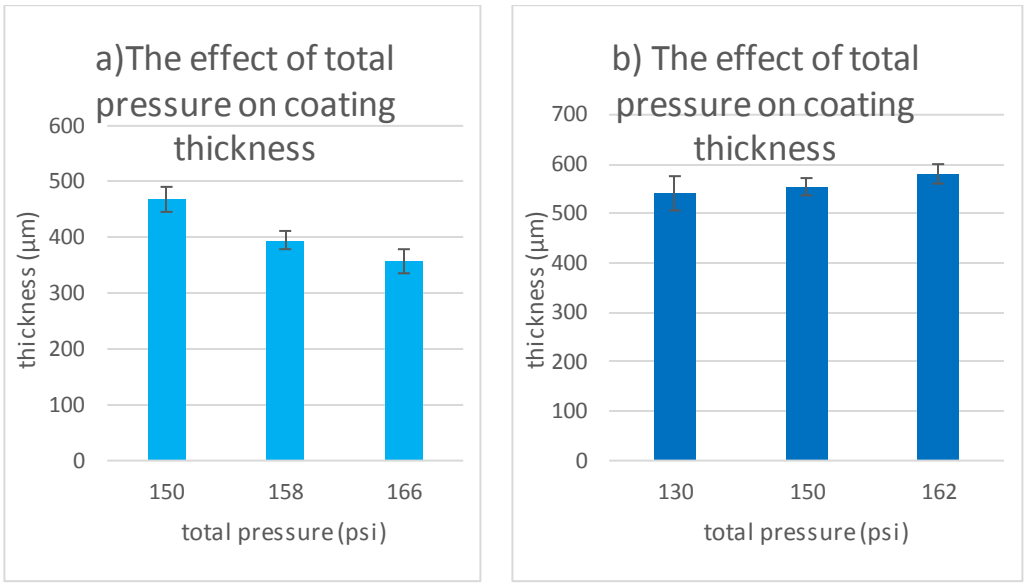

Figure 54. *The effect of total pressure on coating thickness of a) Metcoloy and b) Inconel samples.*

6.6 Effect of spraying wire feed rate on the coatings

Below in Figures 55 and 56, the effect of wire feed rate on oxide and metal contents of coatings can be seen. It should also be remembered that the wire feed rate also controls the current. When wire feed increases, so does the current. The two Figures represent two different Inconel batches. The samples in Figure 55 are from the second spraying session,

while the samples featured in Figure 56 are from session three. They have slightly different spraying parameters, so they are not directly comparable.

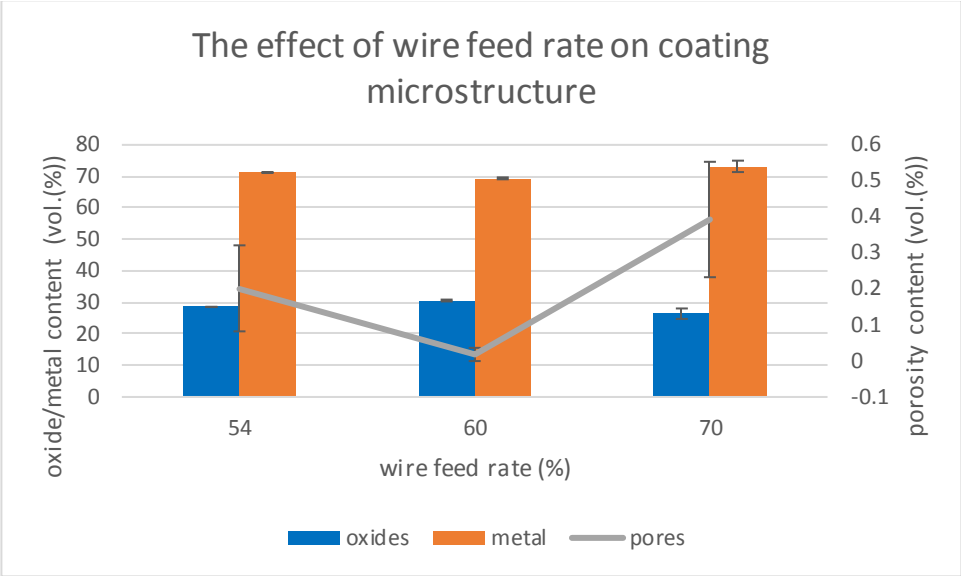

Figure 55. *The effect of wire feed rate on coating composition of batch Inconel 2. The spraying parameters for the samples in this batch are in Table 22*

In both of the batches, the amounts of both oxide and metal seem to stay much the same. The sample sprayed with highest wire feed rate in Figure 55 has slightly lower oxide content than the other samples in either of the batches, but this could be simply a coincidence.

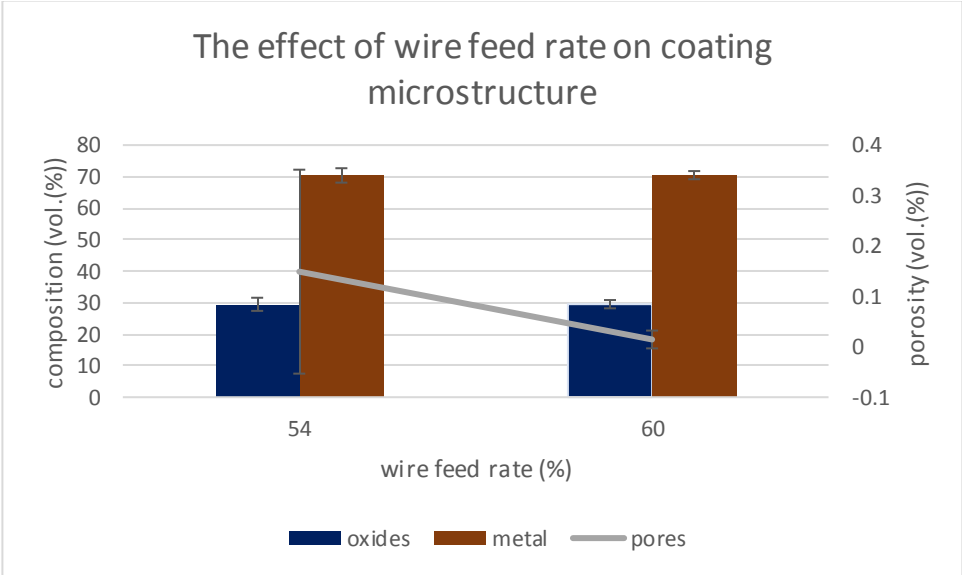

Figure 56. *The effect of wire feed rate on coating composition of batch Inconel 3. The spraying parameters for the samples in this batch are in Table 23*

In the batch which is denoted Inconel 2 in Figure 57 a, both the mean and maximum values of hardness increase as the wire feed rate increases. The increase is more linear in the mean than in the maximum values of Vickers hardness. In the batch called Inconel 3 that can be seen in Figure 57 b below, the mean values of hardness decrease slightly as wire feed, and current, increase, while the opposite occurs in the maximum values of hardness. It could be that the decrease in the mean hardness values in Figure 57 is due to an error, and increase in wire feed rate does, in fact, correlate with an increase in hardness.

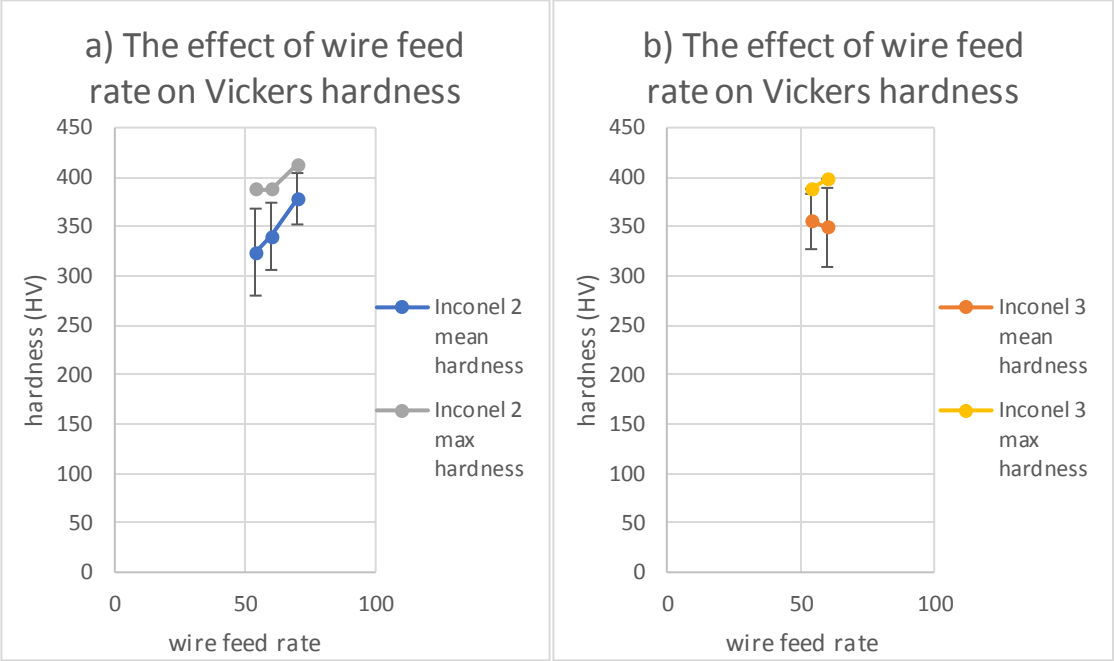

Figure 57. *The effect of wire feed rate on coating hardness of a) batch Inconel 2 and b) batch Inconel 3.*

Based on Figure 58 below, it seems that wire feed rate doesn't have an effect on the surface roughness of coatings, since all the coating samples have very similar values of both Ra and Rz.

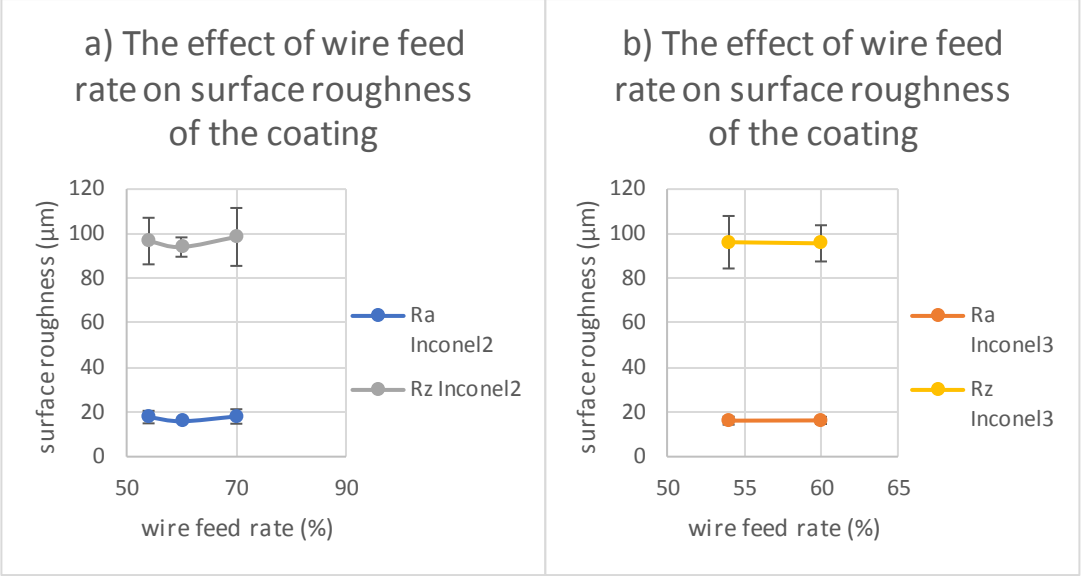

Figure 58. *The effect of wire feed rate on coating surface roughness of a) Inconel 2 and b) of Inconel 3.*

As could be guessed, the thickness of the coating increases as the wire feed rate increases, as Figure 59 below shows. After all, increasing wire feed rate does increase the production rate of droplets at the wire tips [17]. The rise of the thickness seems to be quite linear. In the batch Inconel 3, however, the raise in the thickness of the coatings is much smaller than in batch Inconel 2.

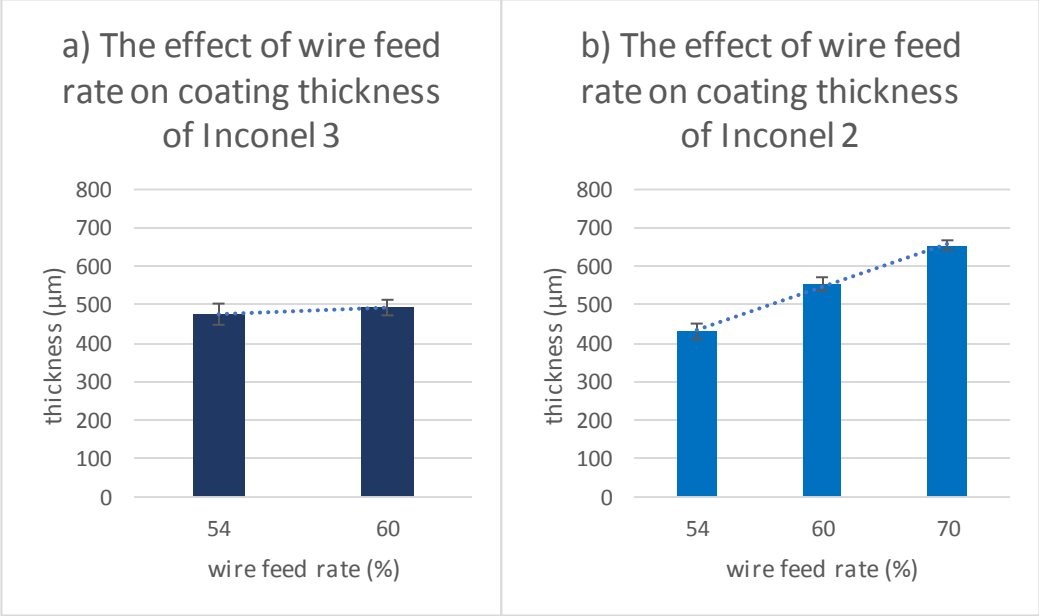

Figure 59.*The effect of wire feed rate on coating thickness of a)Inconel2 and b) of Inconel 3.*

6.7 Effect of spraying voltage

Based on Figures 62 and 63, it seems that spraying voltage doesn't have a direct effect on the oxide of the coating apart from the amount of pores. All the samples which voltage was varied were made of Inconel. The two different batches, called Inconel 2 and Inconel 3 (the number refers to spraying session) have slightly different spraying parameters, so they are not necessarily directly comparable to each other.

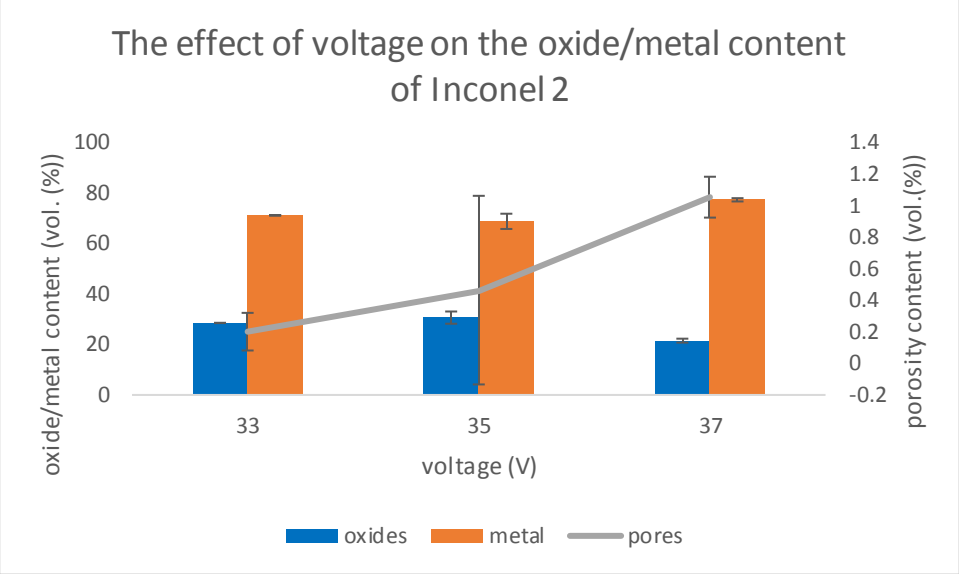

Figure 60. *The effect of voltage on coating composition of batch Inconel 2.*

In the batch featured in Figure 60 above, the amount of oxides in the middle sample is lower than either in the first or last sample of that batch. In the batch marked in Figure 61 below, the oxide and metal contents of the two samples appear to be almost exactly the same. In both batches, porosity seems to increase as voltage increases. Increase in voltage causes a decrease in spray velocity [17], which in turn results in an increase in porosity [22], so this observation makes sense, though since the porosity contents are very low, the porosity results are not very reliable.

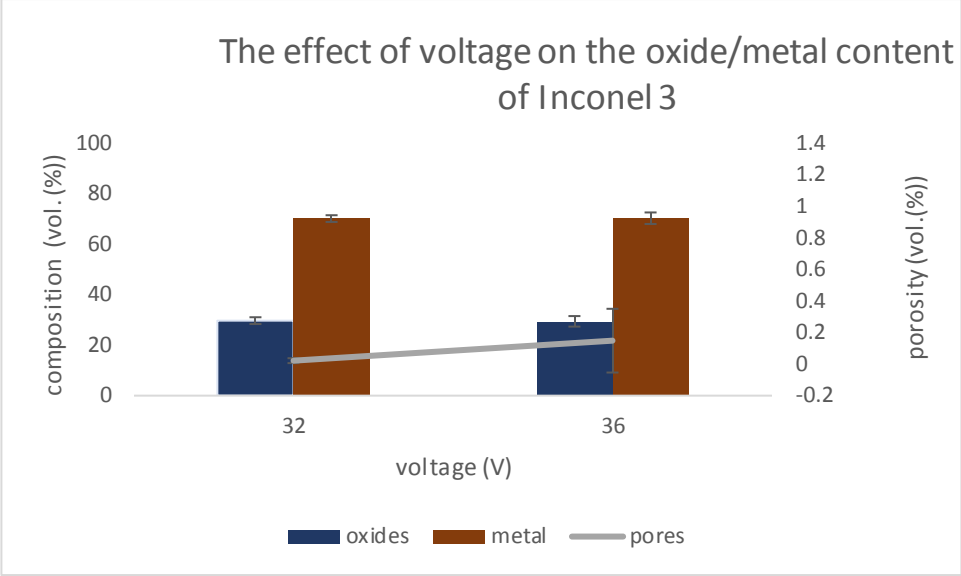

Figure 61. *The effect of voltage on coating composition of batch Inconel 3.*

Based on Figure 62, it looks like voltage doesn't have a direct effect on the hardness of the coatings. In the batch Inconel 3, which contains three samples, the hardness increases from the first sample to the second, but then decreases from the second sample to the third. In the other batch, hardness decreases slightly as voltage increases. The differences between the samples are, in any case, quite small, and could be caused by error.

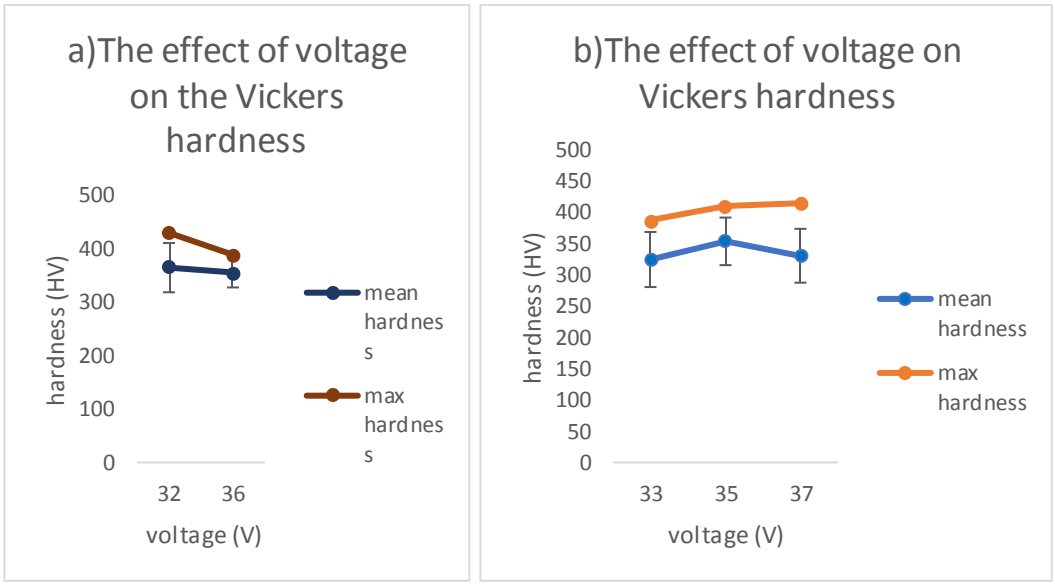

Figure 62. *The effect of voltage on mean and maximum hardness of a) batch Inconel 2 and b) batch Inconel 3.*

The surface roughness of the coatings stays much the same regardless of the voltage used in spraying (Fig. 63). This applies to Ra values as well as Rz values.

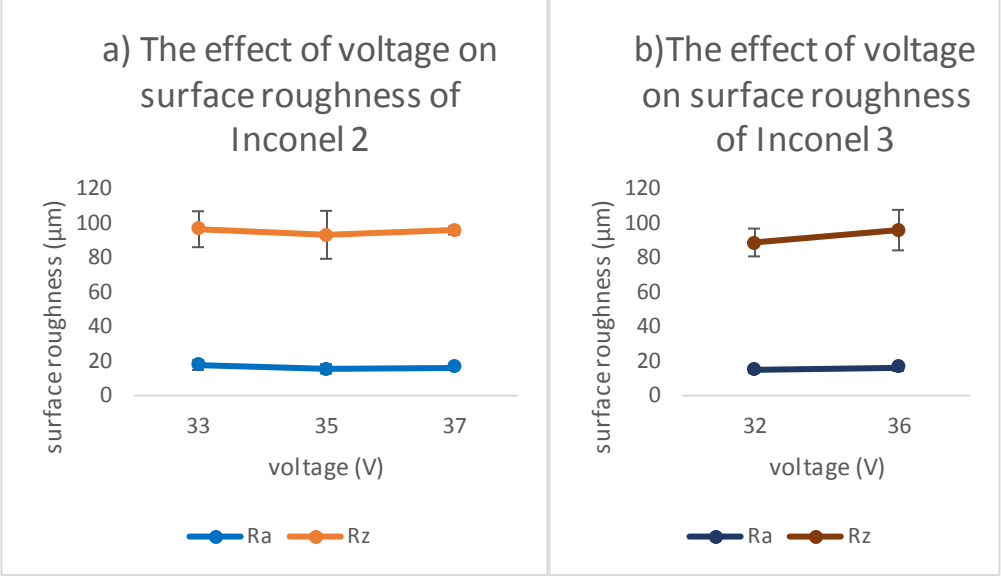

Figure 63 *The effect of voltage on surface roughness of a) batch Inconel 2 and b) batch Inconel 3.*

Thickness of the coatings doesn't seem to correlate with voltage, either, at least based on Figure 64 below.

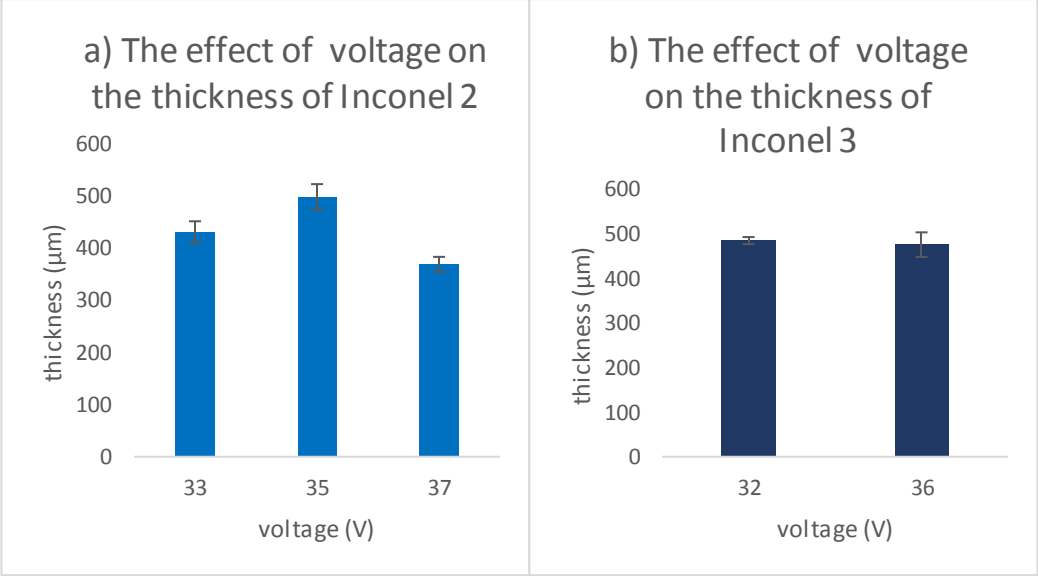

Figure 64 *The effect of voltage on coating thickness of samples from a) batch Inconel 2 and b) batch Inconel 3.*

6.8 Effect of spraying distance

Below in Figures 65, 66 and 67, there can be seen the effect of distance on oxide and metal contents of coatings from three different batches of samples. The parameters of the two Inconel batches were not the same, so the batches are not directly comparable. Both

in the Metcoloy batch of samples and the batch Inconel 4 batch of samples the specimens were sprayed simultaneously. With the amount of pores so low, it is not possible to say anything definite about how well they correlate with the distance. In fact, the amount of pores seemingly does not correlate with distance in any way whatsoever in any of the batches, even though according to Figure 7 mentioned in Chapter 3.2, the porosity should increase as the spraying distance increases.

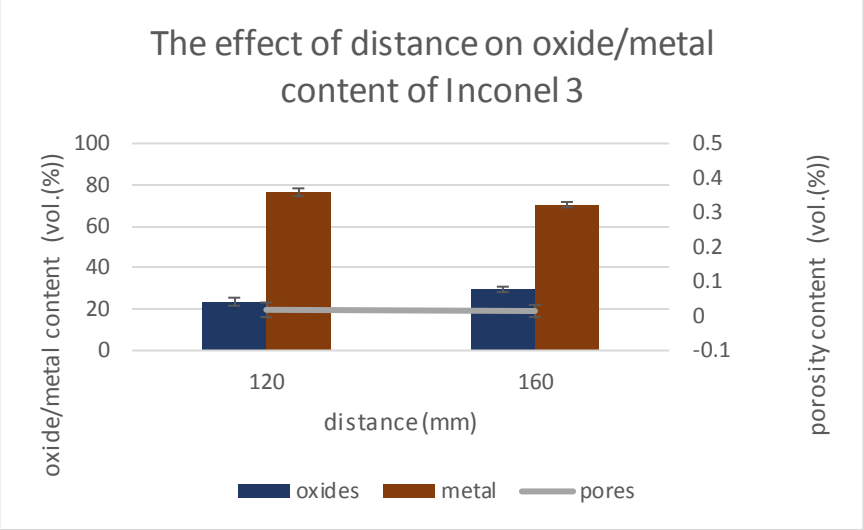

Figure 65 *The effect of distance on coating composition of samples from batch Inconel 3.*

In Figure 65 above, as distance increases, the oxide content of the coating slightly increases. The same occurs in Figure 66 below. The differences between the oxide content of the samples is, however, very small.

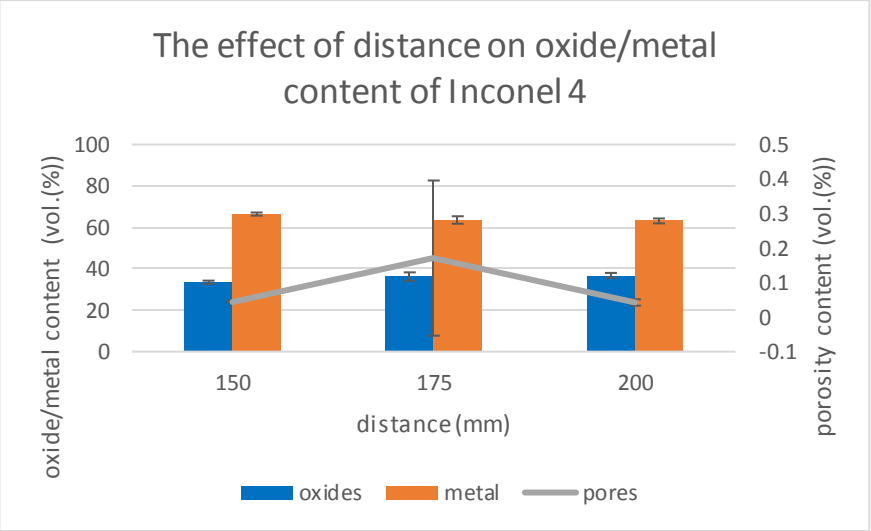

Figure 66 *The effect of distance on coating composition of samples from batch Inconel 4.*

In the case of the three Metcoloy samples, shown in Figure 67 below, the same trend as in the Inconel batches above can be seen: the increase in distance results in very slight increase of oxide content in the coating. Increased distance increases the oxide content because the sprayed coating droplets have more time to oxidize in-flight when the distance is longer [35].

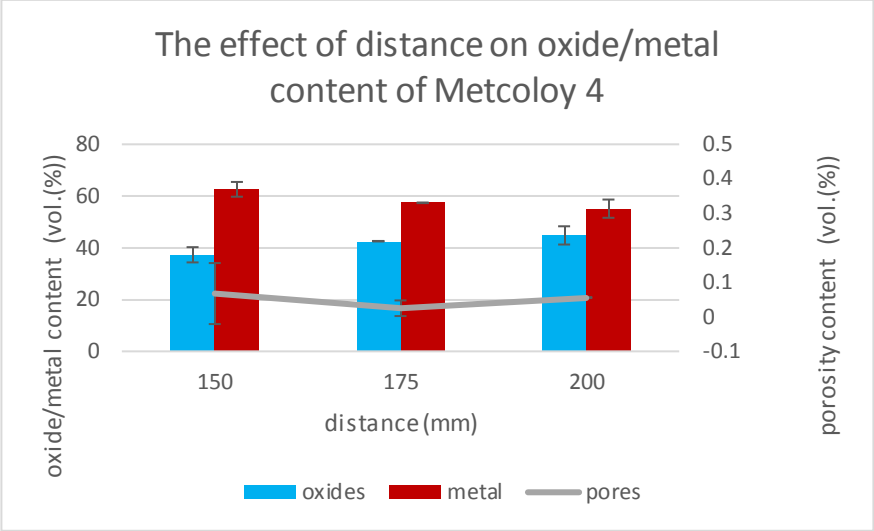

Figure 67. *The effect of distance on coating composition of samples from batch Metcoloy 4.*

In Figure 68 below it can be seen that in batch Inconel 3 as the distance increases, so does the hardness of the coating. In Inconel 4 batch, the sample sprayed from furthest distance has smaller maximum hardness value than the other two samples sprayed in the same batch (Fig. 68 b). Even so, the mean hardness in this batch does increase as the distance increases.

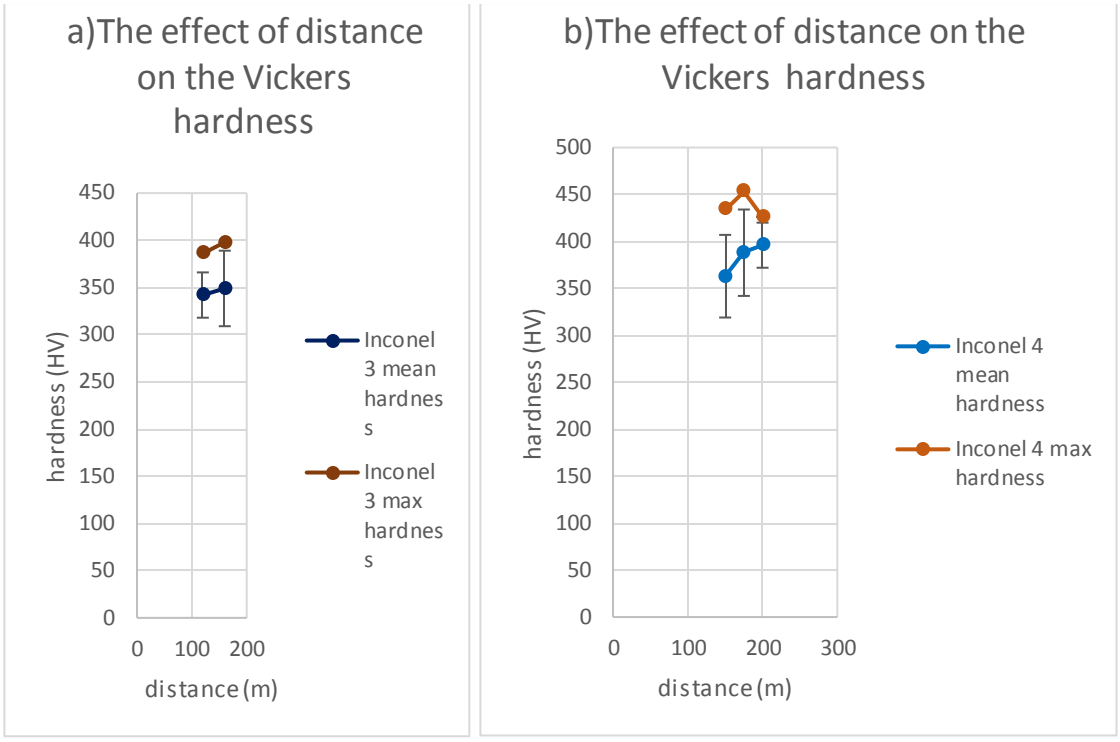

Figure 68 *The effect of distance on mean and maximum hardness of samples from a) batch Inconel 3 and b) batch Inconel 4.*

In the Metcoloy batch (Fig. 69), the hardness increases quite steadily as the distance increases. In all of the batches, the rise in hardness correlates with the slight rise in oxide content. This is quite expected, since oxides generally increase the hardness of a coating [2].

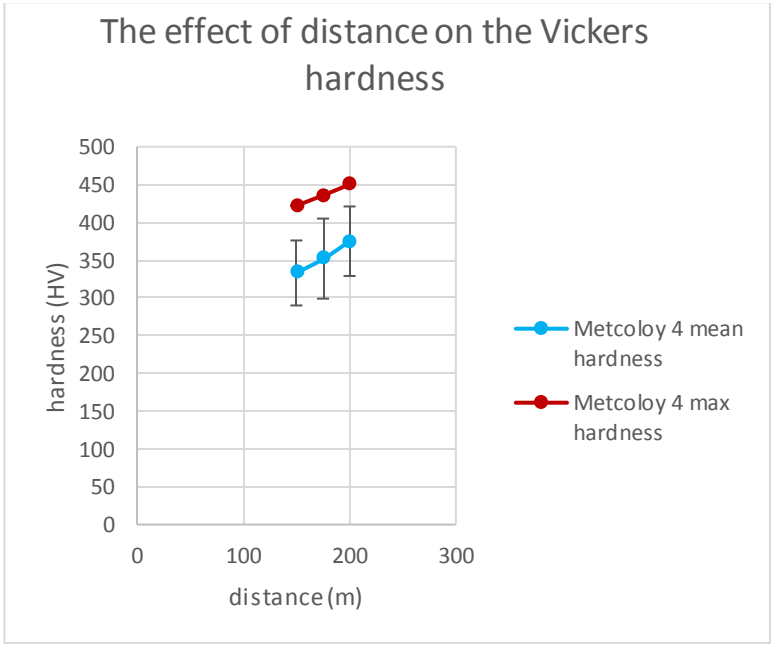

Figure 69. *The effect of distance on mean and maximum hardness of samples from batch Metcoloy 4.*

Hardness values of all the coating samples made in this study was plotted against the oxide content of the coatings (Fig.70) There does not seem to be any correlation between the amount of oxides and the hardness of the coating when all the samples are considered.

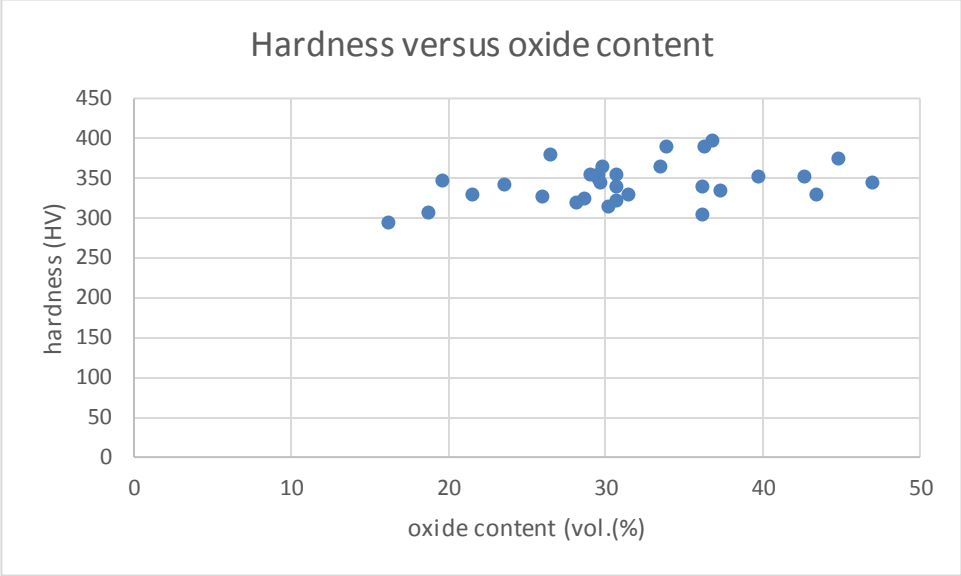

Figure 70. *Hardnesses of all the coatings made for this thesis plotted against their oxide content*

From Figure 71 below can be deduced that in the two Inconel batches, the surface roughness decreases as the spraying distance increases.

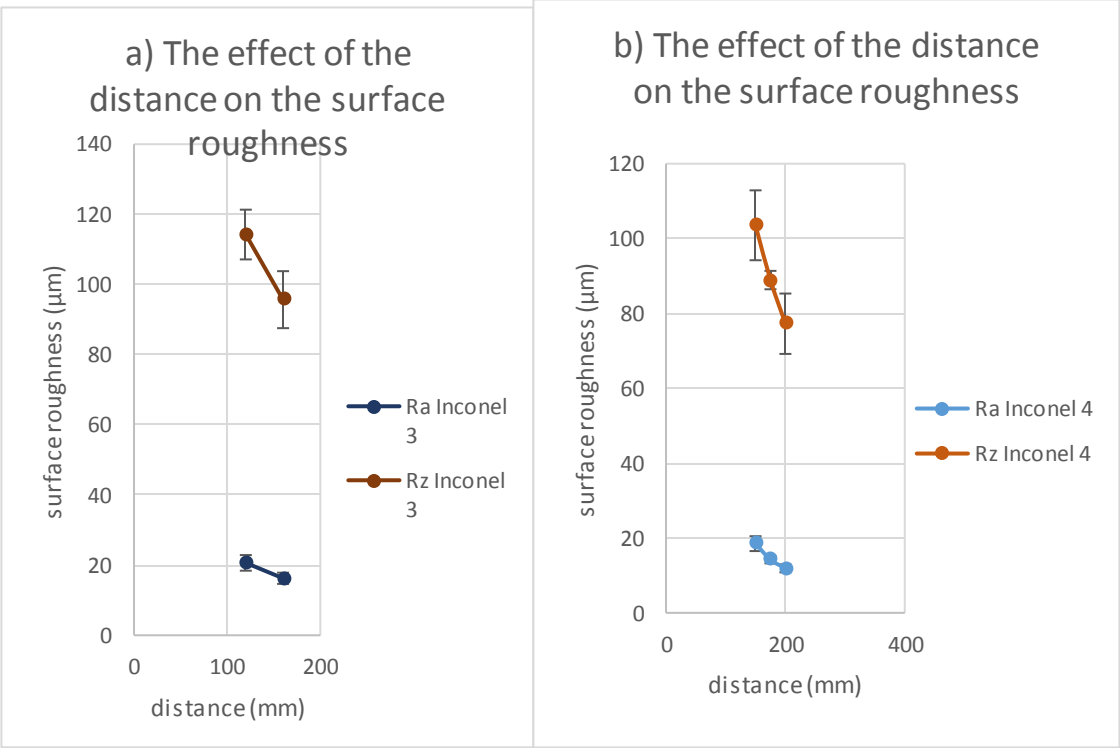

Figure 71 *The effect of distance on surface roughness of samples from batch a) Inconel 3 and b) Inconel 4.*

In the Metcoloy batch, too, the same correlation can be seen (Fig.73, below). This correlation can be seen in both Ra and Rz values of all three batches.

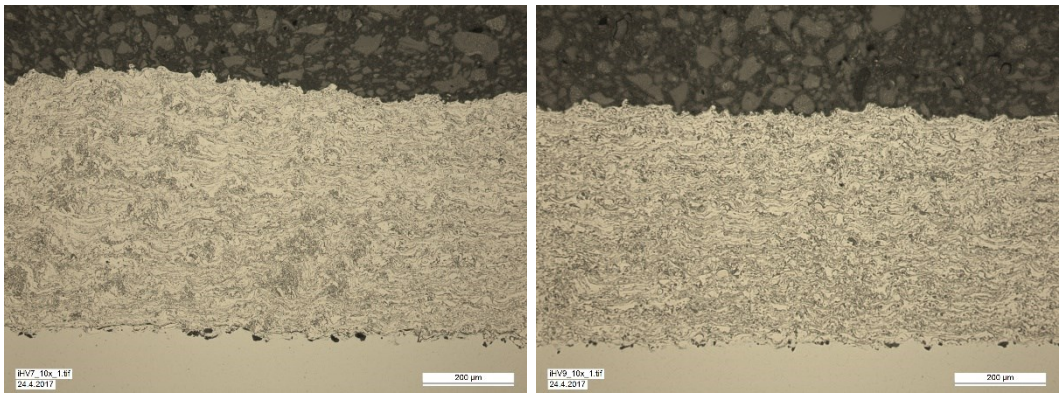

Figure 72. *On the left: an image of sample iHV7; on the right: an image of sample iHV9. Magnification is 10 in both images.*

In the Inconel samples of both batches, there can be seen increase in homogeneity of the coating microstructure in the optical microscope images. Two such images can be seen above in Figure 72, where are images of samples iHV7 and iHV9. The decreased surface roughness may be due to increase in coating homogeneity.

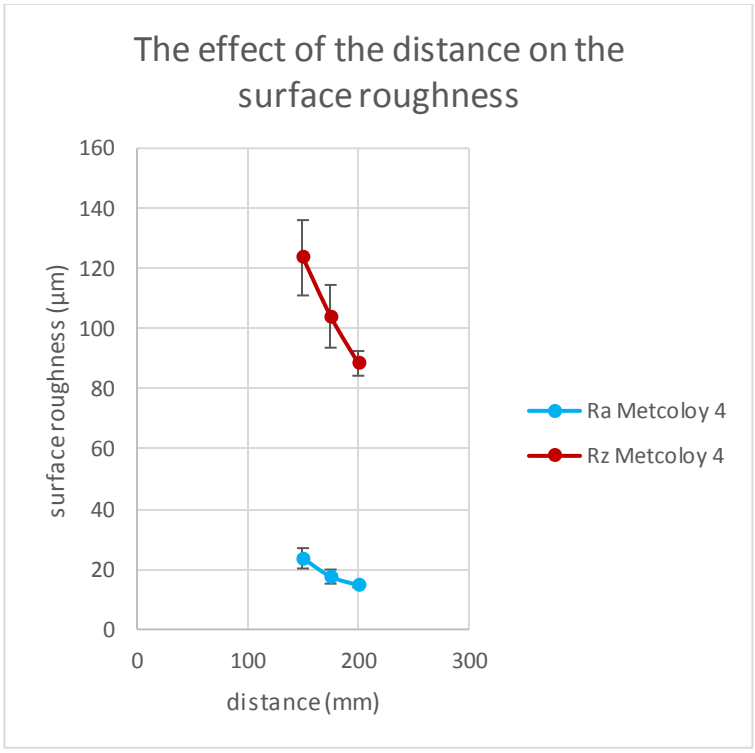

Figure 73. *The effect of distance on surface roughness of samples from batch Metcoloy 4.*

There does not seem to be any direct correlation between the distance and thickness of the coating. In Inconel 3 batch of two samples (Fig. 74a), the thickness increases as distance increases, but in the other Inconel batch (Fig. 74b), thickness seems to decrease as the spraying distance increases.

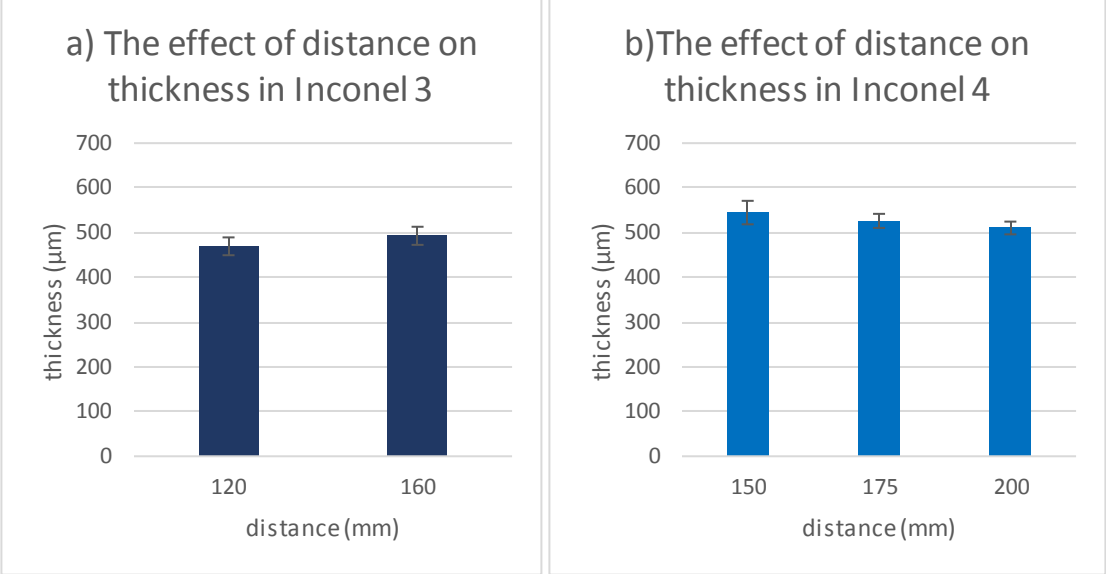

Figure 74. *The effect of distance on thickness of samples from batch a) Inconel 3 and b) Inconel 4.*

In the Metcoloy batch (Fig. 75, below), the thickest coating is in the middle sample, so there seems to be no correlation at all between the distance and coating thickness. The differences in the thicknesses of the coatings are quite small, in all of the batches.

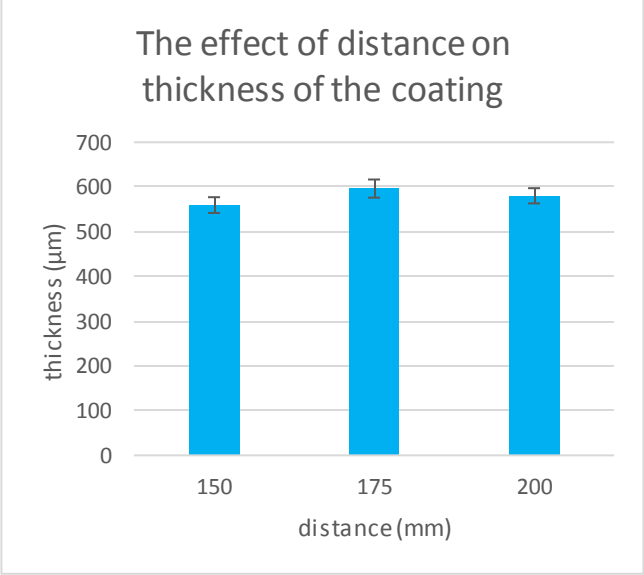

Figure 75 *The effect of distance on thickness of samples from batch Metcoloy 4.*

6.9 Effect of using propane as a process gas

In Figure 76 below, three Inconel samples sprayed with the combustion flame are compared with three Inconel samples sprayed without the combustion flame. HV4 and HV7, iHV1 and iHV2, and iHV5 and iHV5, were each pair respectively sprayed with the same parameters apart from gas pressure. In the Figure 76, the samples sprayed with the combustion flame are yellow while the samples sprayed without the flame are green. The bars with lighter color mark the amount of oxides, while the bars with darker color mark the amount of metal.

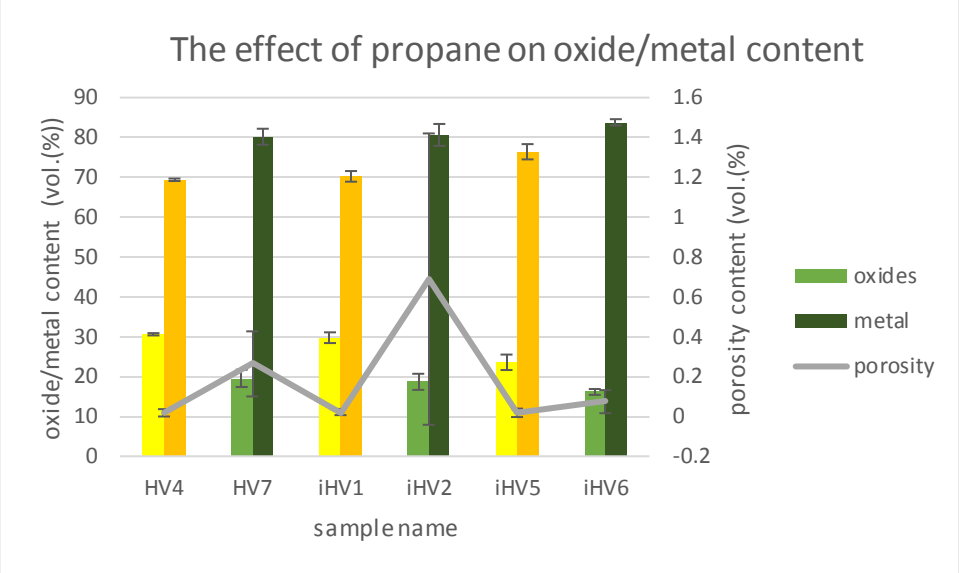

Figure 76. *The effect of using propane on coating composition. The bars in yellow mark samples that were sprayed using propane, the bars in green mark samples that were sprayed without using propane. Regardless of the color, the smaller bar on the left always denotes the amount of oxides and the longer bar on the right denotes the amount of metal in the coating.*

In all the samples sprayed with the combustion flame, the oxide content is higher and metal content lower than in samples sprayed without the flame. The amount of porosity, on the other hand, is higher in all of the samples sprayed without the flame. This makes sense, since the coatings sprayed with the combustion flame look clearly denser in microscopic images than coatings sprayed without the flame, and previous studies indicated that this would be the case [2]. Since using the combustion flame means also higher gas velocity, which can lead to higher oxidation [22], the difference in oxide content is also quite logical, even though propane is supposed to shield the particles from the oxidation.

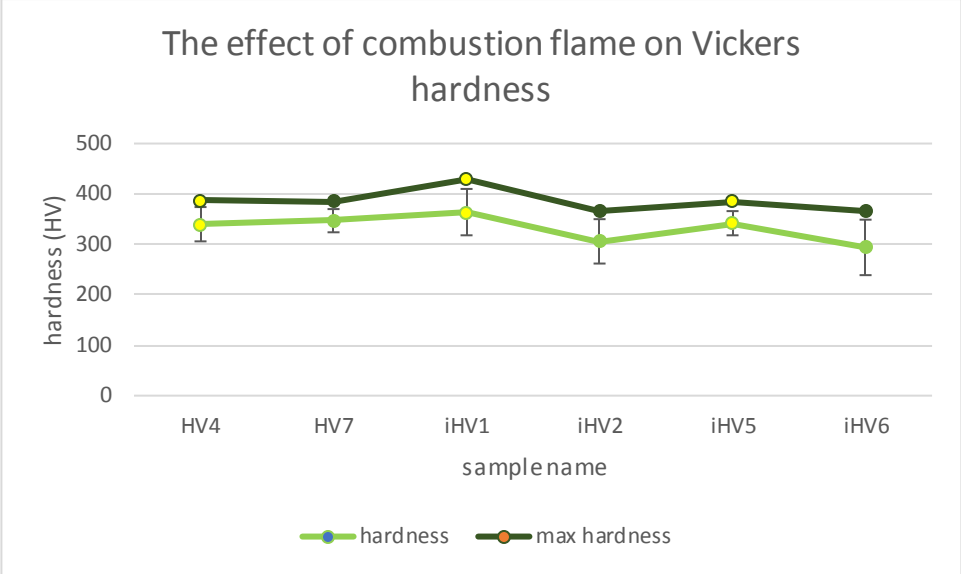

Figure 77. *The effect of propane as atomization gas on coating hardness. The yellow dots mark samples sprayed with propane, the dots that are the same colour as the outlines mark samples sprayed without propane*

In Figure 77 above, the effect of using the combustion flame on hardness can be seen. Apart from HV4 and HV7, of each pair, the sample sprayed without the combustion flame has lower hardness. HV7, sprayed without the combustion flame, seems to have higher hardness than its pair HV4. However, HV4 has almost the same maximum hardness value than HV7, so the lower hardness of sample HV4 could be simply an error. Since the samples sprayed with the combustion flame have higher oxide contents, it is logical that they would also have higher hardnesses.

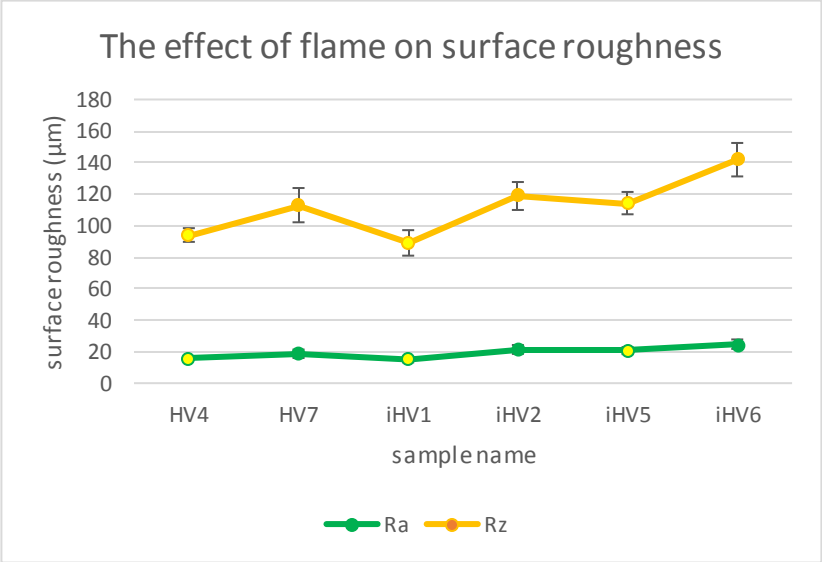

Figure 78. *The effext of propane as carrier gas on surface roughness of the coating. The yellow dots mark samples sprayed with propane, the dots that are the same colour as the outlines mark samples sprayed without propane*

Based on Figure 78, the surface roughness, both Ra and Rz, seem to be greater in the samples sprayed with the combustion flame. This makes sense, since the coatings sprayed without the combustion flame look rougher and less uniform than the coatings sprayed using the combustion flame even with the naked eye. The higher velocity caused by the combustion flame also produces finer particles [22], so it is not a surprise the surface roughness would be lower in the coatings sprayed with the flame.

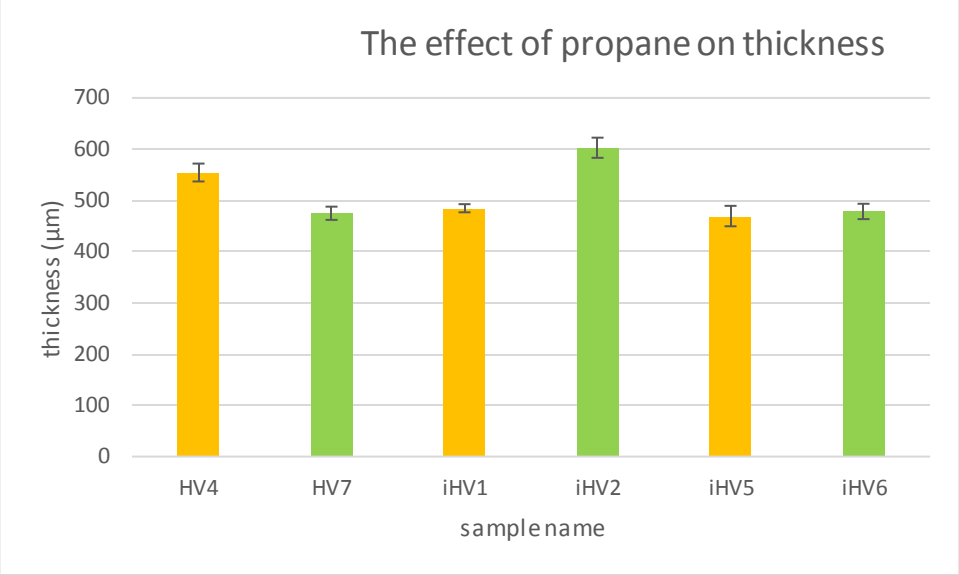

Figure 79. *The effect of propane as carrier gas on coating thickness. The yellow bars mark samples sprayed with propane, the green bars mark samples sprayed without propane*

From Figure 79 can be seen that in iHV1 and iHV2, as well as iHV5 and iHV6, the sample sprayed using propane is thinner than the sample sprayed without propane. However, HV4 is clearly thicker than HV7, even though it was sprayed using the combustion flame. It could be that there is no direct correlation between the coating thickness and whether or not the combustion flame was used.

6.10 Comparison of HVAF arc coatings and conventional arc spray coatings

Below in Figure 80 can be seen two different Metcoloy batches: one is sprayed with Smart Arc, the other with HVAF Arc. It can be seen from the graph that the oxide content is slightly higher in the SmartArc samples than in HVAF Arc samples. The two sets of coatings were sprayed so that the samples have different distances, but otherwise same parameters within the set. This is also the case in the Inconel coatings that are featured in Figure 81.

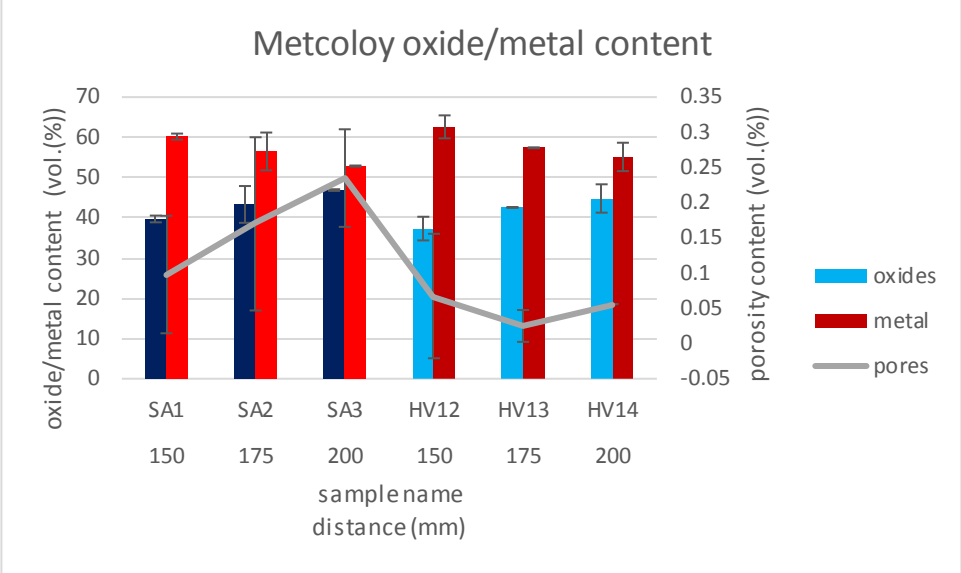

Figure 80. *Comparison of coating compositions of Metcoloy 4 made with Smartarc and HVAF Arc.*

In Figure 81, below, two Inconel batches are compared. Of them, too, the other batch is sprayed with SmartArc, the other with HVAF Arc. Here the SmartArc coatings seem to have slightly less oxides than HVAF Arc coatings. This is a bit puzzling, since the samples sprayed without propane (Fig. 76) using HVAF Arc have less oxides than either coatings featured in Figure 81, while logically, those coatings should resemble SmartArc coatings, as they both are sprayed without the combustion flame.

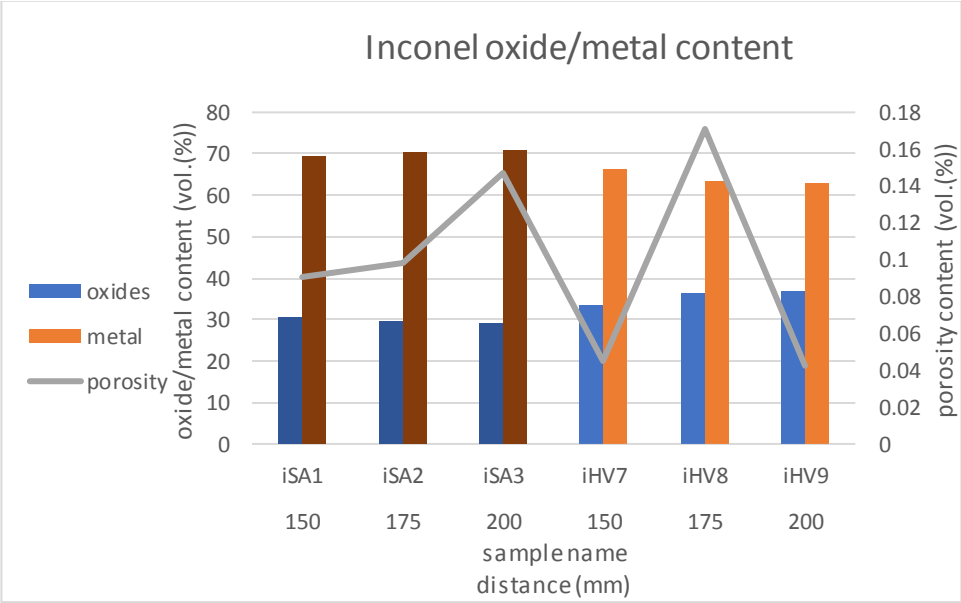

Figure 81. *Comparison of coating compositions of Inconel 625 made with Smartarc and HVAF Arc.*

The hardnesses of the two Metcoloy coating sets (Figure 82, below), on the other hand, seem to be quite similar, though in SmartArc, the increasing distance doesn't result in steadily increasing hardness, as in its Metcoloy counterparts.

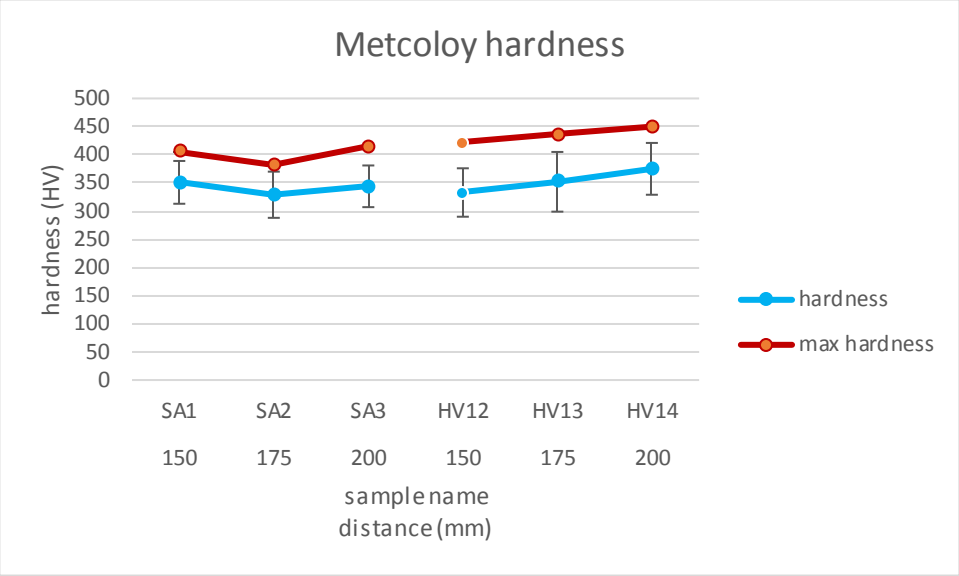

Figure 82. *Comparison of coating hardnessess of Metcoloy 4 coatings made with Smart-arc and HVAF Arc.*

In the Inconel samples the hardness values are not as similar (Figure 83 below) as in the Metcoloy samples. In the Inconel samples, the HVAF Arc samples have somewhat higher hardness values than SmartArc coatings. In both sets the increasing distance results in steadily increasing mean hardness. The maximum hardness values, however, do not correlate with the mean hardness values, unlike in the Metcoloy samples.

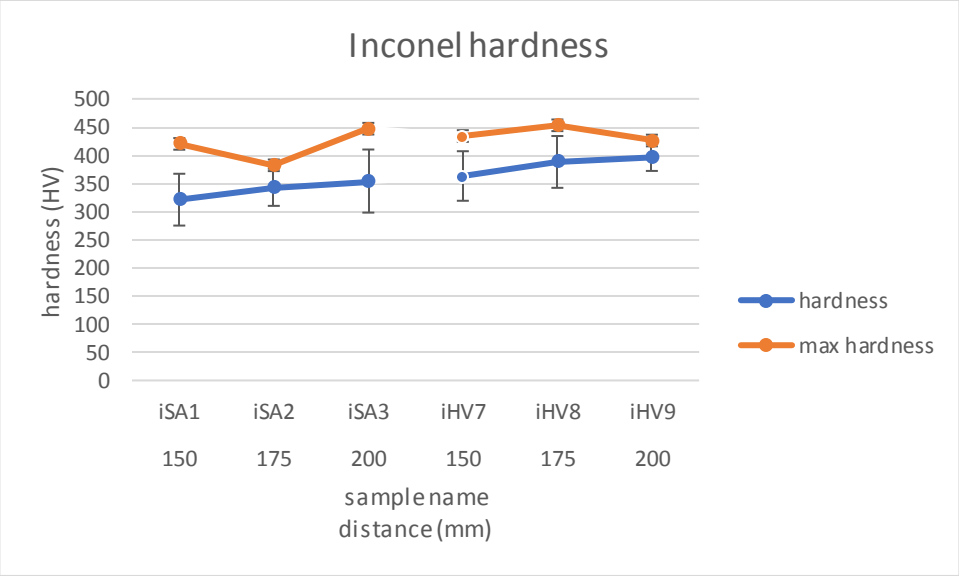

Figure 83. *Comparison of coating hardnessess of Inconel 625 coatings made with Smart-arc and HVAF Arc.*

Based on the Figure 84, shown below, it seems that surface roughness is not much affected by which device was used. Apart from the Rz value of sample HV12, the samples have surface roughness values that are very alike.

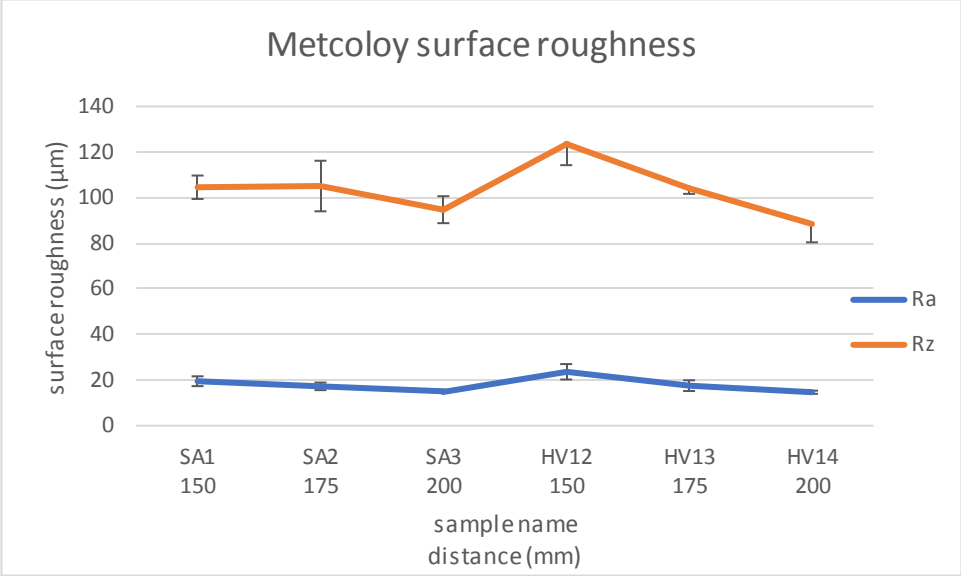

Figure 84. *Comparison of coating surface roughnesses of Metcoloy 4 coatings made with Smartarc and HVAF Arc.*

In the Inconel samples, too, the surface roughness values are very similar (Fig. 85). In this, too, the SmartArc coatings differ from the coatings made with HVAF Arc without using propane, since those coatings have distinctly rougher surfaces than the HVAF Arc coatings sprayed using the combustion flame.

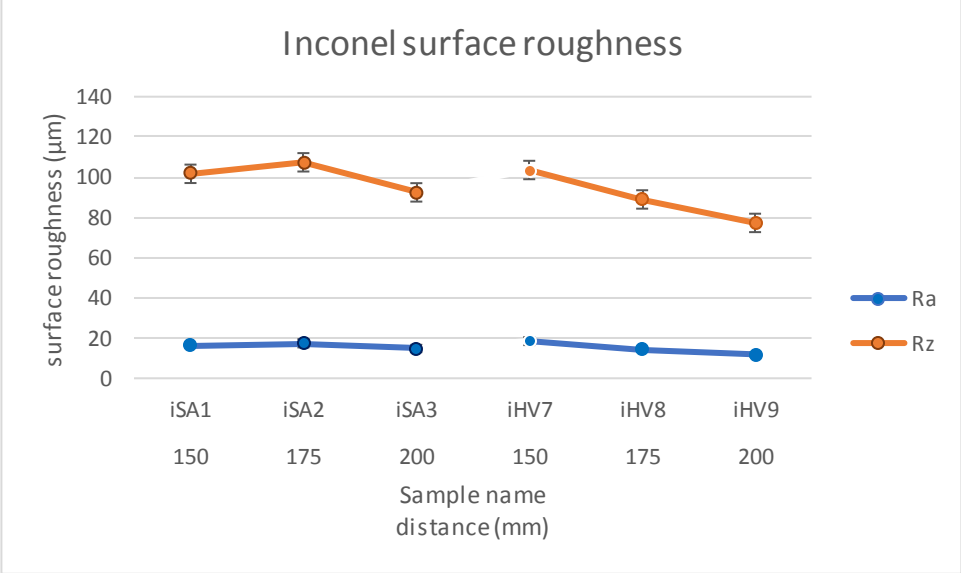

Figure 85. *Comparison of coating surface roughnesses of Inconel 625 coatings made with Smartarc and HVAF Arc.*

From Figure 86 below can be seen that the SmartArc coatings are slightly thicker than the HVAF Arc coatings. Neither sets show a clear correlation with the distance and the thickness of the coating.

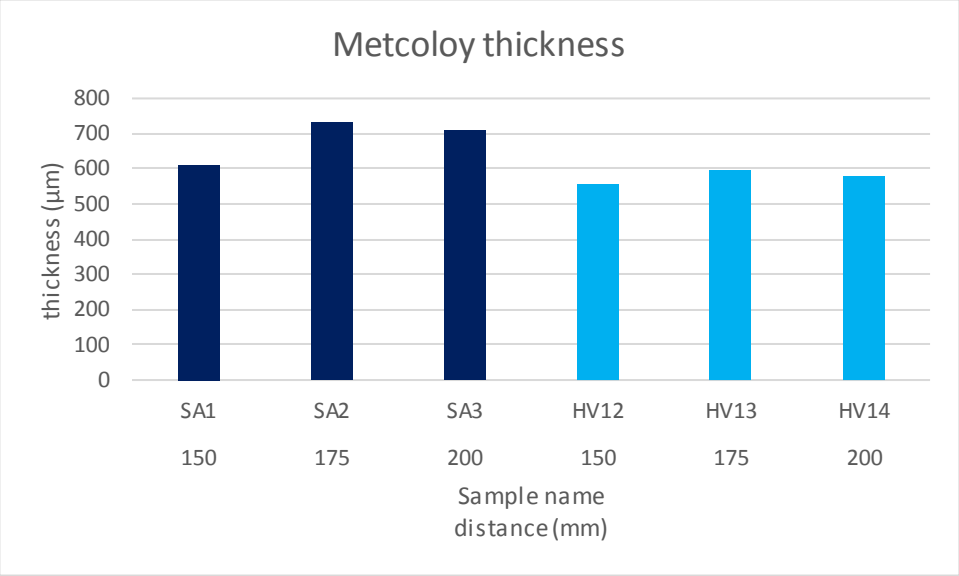

Figure 86. *Comparison of coating thicknesses of Metcoloy 4 coatings made with Smart-arc and HVAF Arc.*

In the Inconel samples, too, the SmartArc coatings are slightly thicker than HVAF Arc samples (Fig. 87). The differences in thickness are smaller in Inconel 625 samples than in Metcoloy 4 samples.

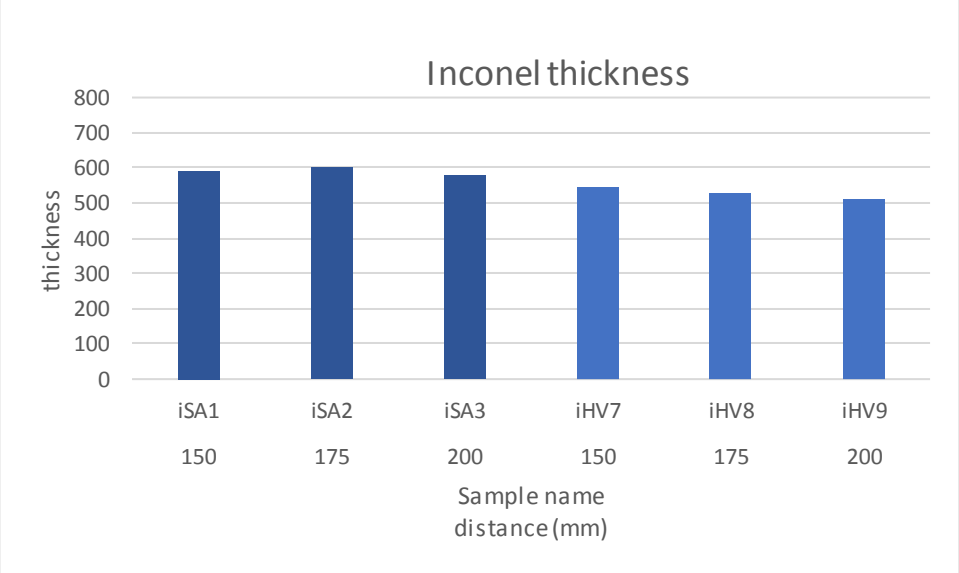

Figure 87. *Comparison of coating thicknesses of Inconel 625 coatings made with Smart-Arc and HVAF Arc.*

6.11 Erosion wear resistance of the coatings

Below in Figure 88 the results of the erosion test can be seen. The samples used in the test were the three pairs of samples that were also used in comparing the effect of combustion flame on the coatings. So HV4 and HV7, iHV1 and iHV2, and iHV5 and iHV6 form pairs which were sprayed with the same parameters, apart from the combustion flame, respectively. Samples HV7, iHV2, and iHV6 were sprayed without the combustion flame, the rest of the samples with it.

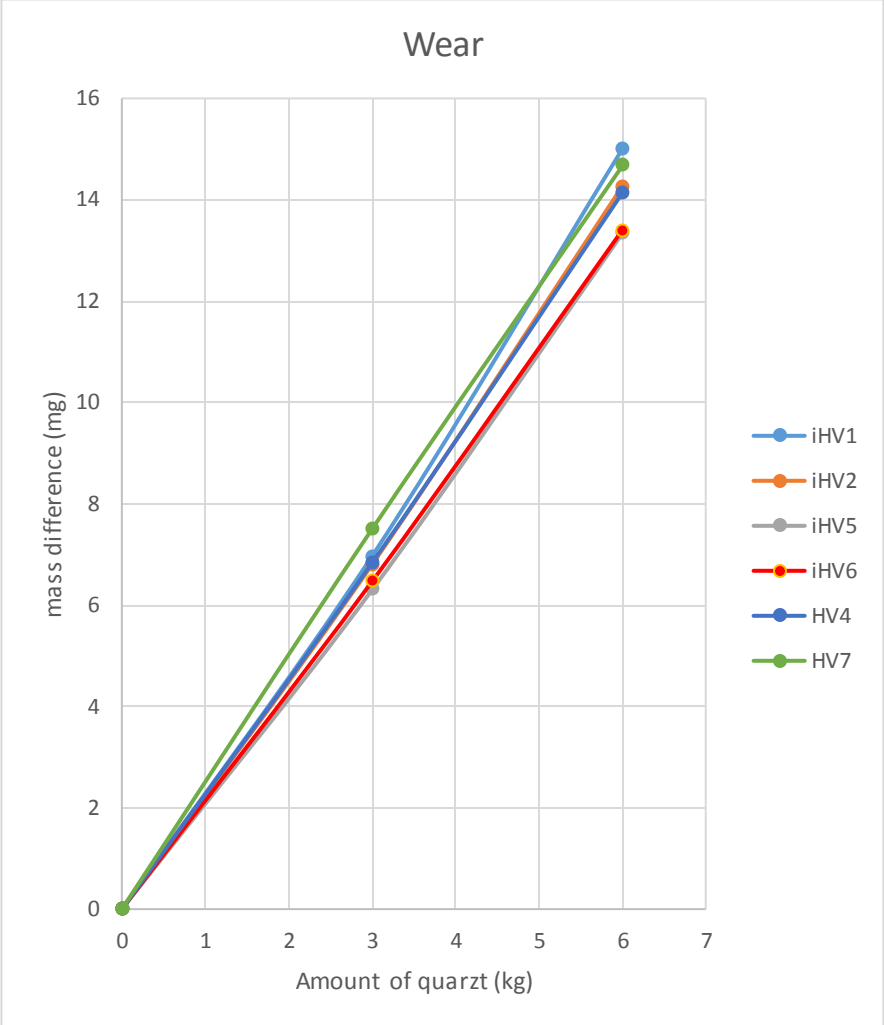

Figure 88. *Results from the erosion test*

It is clear from the Figure 88 that the test results of all the samples are very close to one other. Mostly worn sample is iHV1, while the least worn is iHV5, though iHV6 is almost as little worn. Of the samples sprayed without the flame, iHV6 and HV7 are more worn than their counterparts that were sprayed with the flame. However, as was previously mentioned, the difference between iHV5 and iHV6 is almost negligible. The fact that iHV1 is more worn than iHV2 is quite perplexing considering that iHV2 has more pores and lesser hardness than iHV1. While higher hardness doesn't always lead to better wear resistance, lesser porosity generally does [8]. On the other hand, since the differences

between the samples are very small, they could be due to error of some kind or just coincidental. Brinell hardness of Inconel 625 is for as-rolled plate 175-240 HB [24]. This corresponds roughly to 179-248 HV. [13] The hardnesses of the Inconel samples studied in this thesis are around 300-390; clearly, the coating process of HVAF arc raises the hardness of Inconel 625 wire considerably.

6.12 Corrosion resistance of the coatings

Below in Figure 89, the results of the immersion test of three Metcoloy 4 samples can be seen. These three samples started showing some rust on the second day of the experiment, approximately 25 h after the experiment started. However, the rust never spread any further in any of the samples; instead, the rust spots stayed the same for the rest of the experiment. Approximately at the same time in the figure, the lines of HV2 and HV3 have a little drop, after which they never get so low again. This drop coincides with the arrival of rust and indicates that the increase in the lines after the small drop is caused by the corrosion products blocking the pores in the coating. All in all, it is evident from the Figure 90 that the Metcoloy coatings cannot withstand corrosion very well.

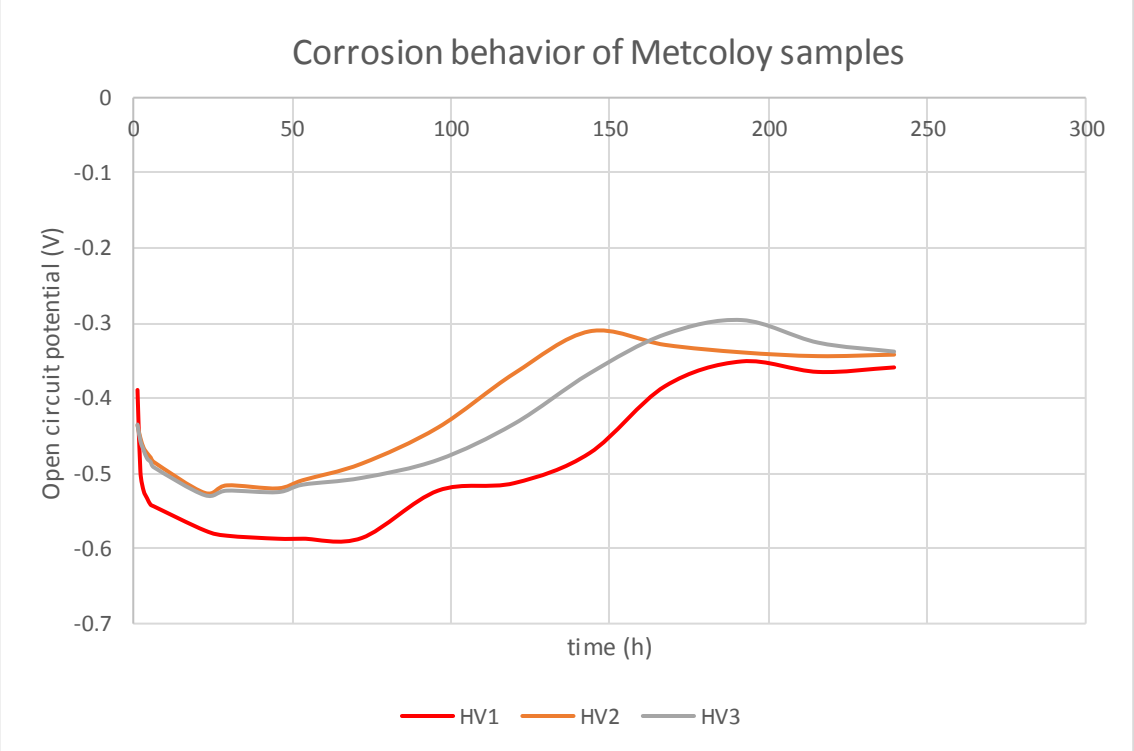

Figure 89. *Results of the corrosion test for Metcoloy 4 samples*

Below in Figure 90, the results of the immersion test of Inconel 625 samples can be seen. The sample HV8X is much thinner than the rest of the samples, and this is quite likely the reason why its substrate started to rust on the second day of the experiment, and continued to rust further all the way to the end of the test. Sample iHV3 started to leak on the

last day of the experiment, and so the final measurement of it was not included in the graph below.

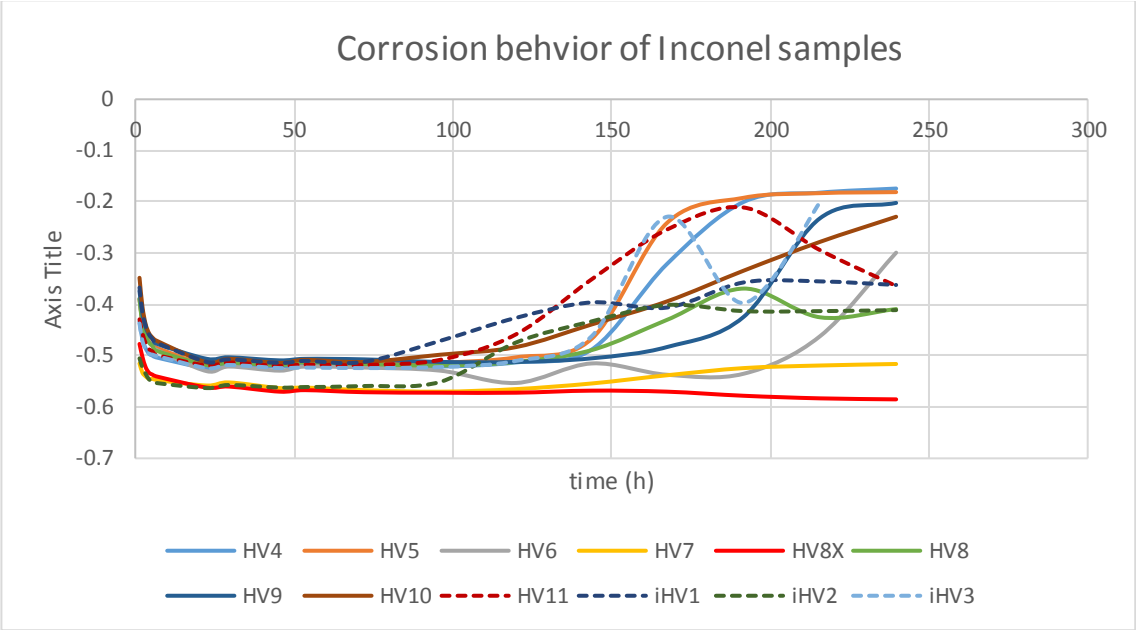

Figure 90. *Results of the corrosion test for Inconel 625 samples*

Of the rest of the Inconel samples, HV4, HV5, HV9, and iHV3 never started showing any signs of rust. HV7, HV8, iHV2, iHV1, HV11, HV10 and HV6 started showing some signs of rust on the seventh day of the experiment. In the end, only samples HV8X and HV8 could be said to be heavily rusted, while the rest developed only some quite small spots.

While the thinnest sample (HV8X) started to corrode quite soon and quite heavily, the thickest sample (HV9) attained quite high a value and never started showing any signs of rust. The rest of the samples that didn't show any rust (HV4, HV5, iHV3) weren't particularly thick, apart from HV5, though neither were they very thin. This seems quite logical, since the corrosion resistance of the coating is determined by its porosity and thickness [2]. However, based on the Figure 90, it must be said that these Inconel 625 coatings do not withstand corrosion any better than the HVAF Arc Metcoloy4 coatings. The lines in the graph rise after the small drop around 25 hours because corrosion products block the pores in the coating, just as they do in the Metcoloy coatings.

7. DISCUSSION

In all the studies from open literature concerning either HVAF Arc or AAS, the coating has a finer microstructure than that of made with conventional arc spray gun [2],[18], [32]. It is also mentioned that coatings made from alloy 671 and 625 are also denser than their counterparts sprayed with conventional arc spray machine [32]. These findings match the results of this thesis, for in all of the images, the HVAF Arc coatings have a finer and denser structure than either SmartArc or HVAF Arc coatings made without using combustion products of propane and air as atomizing gas. The findings also match the theory that increased velocity of the particles in the spraying jet results in a finer coatings structure [2].

In study by Verstak and Baranovski, HVAF arc aluminium coating had isolated oxide inclusions instead of oxide scales, and in HVAF arc coatings made from alloy 671 and 625, respectively, the amount of oxides in the coatings was similar to conventional electric arc spraying [30]. In the study by Nuzzo, the coatings are clearly quite heavily oxidized. [18] The amount of oxides in the AAS coatings is not discussed in any of the studies conducted by Boronenkov and Korobov. [2] The former two results, especially the results from Nuzzo are quite similar to what is observed in the studies conducted for this thesis: the HVAF arc coatings are quite heavily oxidized. In fact, in the studies made for this thesis, the amount of oxidation is typically greater in HVAF arc coatings than in conventionally sprayed arc coatings, with the exception of the three Metcoloy samples compared to similar SmartArc samples.

In theory, the propane used as a process gas in HVAF Arc should decrease the amount of oxidation [32], but that does not seem to be the case. It is of course possible that by using propane, the oxidation of the HVAF Arc coatings is less than it would be with the same velocity obtained without using propane. High velocity of the atomizing gas flow leads to increased oxide content compared to lower velocity, because the smaller particles produced by high velocity have greater specific surface area that is in contact with oxygen [22].

In a study by Verstak and Baranovski, the porosity of alloys 671 and 625 porosity less than 2% [32], and in AAS stainless steel coating by Boronenkov and Korobov, the porosity of the coating is about 2-3%. These low values match the porosity results obtained in this thesis.

While Fe-Cr-B-C cored wire coatings had a similar microhardness as conventional arc sprayed coatings in a study by Verstak and Baranovski, [32], AAS coatings had better microhardness than conventionally arc sprayed coatings in a study by Boronenkov and

Korobov [2]. In the study by Nuzzo, the Metcoloy 2 coatings have Vickers hardness values quite alike to hardness values obtained in the studies for this thesis [18]. In the studies for this thesis, it is also noted that the HVAF Arc sprayed coatings usually have 40-50 HV higher Vickers hardness values than the coatings sprayed with HVAF Arc without using the combustion flame. On the other hand, SmartArc coatings have about the same hardness values as the HVAF Arc coatings when the material used is Metcoloy 4. In the coatings made with Inconel 625, HVAF Arc coatings have slightly higher hardness values than the similar SmartArc coatings.

In the study by Nuzzo, increasing distance resulted in increased amount of oxidation [18], just as it did in the study of this thesis. The reason why increasing distance can increase amount of oxidation in a coating is that with a longer distance, the particles in the spray jet have more time to oxidize. [35] While in Nuzzo's study the increasing distance doesn't really increase the hardness, in this study of this thesis, it did, though quite slightly.

Both in the HVAS studies [38] [33] and in the studies made for this thesis for HVAF Arc the amount of oxides is greater when the high velocity gun is used instead of conventional arc spraying gun, and the amount of pores in the coatings is about half what it is in coatings made with typical arc spraying gun. In HVAS stainless steel 3Cr13 coating the oxide content was about 17 [38], and in a HVAS stainless steel 4Cr13 coating the oxide content was about 38 % [33]; in the Metcoloy 4 coatings made for this thesis, the SEM analysis results indicate that the oxide content is around 28 %. So the exact values for the oxide content do not match very well between HVAS and HVAF Arc, though it should be noted that the coating materials are not identical, either. At least when stainless steel is used as the coating material, the hardness of HVAS coatings made of stainless steel [38] is relatively close the hardness values obtained for HVAF Arc Metcoloy 2 coatings in the study by Nuzzo [18]. Therefore, it would seem that HVAS and HVAF Arc produce relatively similar coatings, but it is not clear, exactly how similar.

It would seem that the benefits of HVAF Arc coatings are the fine structure, low porosity and maybe a somewhat greater hardness than in conventional arc sprayed coatings. Whether or not the HVAF Arc coatings are harder than conventionally sprayed coatings seems to depend somewhat on the coating material used. On the other hand, HVAF Arc produces coatings that are a least as good as the conventional arc sprayed coatings, and their deposition rate seems also to be quite similar. For applications where the heavy oxidation of the coating is not a problem, such as applications that mainly require hardness from the coating, HVAF Arc might be quite suitable, especially if high deposition rate is needed. HVAF Arc apparatus might also be improved if the wire feeding system was changed into a push/pull feeding mechanism; this would likely eliminate the tendency of Inconel 625 wire of getting stuck in the gun.

In the future, it might be enlightening to see how other process gas than propane would affect the coating quality – would the coatings be less oxidized? The adhesion strength of

HVAF Arc coatings compared to conventional arc sprayed coatings has not been tested yet, either. A study comparing HVAS and HVAF arc would also be quite interesting, since right now, it is not certain how close to each other they really are.

8. CONCLUSIONS

With HVAF Arc, it is possible to produce coatings with fine microstructure and low porosity. However, it seems that the amount of oxidation in the coatings is relatively high, and at least when Inconel 625 is used as the coating material, the amount of oxides in the coating is higher than when using either conventional arc spraying apparatus or HVAF Arc without the combustion flame. Also, the coatings do not seem to be corrosion resistant at all. The hardness of HVAF arc coatings seems to be either as high, or somewhat higher, as in typical arc sprayed coatings.

The spraying parameters of HVAF Arc cannot be adjusted very much. Gas parameters about 70 psi propane, 80 psi of air seem to work best, though it is possible to adjust both values slightly upwards. The ratio of the gases should be about 7:8, though. Voltage of 33-36 V is recommended; about 33 V is enough for material like Metcoloy 4, while Inconel 625 seems to work better with about 36 V. Wire feed rate can be about 52-60%; it is possible to use a higher wire feed rate, but this will result in a quite thick coating. HVAF Arc apparatus might also be improved if the wire feeding system was changed into a push/pull feeding mechanism.

Most of the time varying the spray parameters causes relatively little difference in the coating qualities. The exception is when the combustion flame is not used and the HVAF Arc is basically turned into conventional arc spraying apparatus. This results in a coarser microstructure, rougher surface, and slightly less hard coating with more porosity and lower amount of oxides. However, there are some slight differences obtained when varying parameters when using HVAF Arc with the combustion flame. By increasing total gas pressure, the amount of oxides in the coating is slightly reduced, if the wires used are made of Metcoloy 4. If the wires are made of Inconel 625, the amount of oxides increases somewhat as the pressure is increased. Raising voltage raises very slightly the amount of pores in the coating. Increasing wire-feed rate will, naturally, result in a thicker coating. With increased distance, the coating hardness is slightly increased, as well as the amount of oxides it contains, and surface roughness is decreased.

REFERENCES

[1] Bolot, R., Planche, M., Liao, H. & Coddet, C. A three-dimensional model of the wire-arc spray process and its experimental validation. journal of materials processing technology 200 (2008), pp. 94–105

[2] Boronenkov, V. & Korobov, Y. Fundamentals of Arc Spraying. Physical and Chemical Regularities. 449 p.

[3] Brake, M., Hall, A., & Madison, J. Designing energy dissipation properties via thermal spray coatings Surface & Coatings Technology 310 (2017), pp. 70–78.

[4] Espallargas, N. Future Development of Thermal Spray Coatings. 2015, Elsevier Ltd. 286 p.

[5] Gedzevicius, I. & Valiulis, A. Analysis of wire arc spraying process variables on coatings properties. Journal of Materials Processing Technology 175 (2006), pp. 206–211

[6] Hangong, W., Liuying, W., Xunjia, S. & Xuetao, Z. Research on Microstructure and Properties of Coating Produced by High Velocity Electric Wire Arc Spraying of TiB2/Al2O3 Cored Wire. Thermal Spray 2004: Advances in Technology and Application. (May 10, 2004).

[7] Institute of Technology of Metals. Development of the institute: activated arc spray – hypersonic metallization. [Online.] Available at (referred at 17.5.2017) http://www.itm.by/en_ver/index.php?mod=science&act=c15

[8] Kleis, I. & Kulu, P. Solid Particle Erosion: occurrence, prediction and Control. Springer Science & Business Media, 2008, 205 p.

[9] Koch, C. Nanostructured Materials. Processing, Properties, and applications. Second edition. 2007, William Andrew Inc. 760 p.

[10] Kutz, M. Handbook of Environmental Degradation of Materials. 2005, William Andrew Inc. 580 p.

[11] Liao, H., Zhu, Y., Bolot, R., Coddet, C. & Ma, S. Size distribution of particles from individual wires and the effects of nozzle geometry in twin wire arc spraying. Surface & Coatings Technology 200 (2005), pp. 2123– 2130

[12] Liu, G., Rozniatowski, K. & Kurzydlowski, K. Quantitative characteristics of FeCrAl films deposited by arc and high-velocity arc spraying. Materials Characterization 46 (2001), pp. 99– 104

[13] Maher. Hardness Conversion Chart. November 6, 2014. Available: http://www.maher.com/media/pdfs/hardness-conversion-chart.pdf

[14] Metal-Monster. Arc Spray. [Online.] Available at (referred at 9.2.2017) http://www.metal-monster.com/ArcSpray.html.

[15] Newbery, A. & Grant, P. Large arc voltage fluctuations and droplet formation in electric arc wire spraying. Powder Metallurgy 46 (2003)3, pp. 229-235

[16] Newbery, A. & Grant, P. Oxidation during electric arc spray forming of steel. Journal of Materials Processing Technology 178 (2006), pp. 259–269

[17] Newbery, A., Grant, P. & Neiser, R. The velocity and temperature of steel droplets during electric arc spraying. Surface & Coatings Technology 195 (2005), pp. 91– 101

[18] Nuzzo, Manon. Microstructural characterization of coatings deposited by novel high velocity thermal spray process. Report. Tampere University of Technology. 46 p.

[19] Oerlikon Metco. Material Product Data Sheet. Nickel Chromium Thermal Spray Wires. DSMTS-0052.72016 available: https://www.oerlikon.com/.../oerlikon_DSMTS-0052.7_NiCr_Wires..

[20] Oerlikon Metco. Thermal Spray Materials Guide. April, 2015. Available: https://www.oerlikon.com/.../metco/oerlikon_TS_MaterialGuide_EN...

[21] Oseir. How does SprayWatch work? [Online.] Available at (referred at 17.5.2017) http://www.oseir.com/docs/templates/basic.php3?page_id=54

[22] Planche, M., Liao, H., & Coddet, C. Relationships between in-flight particle characteristics and coating microstructure with a twin wire arc spray process and different working conditions. Surface and Coatings Technology 182 (2004), pp. 215–226

[23] Pourmousa Abkenar, A. WIRE-ARC SPRAYING SYSTEM: Particle Production, Transport, and Deposition. Doctoral thesis. Canada 2007. Graduate Department of Mechanical and Industrial Engineering University of Toronto. 149 p.

[24] Special Metals. Inconel alloy 625. August 13, 2013. Available: http://www.specialmetals.com/assets/documents/alloys/inconel/inconel-alloy-625.pdf

[25] Steel grades. The steel grade sharing platform. [Online.] Available at (referred at 23.5.2017) http://www.steel-grades.com/Steel-Grades/Special-Steel/3cr13.html

[26] Sulzer Metco. Metcoloy #2 wire. Technical Bulletin #10-023. Oct 2000, 3 p. Available: http://www.gordonengland.co.uk/sef/attachment.php?aid=371

[27] Tampere University of Technology. Erosion tester. [Online.] Available at (referred at 17.5.2017) http://www.tut.fi/en/research/research-fields/materials-science/research-equipment/wear-research/erosion-tester/index.htm

[28] Toma, S., Bejinariu, C., Baciu, R. & Radu, S. The effect of frontal nozzle geometry and gas pressure on the steel coating properties obtained by wire arc spraying. Surface & Coatings Technology 220 (2013), pp. 266–270

[29] Uniquecoat. HVAF arc 300 TM. [Online.] Available at (referred at 17.5.2017) http://www.uniquecoat.com/hvafarc.html

[30] Uniquecoat technologies, LLC. Turboarc 300 HVAF-Arc Theral Spray System. Owner's manual, number 4012005-001, April, 2011

[31] United States Patent 5 296 667. High velocity electric-arc spray apparatus and method of forming materials. Marantz, R., Marantz, D. & Kowalsky, K. (March 22, 1994.) 17 p.

[32] Verstak, A., & Baranovski, V. (2004). *HVAF arc spraying.* ITSC 2004: International Thermal Spray Conference 2004: Advances in Technology and Application; Osaka; Japan; 10-12 May 2004

[33] Vuoristo, P., Thermal Spray Coating processes, in:Hashmi, S. Comprehensive Materials Processing. 2014, Elsevier Ltd.

[34] Wang, H., Zha, B., Su, X., Yang, H. & Wang, L. Technique and application of high velocity arc spraying. Thermal Spray 2001: New Surfaces for a New Millenium. Proceedings of the international Thermal Spray Conference. Materials Park, US: ASM International, 2001.

[35] Wang, R., Zhang, T., Xu, L., & Huang, X. (2004). Low porosity and fine coatings produced by a new type nozzle of high velocity arc spray gun. ITSC 2004: International Thermal Spray Conference 2004: Advances in Technology and Application; Osaka; Japan; 10-12 May 2004

[36] Wang, R., Xu, L., Zhang, T., & Huang, X. (2004). *The properties of the high productive high velocity arc sprayed coatings and its applications.* ITSC 2004: International Thermal Spray Conference 2004: Advances in Technology and Application; Osaka; Japan; 10-12 May 2004.

[37] Wang, X., Heberlein, J., Pfender,E. & Gerberich, W. Effect of Nozzle Configuration, Gas Pressure, and Gas Type on Coating Properties in Wire Arc Spray. Journal of Thermal Spray Technology 8 (1999)4, pp.565-575

[38] Xu, B., Zhang, W., Ma, S., Tian, B. & Liang, X. Structure and Properties of Coatings Deposited by High Velocity Arc Spray Technique. Journal of Tribology 122 (2000).pp. 646-649

[39] Xu, B.-S., Zhu, Z.-X., Zhang, W., Ma, S.-N.The microstructure and high temperature sliding wear behavior of Fe-Al coating produced by high velocity arc spraying (2004) Proceedings of the International Thermal Spray Conference, pp. 1052-1055.

[40] Zhu, Y, Liao, H., Coddet, C. & Xu, B. Characterization via image analysis of cross-over trajectories and inhomogeneity in twin wire arc spraying. Surface and Coatings Technology 162 (2003), pp. 301–308

APPENDIX A: OPTICAL MICROSCOPE IMAGES WITH MAGNIFICATION 10

In this appendix, a cross-sectional image, with magnification 10, of every sample prepared for this thesis is shown.

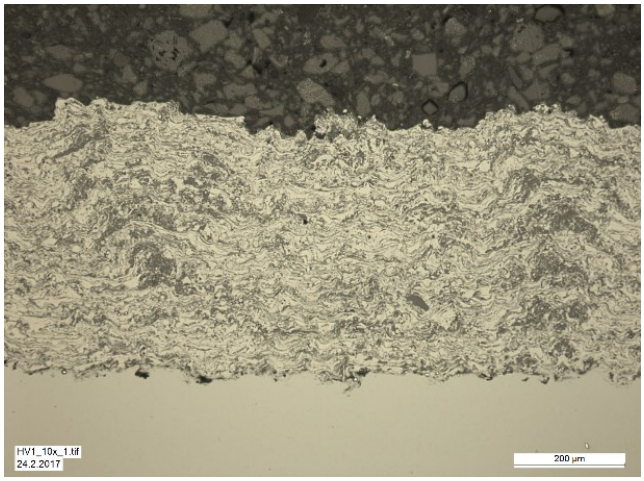

Figure 91. *A cross-sectional image of sample HV1. Magnification 10x.*

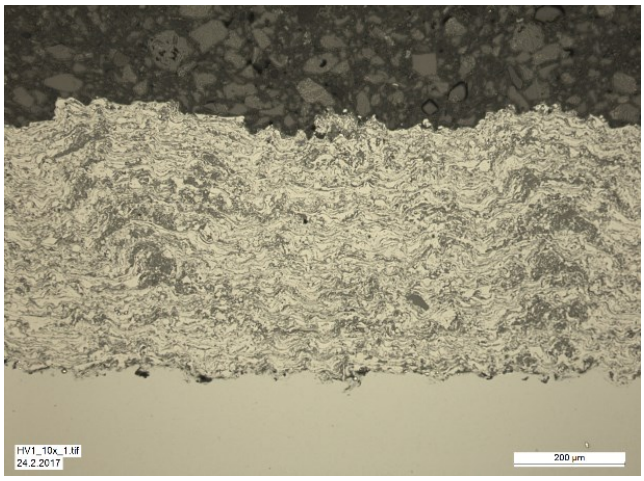

Figure 92. *A cross-sectional image of sample HV2. Magnification 10x.*

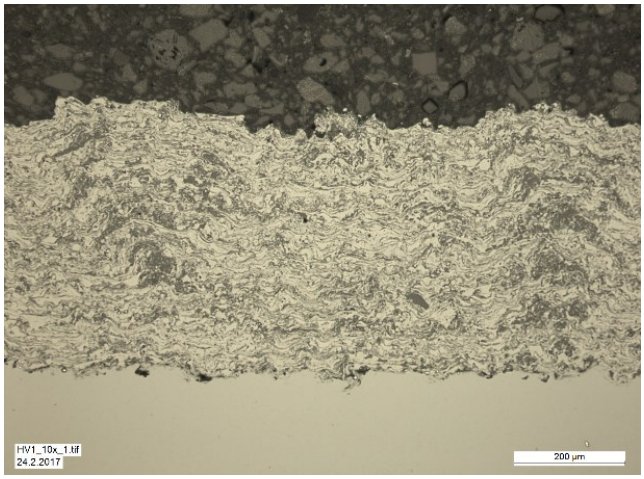

Figure 93. *A cross-sectional image of sample HV3. Magnification 10x.*

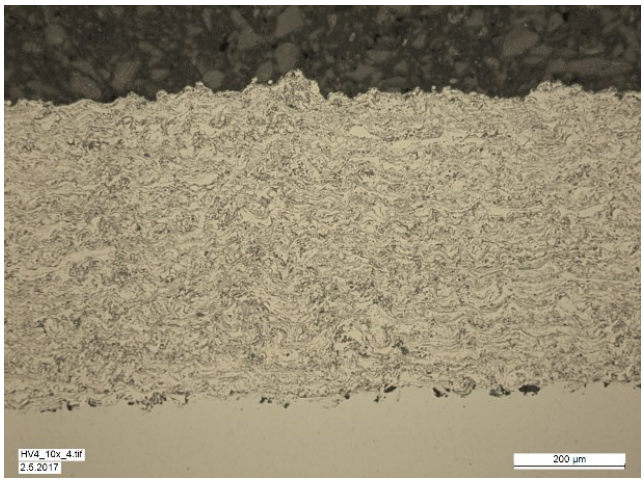

Figure 94. *A cross-sectional image of sample HV4. Magnification 10x.*

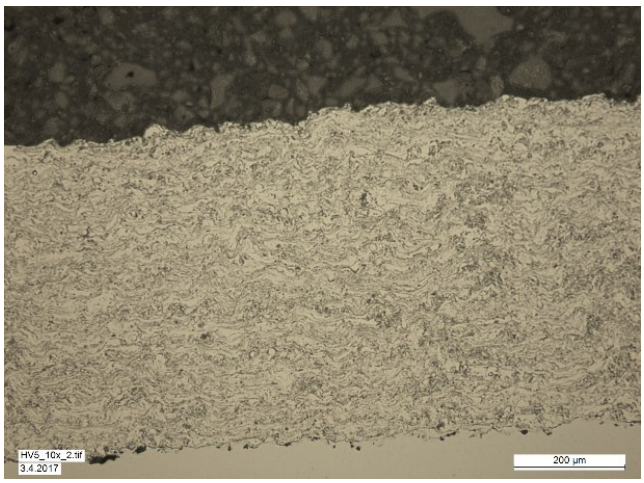

Figure 95. *A cross-sectional image of sample HV5. Magnification 10x.*

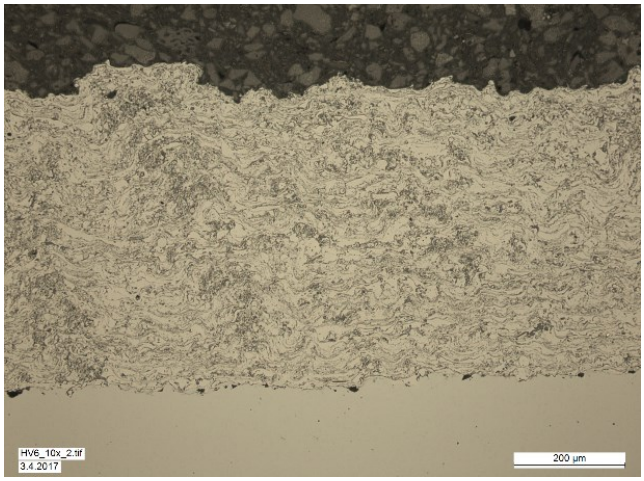

Figure 96. *A cross-sectional image of sample HV6. Magnification 10x.*

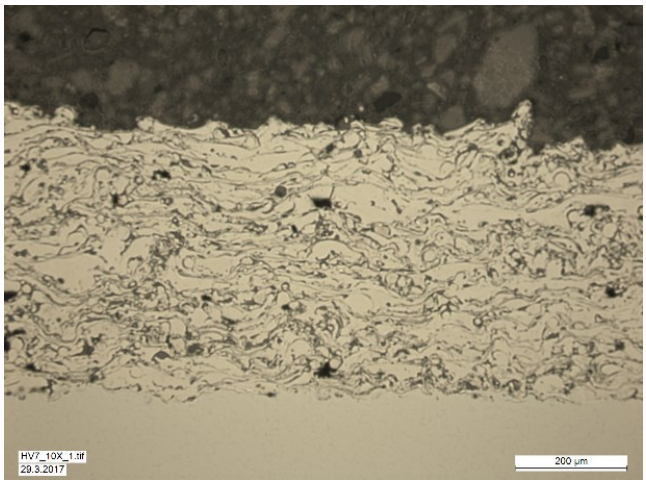

Figure 97. *A cross-sectional image of sample HV7. Magnification 10x.*

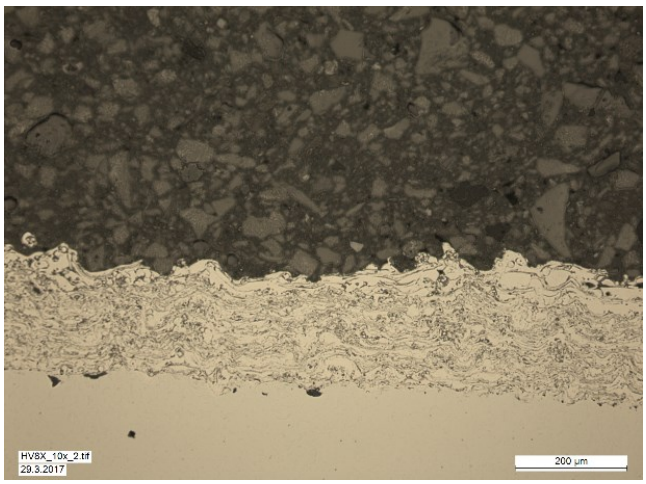

Figure 98. *A cross-sectional image of sample HV8X. Magnification 10x.*

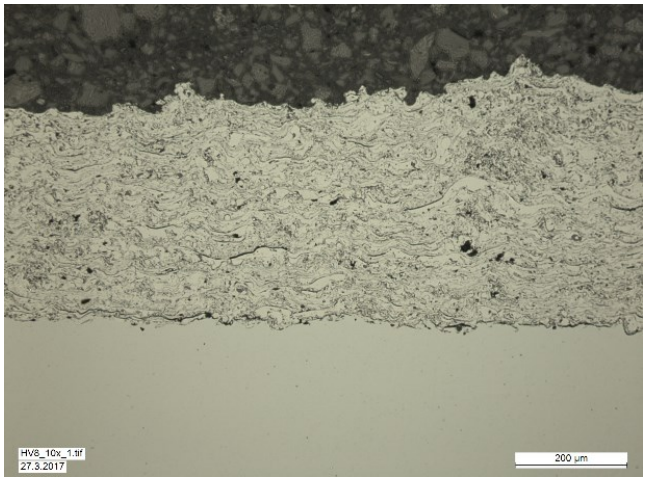

Figure 99. *A cross-sectional image of sample HV8. Magnification 10x.*

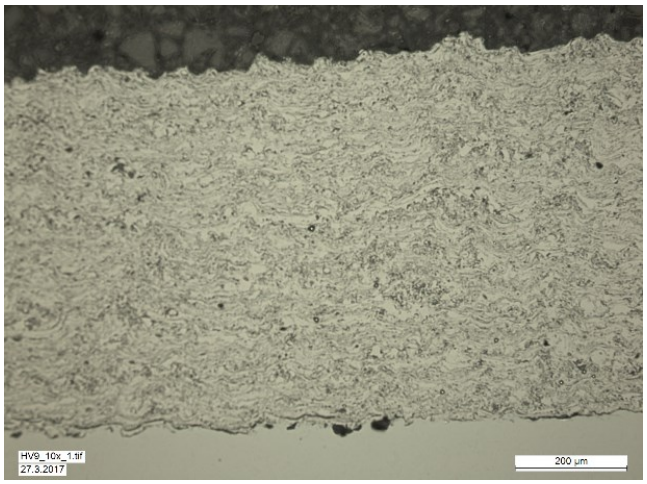

Figure 100. *A cross-sectional image of sample HV9. Magnification 10x.*

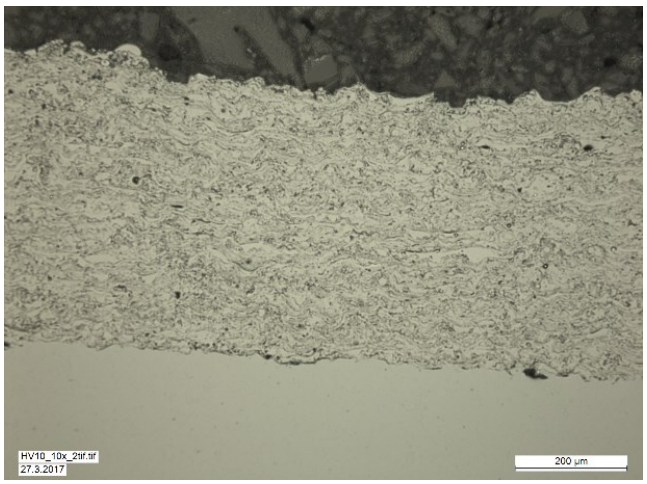

Figure 101. *A cross-sectional image of sample HV10. Magnification 10x.*

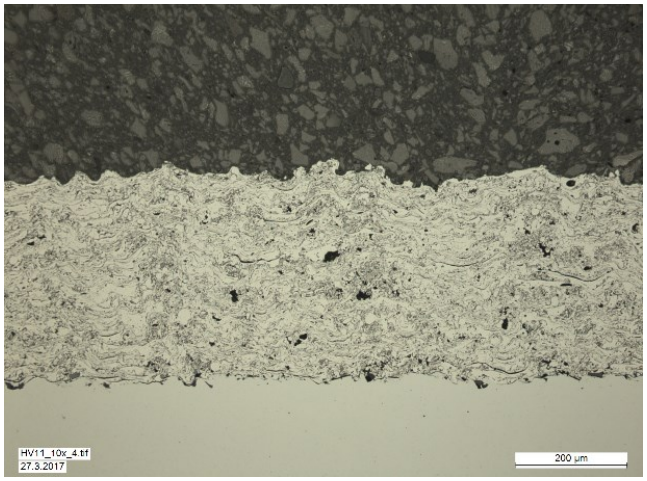

Figure 102. *A cross-sectional image of sample HV11. Magnification 10x.*

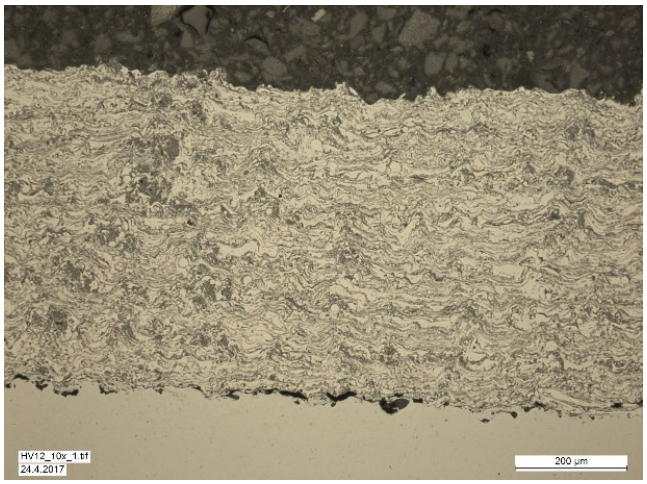

Figure 103. *A cross-sectional image of sample HV12. Magnification 10x.*

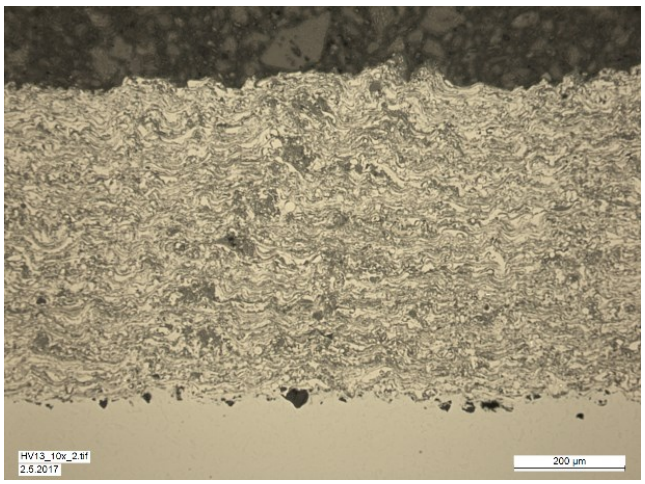

Figure 104. *A cross-sectional image of sample HV13. Magnification 10x.*

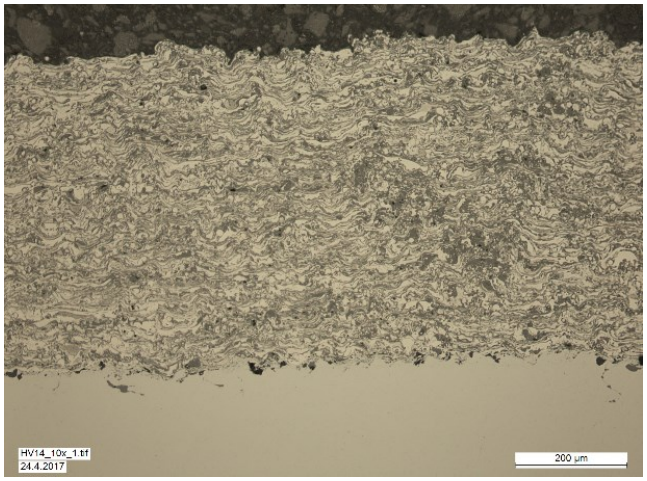

Figure 105. *A cross-sectional image of sample HV14. Magnification 10x.*

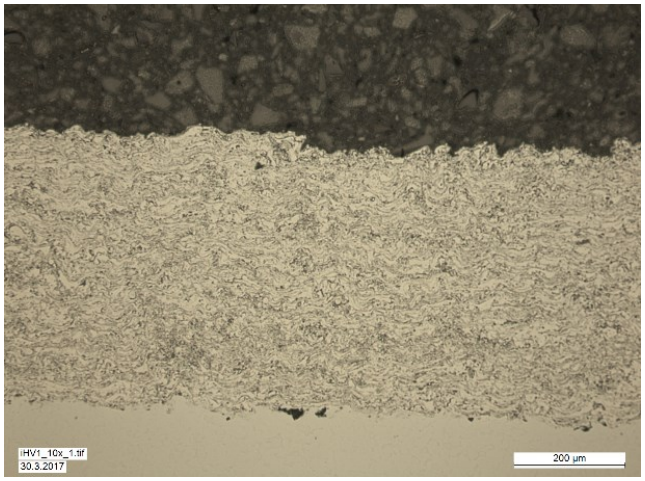

Figure 106. *A cross-sectional image of sample iHV1. Magnification 10x.*

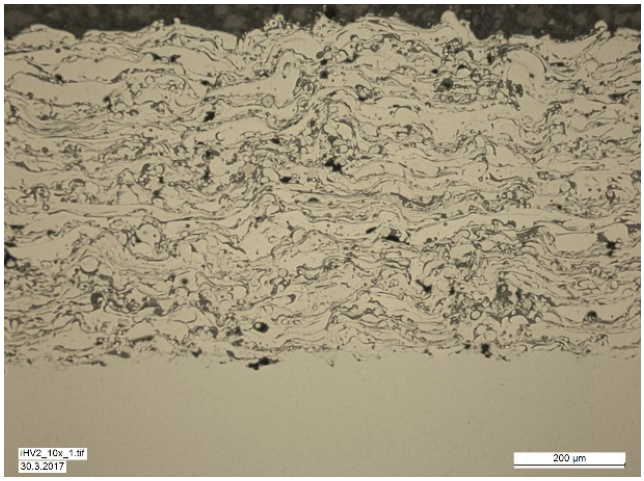

Figure 107. *A cross-sectional image of sample iHV2. Magnification 10x.*

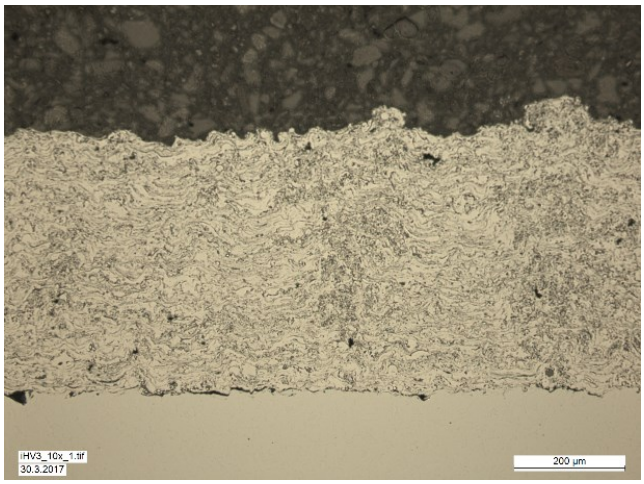

Figure 108. *A cross-sectional image of sample iHV3. Magnification 10x.*

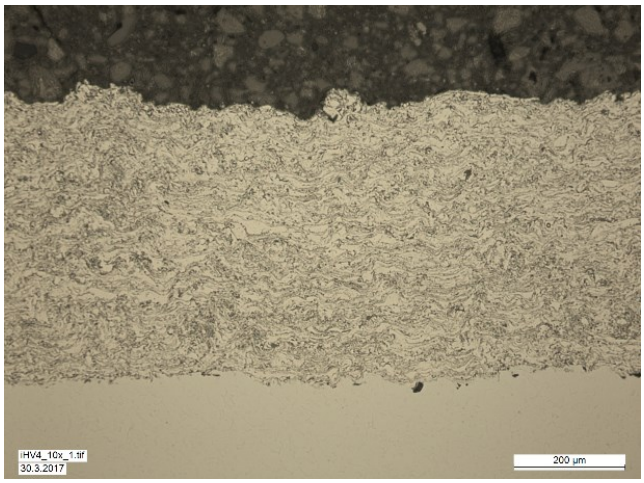

Figure 109. *A cross-sectional image of sample iHV4. Magnification 10x.*

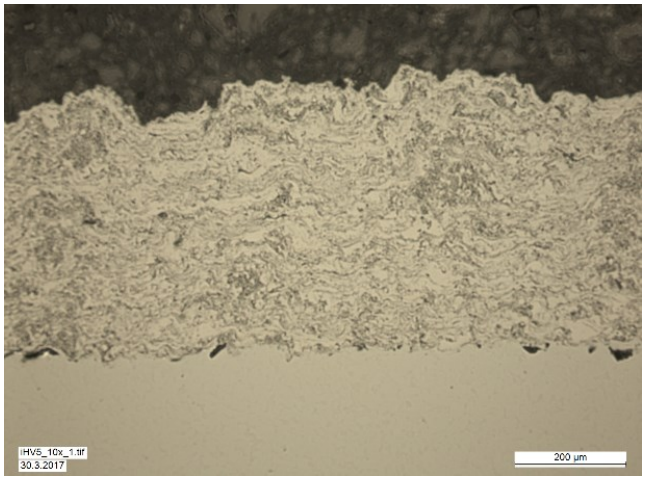

Figure 110. *A cross-sectional image of sample iHV5. Magnification 10x.*

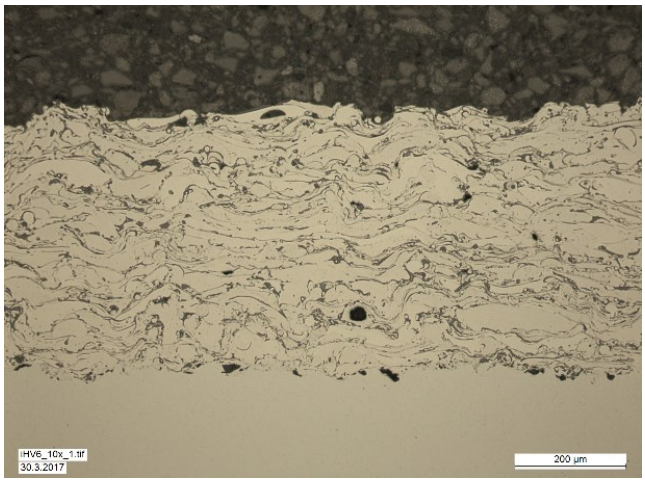

Figure 111. *A cross-sectional image of sample iHV6. Magnification 10x.*

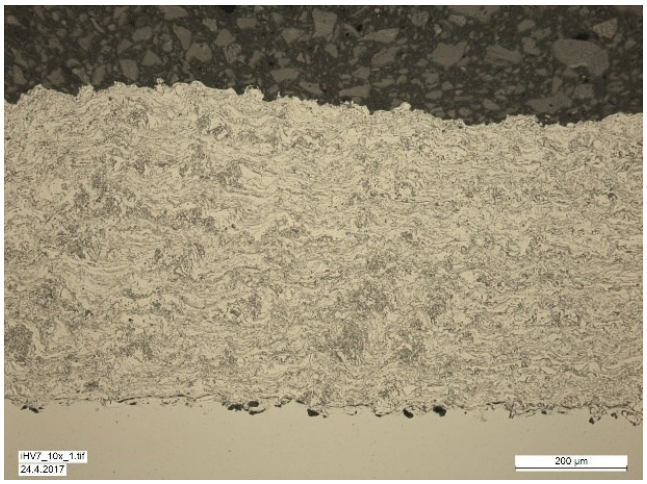

Figure 112. *A cross-sectional image of sample iHV7. Magnification 10x.*

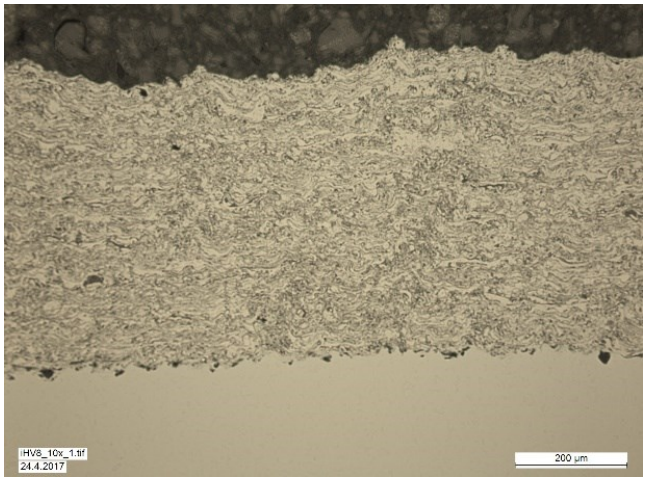

Figure 113. *A cross-sectional image of sample iHV8. Magnification 10x.*

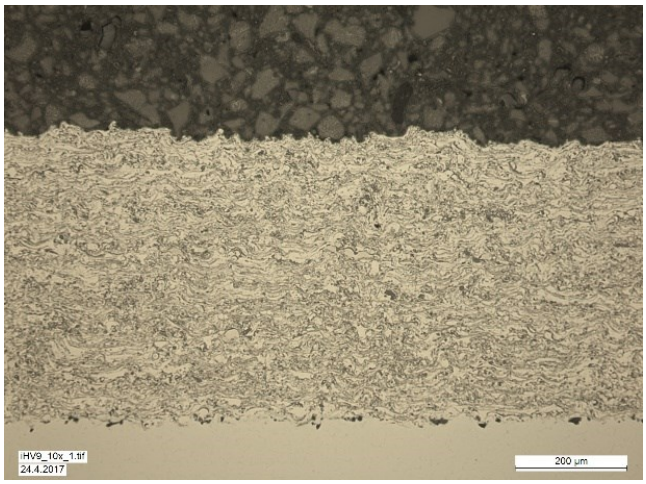

Figure 114. *A cross-sectional image of sample iHV9. Magnification 10x.*

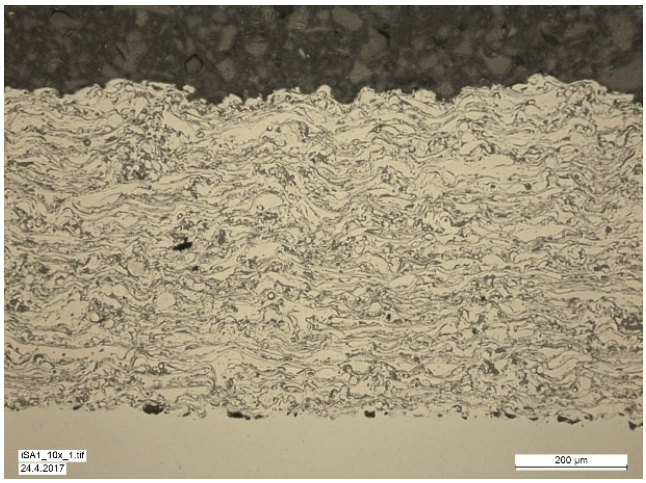

Figure 115. *A cross-sectional image of sample iSA1. Magnification 10x.*

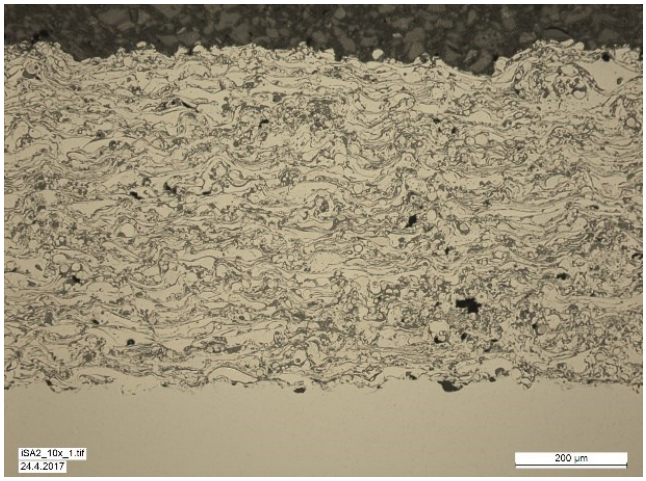

Figure 116. *A cross-sectional image of sample iSA2. Magnification 10x.*

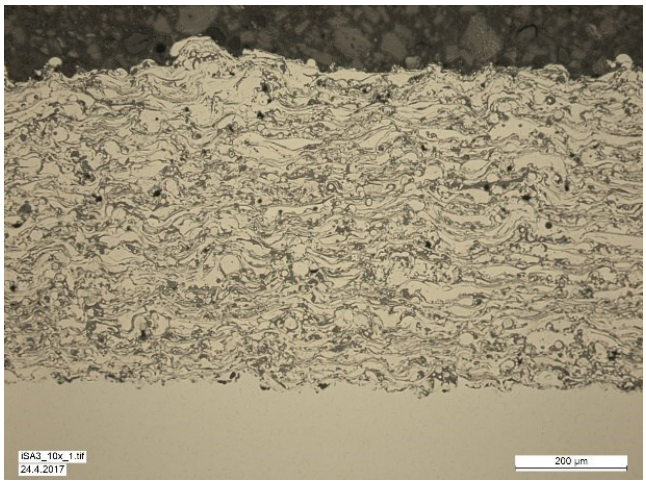

Figure 117. *A cross-sectional image of sample iSA3. Magnification 10x.*

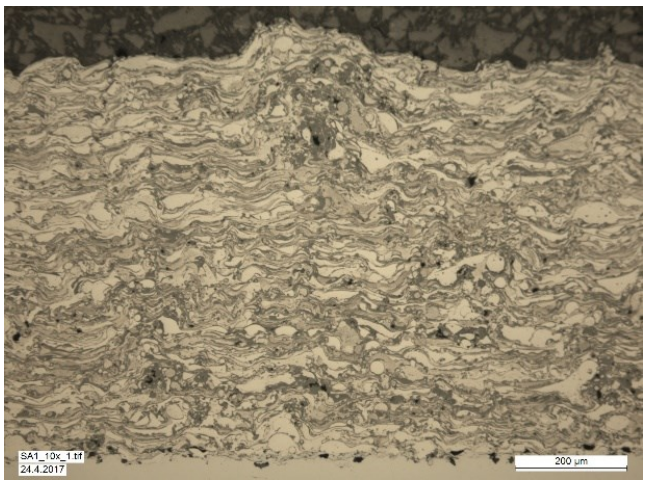

Figure 118. *A cross-sectional image of sample SA1. Magnification 10x.*

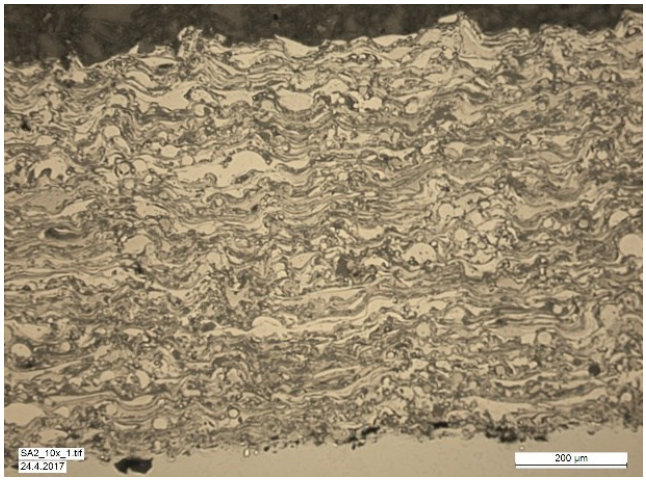

Figure 119. *A cross-sectional image of sample SA2. Magnification 10x.*

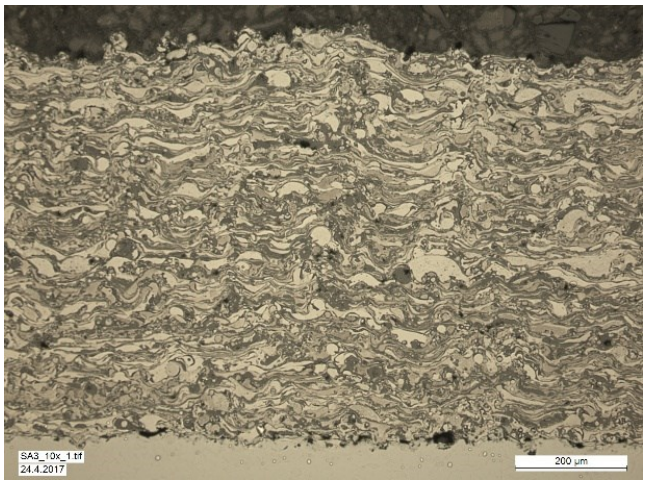

Figure 120. *A cross-sectional image of sample SA3. Magnification 10x.*

APPENDIX B: OPTICAL MICROSCOPE IMAGES WITH MAGNIFICATION 50

In this appendix, a cross-sectional image, with magnification 50, of every sample prepared for this thesis is shown.

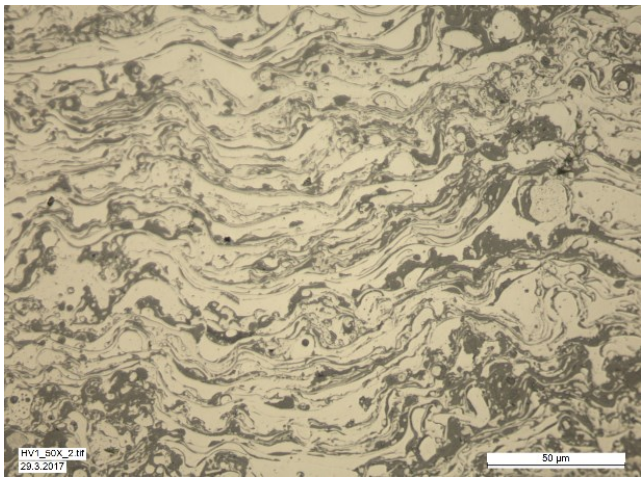

Figure 121. *A cross-sectional image of sample HV1. Magnification 50x.*

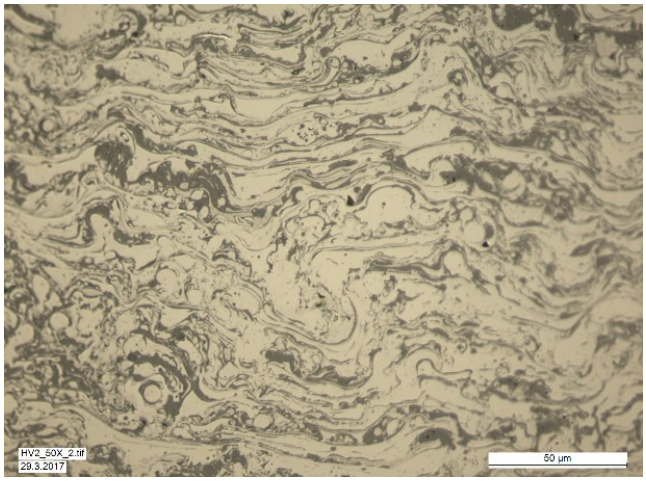

Figure 122. *A cross-sectional image of sample HV2. Magnification 50x.*

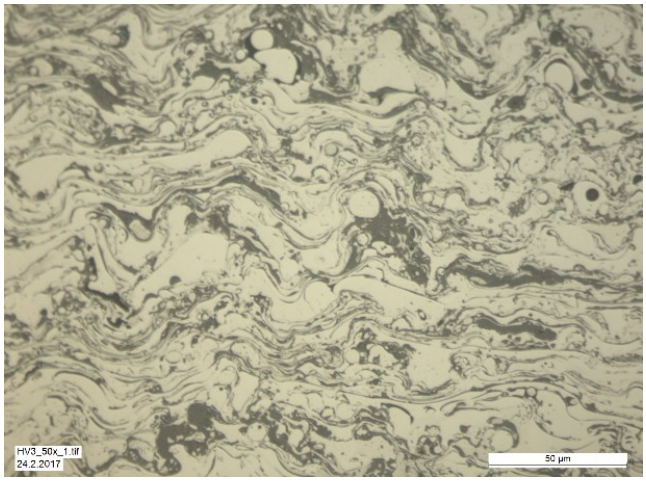

Figure 123. *A cross-sectional image of sample HV3. Magnification 50x.*

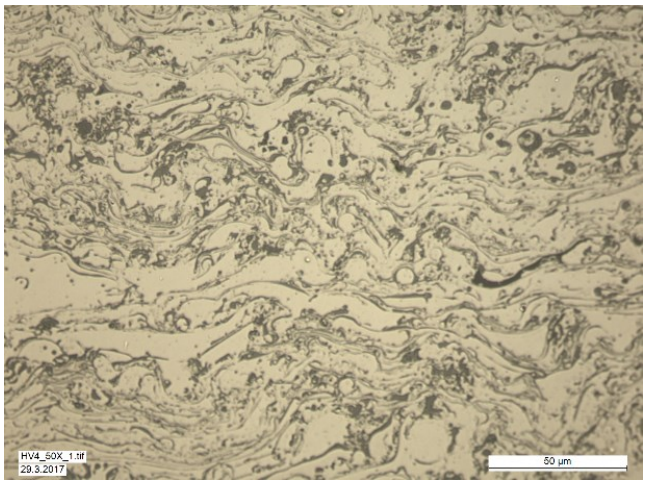

Figure 124. *A cross-sectional image of sample HV4. Magnification 50x.*

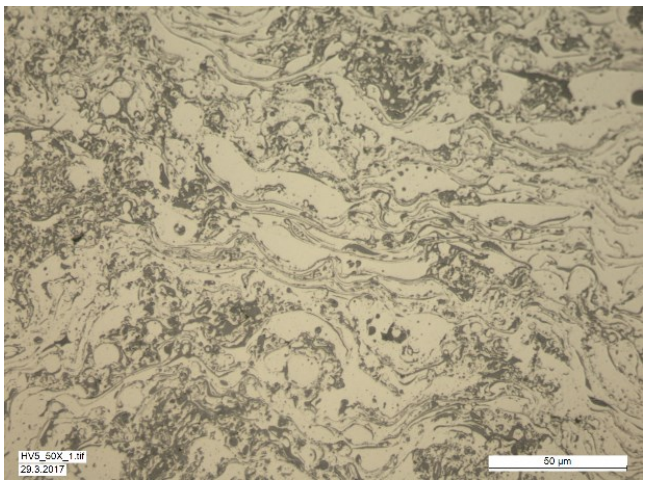

Figure 125. *A cross-sectional image of sample HV5. Magnification 50x.*

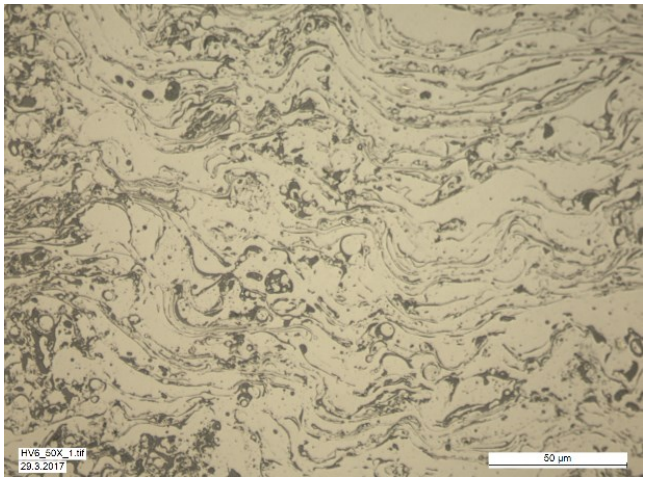

Figure 126. *A cross-sectional image of sample HV6. Magnification 50x.*

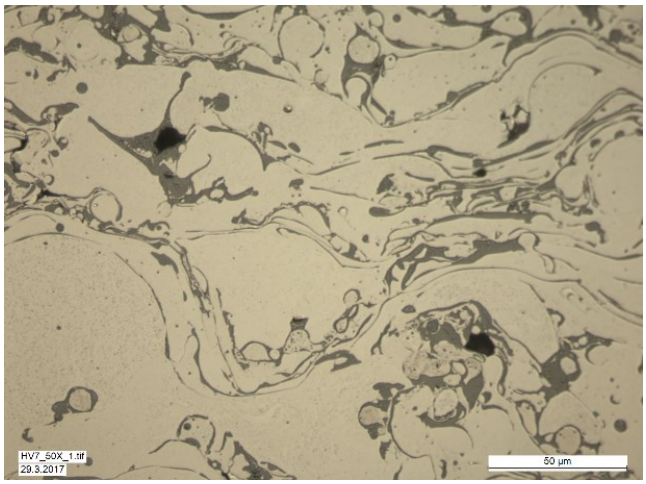

Figure 127. *A cross-sectional image of sample HV7. Magnification 50x.*

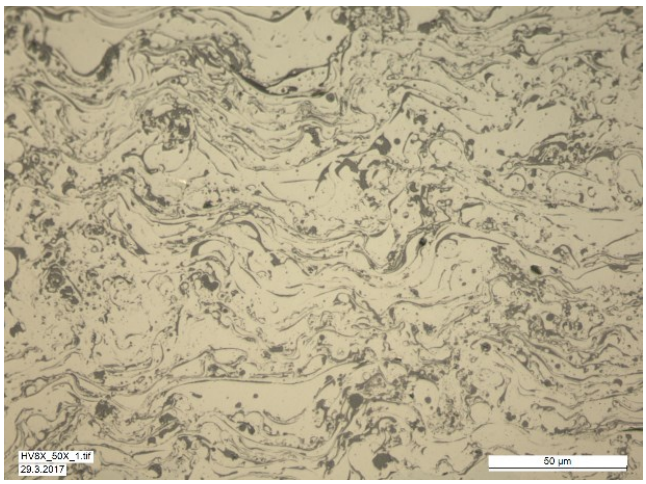

Figure 128. *A cross-sectional image of sample HV8X. Magnification 50x.*

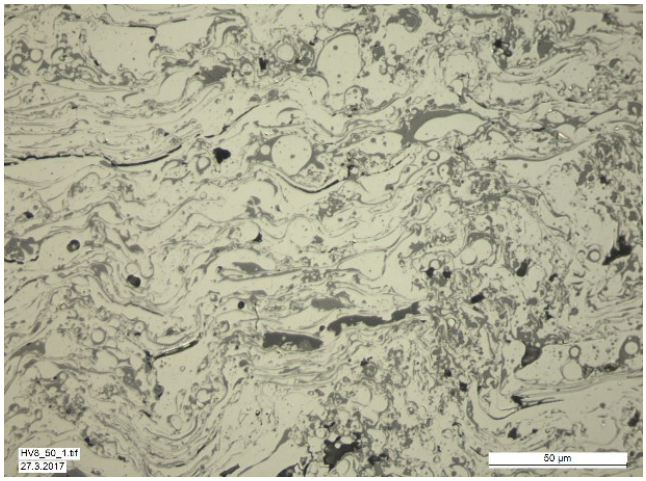

Figure 129. *A cross-sectional image of sample HV8. Magnification 50x.*

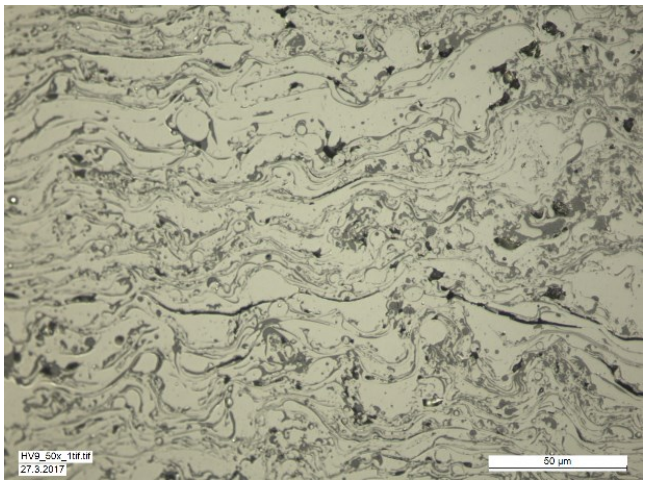

Figure 130. *A cross-sectional image of sample HV9. Magnification 50x.*

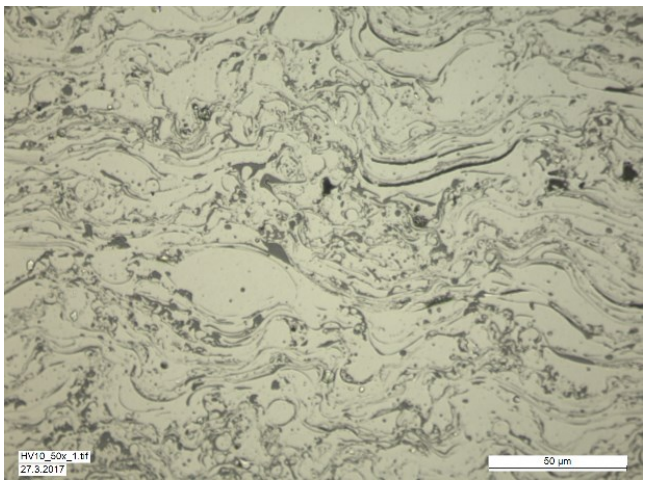

Figure 131. *A cross-sectional image of sample HV10. Magnification 50x.*

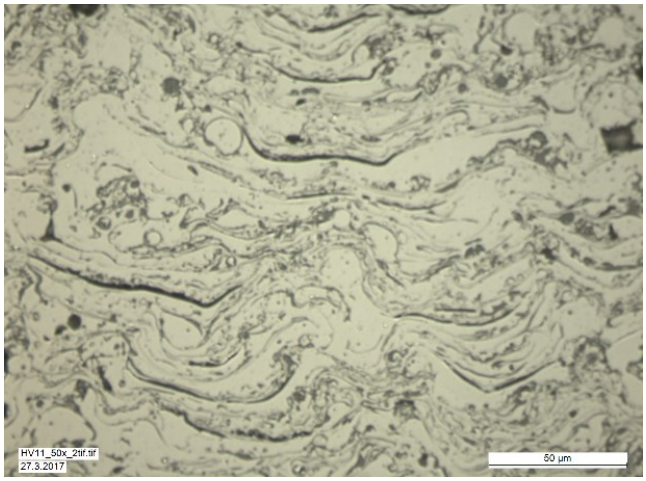

Figure 132. *A cross-sectional image of sample HV11. Magnification 50x.*

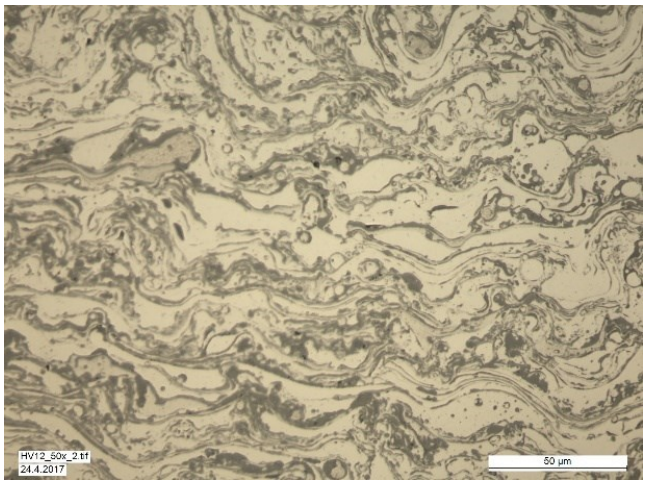

Figure 133. *A cross-sectional image of sample HV12. Magnification 50x.*

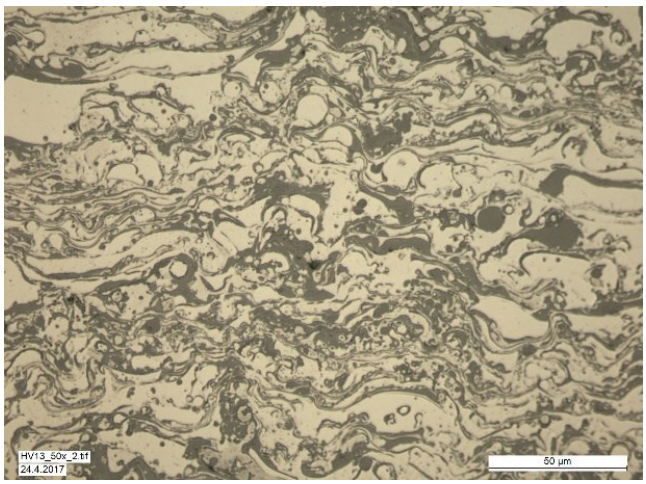

Figure 134. *A cross-sectional image of sample HV13. Magnification 50x.*

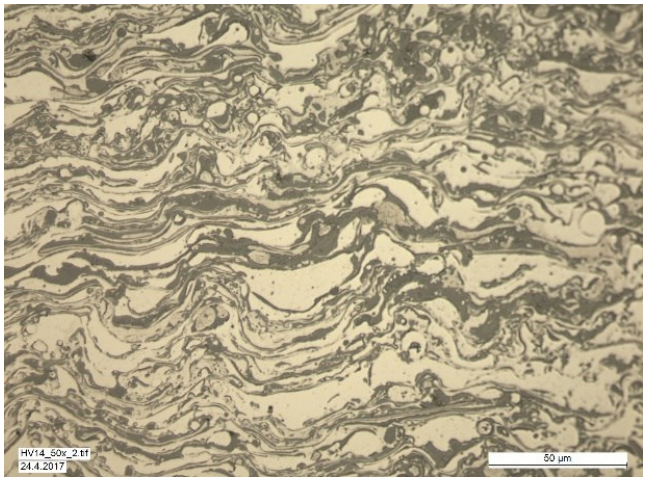

Figure 135. *A cross-sectional image of sample HV14. Magnification 50x.*

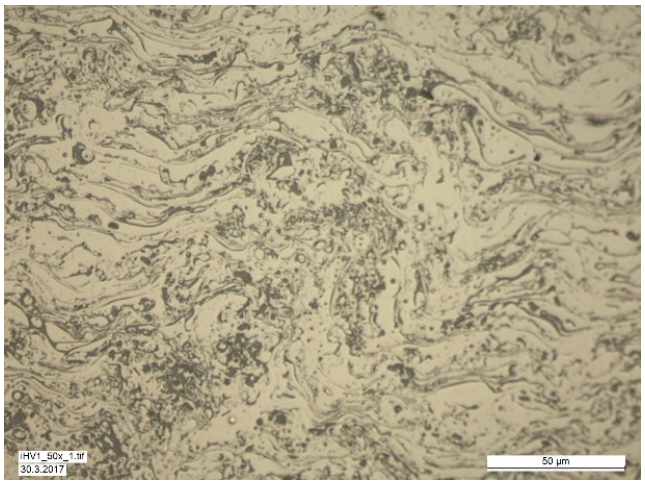

Figure 136. *A cross-sectional image of sample iHV1. Magnification 50x.*

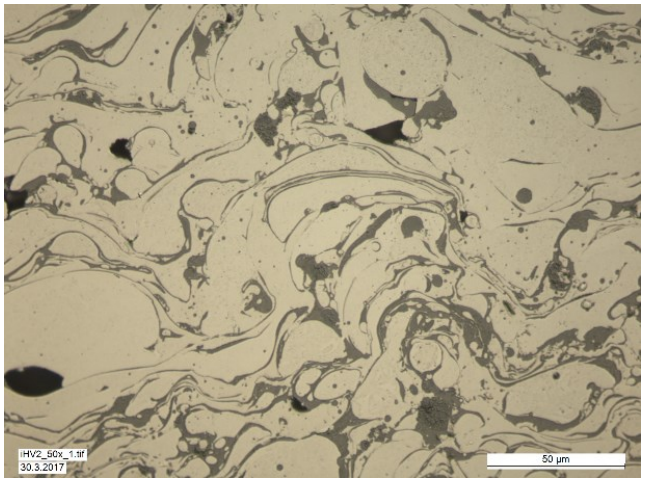

Figure 137. *A cross-sectional image of sample iHV2. Magnification 50x.*

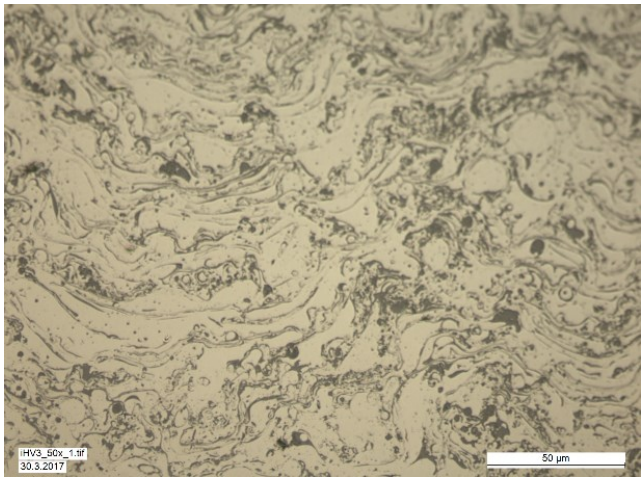

Figure 138. *A cross-sectional image of sample iHV3. Magnification 50x.*

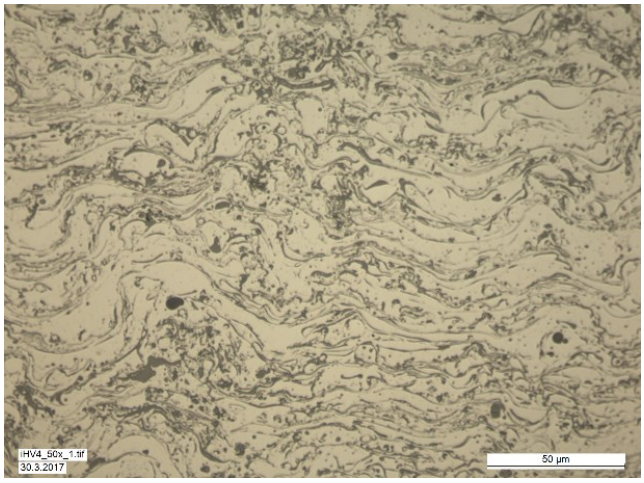

Figure 139. *A cross-sectional image of sample iHV4. Magnification 50x.*

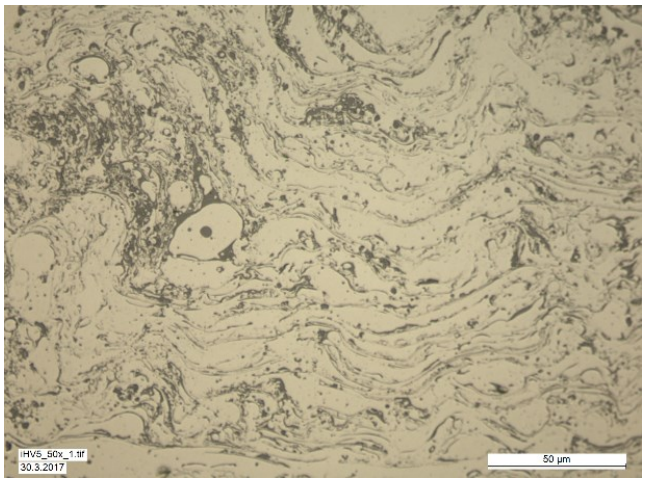

Figure 140. *A cross-sectional image of sample iHV5. Magnification 50x.*

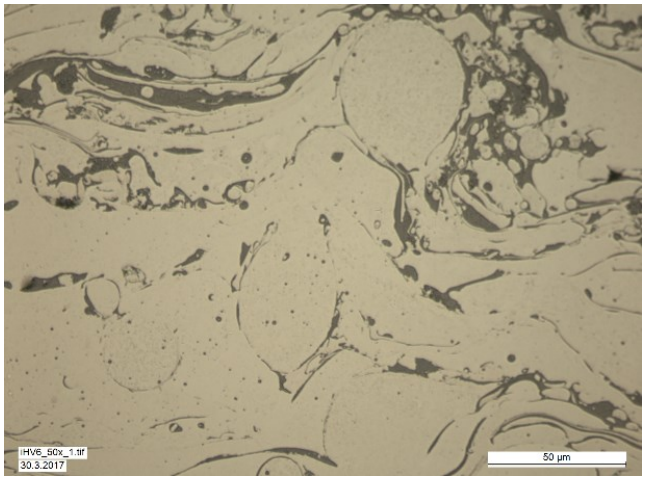

Figure 141. *A cross-sectional image of sample iHV6. Magnification 50x.*

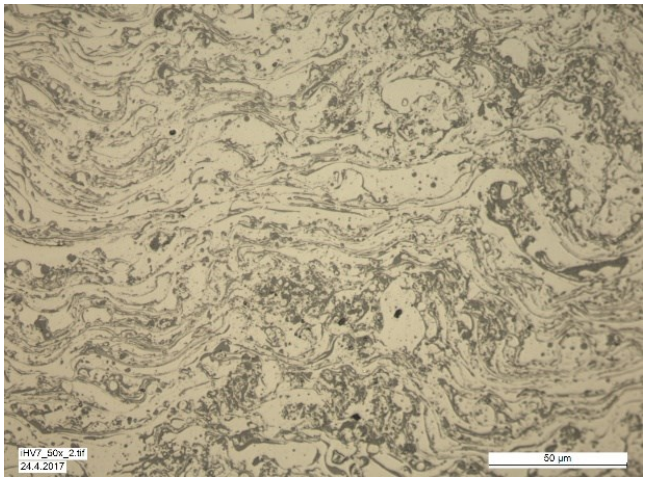

Figure 142. *A cross-sectional image of sample iHV7. Magnification 50x.*

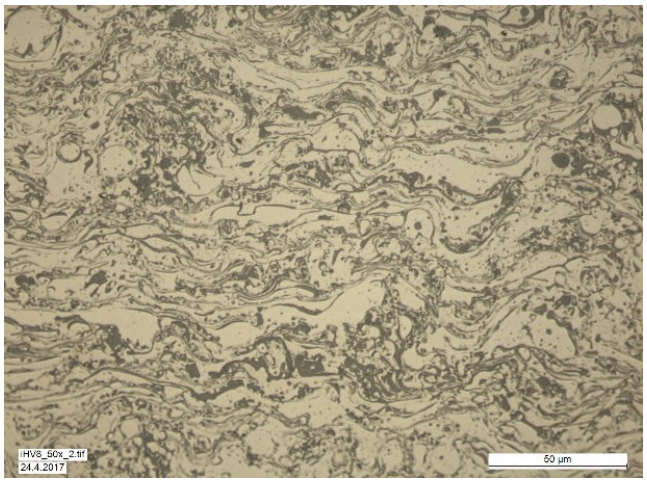

Figure 143. *A cross-sectional image of sample iHV8. Magnification 50x.*

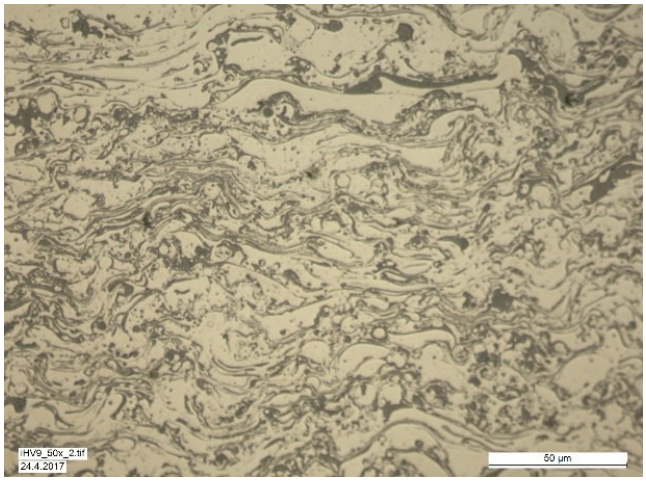

Figure 144. *A cross-sectional image of sample iHV9. Magnification 50x.*

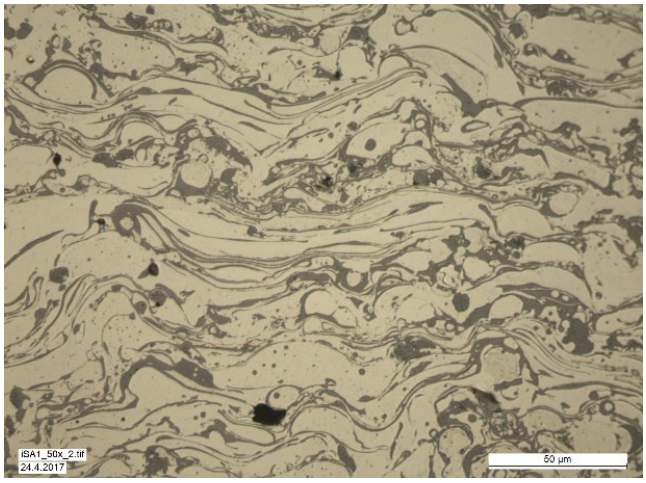

Figure 145. *A cross-sectional image of sample iSA1. Magnification 50x.*

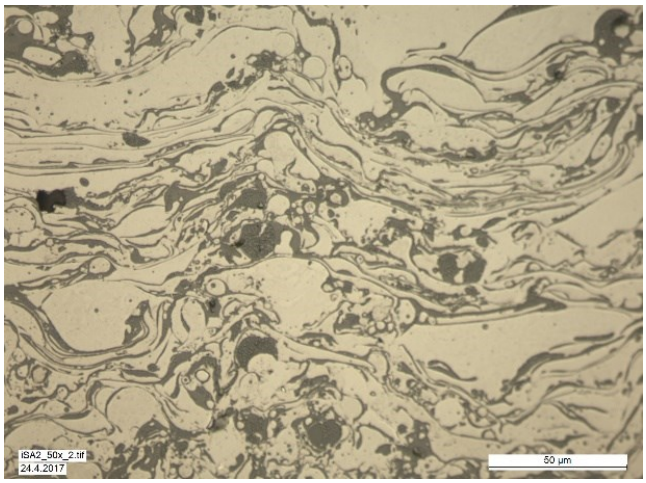

Figure 146. *A cross-sectional image of sample iSA2. Magnification 50x.*

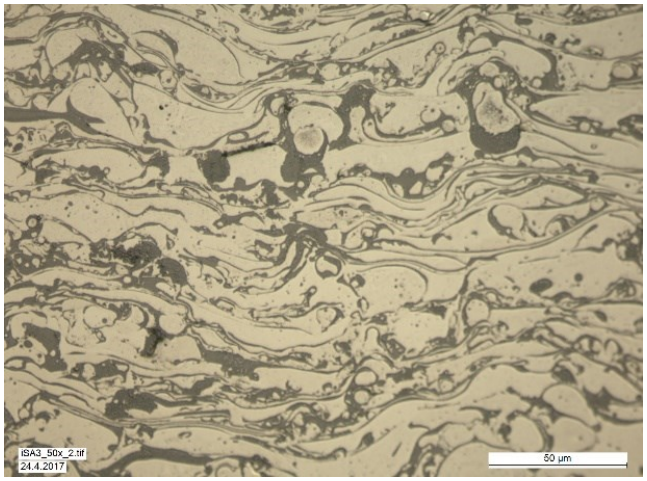

Figure 147. *A cross-sectional image of sample iSA3. Magnification 50x.*

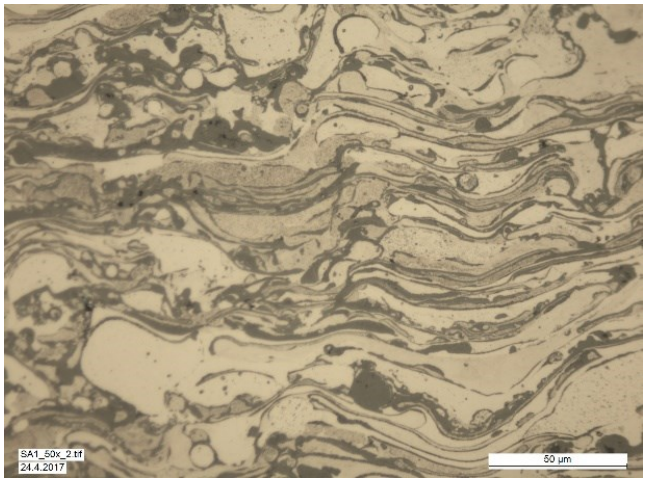

Figure 148. *A cross-sectional image of sample SA1. Magnification 50x.*

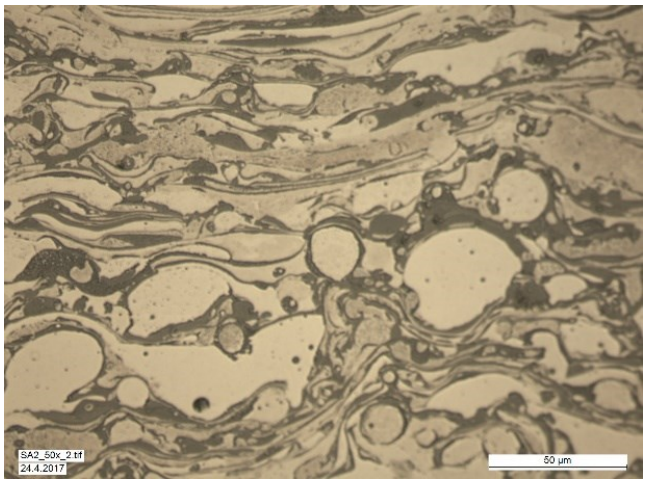

Figure 149. *A cross-sectional image of sample iSA2. Magnification 50x.*

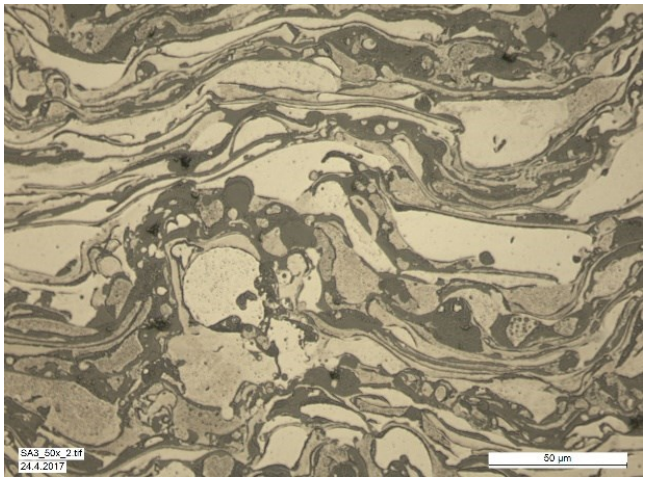

Figure 150. *A cross-sectional image of sample iSA3. Magnification 50x.*